

*What we observe is not nature itself,
But nature exposed to our method of questioning.*

W. Heisenberg

University of Alberta

**Advances in Molecular Sieves and their Applications in
Adsorptive Gas Separation Processes**

by

Christopher Chih-Hao Lin

A thesis submitted to the Faculty of Graduate Studies and Research
in partial fulfillment of the requirements for the degree of

Doctor of Philosophy

in

Chemical Engineering

Department of Chemical and Materials Engineering

©Christopher C. H. Lin

Fall 2009

Edmonton, Alberta

Permission is hereby granted to the University of Alberta Libraries to reproduce single copies of this thesis and to lend or sell such copies for private, scholarly or scientific research purposes only.

Where the thesis is converted to, or otherwise made available in digital form, the University of Alberta will advise potential users of the thesis of these terms.

The author reserves all other publication and other rights in association with the copyright in the thesis and, except as herein before provided, neither the thesis nor any substantial portion thereof may be printed or otherwise reproduced in any material form whatsoever without the author's prior written permission.

Examining Committee

Steven Kuznicki, Chemical and Materials Engineering

Phillip Choi, Chemical and Materials Engineering

Zhenghe Xu, Chemical and Materials Engineering

Jeffrey Stryker, Chemistry

Albert Sacco, Jr., Chemical Engineering, Northeastern University

Dedicated to my mother, Grace

Abstract

The objective of this research was to develop new molecular sieve materials and to examine their applications in adsorptive gas separation processes. Several techniques to modify zeolite molecular sieve materials were developed, including a new pore size control mechanism and novel surface modification procedures. The new materials derived from these modification techniques were found to be potentially useful in many adsorptive gas separation processes.

A novel mechanism was developed to systematically control the pore size of titanium silicate molecular sieves through halogen substitution of terminal hydroxyl groups. These halogen containing zeolites represent a new class of size-selective adsorbents with readily tailored and highly specific pore sizes. Anion-controlled titanium silicates were demonstrated to have promise in multiple areas of size-based separation, particularly light hydrocarbon purification and permanent gas separation. By controlling the type and quantity of the extra-framework cations, titanium silicate molecular sieve adsorbents were modified to separate ethylene and ethane by either the kinetic phenomenon or an equilibrium process. All of these modification techniques were synergistically integrated to illustrate that multi-functional adsorbents can be designed and prepared for many target separations. This approach was demonstrated through the separations of $\text{CO}_2/\text{C}_2\text{H}_6$ and CO_2/CH_4 . Anion-controlled adsorbents were modified to selectively exclude ethane and methane by the steric effect, while the equilibrium and kinetic properties of the

adsorbents were concomitantly adjusted by surface modification. The concept of gas adsorption and separation through nanometals interaction was introduced. Surface-supported nanometals, such as nanosilver, formed on titanium silicate ETS-10 were applied as unique adsorbents to separate gas mixtures, such as Ar/O₂ and N₂/O₂.

Continual research and development in new molecular sieve materials will be crucial to the future of the chemical processing industry, and should be viewed as an avenue for the discovery of next-generation adsorptive gas separation technologies.

Acknowledgements

I thank Dr. Steven Kuznicki for his guidance, support, and mentorship. I am grateful to the members of my examining committee, Dr. Phillip Choi, Dr. Zhenghe Xu, Dr. Jeffrey Stryker, and Dr. Albert Sacco, Jr., for their combined encouragement, fair criticism, and direction. Special thanks to Dr. James Sawada for his valuable insights and advices.

I sincerely thank Lan Wu, Tony Haastrup, Kevin Shi, Tong Qiu, Dr. Alejandro Anson, and every member of our research group, for their general contributions and perspectives. Special thanks to Diane Caird, George Braybrook, Sergei Matveev, Walter Boddez, and Dr. John Duke, for their assistance with various analytical instruments.

Special thanks to Dr. Amy Dambrowitz for her assistance with technical writing and manuscript development.

Special thanks to Dr. Tanya Kuznicki for her assistance with mathematical analysis.

I thank NSERC, Alberta Ingenuity, and the University of Alberta for providing me the funding and support throughout my Ph.D. tenure.

I am indebted to my family and friends, near and far, for providing me the inspiration and motivation to accomplish my goal. Most importantly, I thank Ceanda Mah for her patience and constant support, even during challenging times. Finally, I thank my parents for their commitment to my higher education.

Table of Contents

| | |
|--|----|
| Chapter One. INTRODUCTION | 1 |
| 1.1 Overview | 2 |
| 1.2 Introduction | 4 |
| 1.3 References | 11 |
| | |
| Chapter Two. FUNDAMENTALS OF ADSORPTION AND ADSORPTIVE GAS SEPARATION PROCESSES | 15 |
| 2.1 The Concept of Adsorption | 16 |
| 2.2 Fundamental Forces of Adsorption | 17 |
| 2.3 Single-Component Gas Adsorption | 21 |
| 2.3.1 Isotherm Models | 21 |
| 2.3.2 Langmuir Isotherm | 23 |
| 2.3.3 Langmuir Isotherm with Lateral Interactions | 25 |
| 2.3.4 Freundlich Isotherm | 25 |
| 2.3.5 BET Isotherm | 26 |
| 2.4 Multi-Component Gas Adsorption | 27 |
| 2.4.1 Multi-Component Langmuir Isotherm | 28 |
| 2.4.2 Ideal Adsorbed Solution Theory | 29 |
| 2.5 Henry's Law | 32 |
| 2.6 Selectivity | 33 |
| 2.7 Heat of Adsorption | 33 |
| 2.8 Fundamental Mechanisms of Gas Separation | 35 |
| 2.8.1 Equilibrium Separation | 35 |
| 2.8.2 Kinetic Separation | 35 |
| 2.8.3 Steric Separation | 36 |
| 2.9 Adsorptive Gas Separation Processes | 37 |
| 2.9.1 Adsorbent Design | 37 |
| 2.9.2 Pressure Swing Adsorption | 37 |
| 2.9.3 Temperature Swing Adsorption | 39 |
| 2.10 Conclusions | 41 |
| 2.11 References | 42 |

| | |
|---|----|
| Chapter Three. ANION-CONTROLLED PORE SIZE OF TITANIUM SILICATE MOLECULAR SIEVES | 44 |
| 3.1 Summary | 45 |
| 3.2 Introduction | 46 |
| 3.3 Experimental Methods | 47 |
| 3.4 Results and Discussion | 49 |
| 3.5 Conclusions | 58 |
| 3.6 References | 59 |
| | |
| Chapter Four. SEPARATION OF NITROGEN AND METHANE BY ADSORPTION ON HALOGEN CONTAINING REDUCED PORE ZORITE | 62 |
| 4.1 Summary | 63 |
| 4.2 Introduction | 64 |
| 4.3 Experimental Methods | 66 |
| 4.4 Results and Discussion | 67 |
| 4.5 Conclusions | 70 |
| 4.6 References | 71 |
| | |
| Chapter Five. SEPARATION OF OXYGEN AND ARGON BY ADSORPTION ON HALOGEN CONTAINING REDUCED PORE ZORITE | 73 |
| 5.1 Summary | 74 |
| 5.2 Introduction | 75 |
| 5.3 Experimental Methods | 77 |
| 5.4 Results and Discussion | 80 |
| 5.5 Conclusions | 89 |
| 5.6 References | 90 |
| | |
| Chapter Six. SEPARATION OF ETHYLENE AND ETHANE BY ADSORPTION ON SMALL-PORED TITANIUM SILICATE MOLECULAR SIEVES | 92 |
| 6.1 Summary | 93 |
| 6.2 Introduction | 94 |
| 6.3 Experimental Methods | 95 |
| 6.4 Theoretical Background | 96 |
| 6.5 Results and Discussion | 97 |

| | |
|--|-----|
| 6.6 Conclusions | 105 |
| 6.7 References | 106 |
| Chapter Seven. SEPARATION OF ETHYLENE AND ETHANE BY ADSORPTION ON LARGE-PORED TITANIUM SILICATE MOLECULAR SIEVES | 107 |
| 7.1 Summary | 108 |
| 7.2 Introduction | 109 |
| 7.3 Experimental Methods | 110 |
| 7.4 Theoretical Background | 112 |
| 7.5 Results and Discussion | 115 |
| 7.6 Conclusions | 119 |
| 7.7 References | 120 |
| Chapter Eight. SEPARATION OF CARBON DIOXIDE, ETHANE, AND METHANE BY ADSORPTION ON MODIFIED TITANIUM SILICATE MOLECULAR SIEVES | 122 |
| 8.1 Summary | 123 |
| 8.2 Introduction | 124 |
| 8.3 Experimental Methods | 127 |
| 8.4 Results and Discussion | 128 |
| 8.5 Conclusions | 135 |
| 8.6 References | 136 |
| Chapter Nine. SEPARATION OF NITROGEN, ARGON, AND OXYGEN BY ADSORPTION ON SILVER- EXCHANGED MOLECULAR SIEVES | 138 |
| 9.1 Summary | 139 |
| 9.2 Introduction | 140 |
| 9.3 Experimental Methods | 142 |
| 9.4 Results and Discussion | 143 |
| 9.5 Conclusions | 147 |
| 9.6 References | 149 |
| Chapter Ten. CONCLUSIONS | 151 |
| 10.1 Conclusions | 152 |
| 10.2 Recommendations | 154 |

List of Tables

| | |
|---|-----|
| Table 1-1. Examples of Commercial Adsorptive Separation Processes | 3 |
| Table 2-1. Examples of Industrial Adsorptive Gas Separation Processes | 17 |
| Table 3-1. Quantitative Bulk Elemental Analyses of Anion-Controlled Zorite Analogs | 52 |
| Table 4-1. Physical and Equilibrium Parameters for Ba-RPZ-1 and Ba-ETS-4 | 69 |
| Table 5-1. Equilibrium and Kinetic Parameters for the Adsorption of O ₂ /Ar on Ba-RPZ-1 | 84 |
| Table 5-2. Effective Kinetic Diameters and Molecular Dimensions of Oxygen, Argon, and Nitrogen | 87 |
| Table 6-1. IGC Retention Times for the Adsorption of Ethylene and Ethane on Cation-Exchanged ETS-4 and RPZ-1 at Selected Temperatures | 99 |
| Table 6-2. Limiting Selectivity (α) Calculated from Gravimetric Measurements at 298 K and IGC Measurements at 303 K, 323 K, and 343 K | 100 |
| Table 6-3. UNILAN Parameters for Ethylene Adsorption | 101 |
| Table 6-4. UNILAN Parameters for Ethane Adsorption | 102 |
| Table 7-1. Surface Parameters for the Cation-Exchanged ETS-10 Samples | 111 |
| Table 7-2. Constrained Tóth Parameters for the Adsorption of Ethylene at 298.5 K | 114 |
| Table 7-3. Constrained Tóth Parameters for the Adsorption of Ethane at 298.5 K | 115 |

Table 8-1. Henry's Law Constants (K) and Limiting Selectivities (α) for the Adsorption of Carbon Dioxide, Ethane, and Methane on Selected Titanium Silicate Molecular Sieves 130

Table 8-2. Swing Capacities (1-100 kPa) for the Adsorption of Carbon Dioxide, Ethane, and Methane on Selected Titanium Silicate Molecular Sieves 130

Table 9-1. Langmuir Parameters for the Adsorption Data from 0-120 kPa 147

List of Figures

| | |
|---|----|
| <i>Figure 2-1.</i> The potential energy of selected gas pairs as a function of their distance apart in Å. | 19 |
| <i>Figure 2-2.</i> The IUPAC classification for adsorption isotherms. | 21 |
| <i>Figure 2-3.</i> Schematic of a pressure swing adsorption cycle. | 39 |
| <i>Figure 2-4.</i> Schematic of a temperature swing adsorption cycle. | 40 |
| <i>Figure 3-1.</i> Unit cell representations of anion-controlled zorite analogs. | 50 |
| <i>Figure 3-2.</i> Powder X-ray diffraction of as-synthesized anion-controlled zorite analogs. | 53 |
| <i>Figure 3-3.</i> Chromatographic separation of O ₂ /Ar on anion-controlled zorite analogs. | 55 |
| <i>Figure 3-4.</i> Equilibrium adsorption isotherms of anion-controlled zorite analogs. | 57 |
| <i>Figure 4-1.</i> Powder X-ray diffraction of as-synthesized (a) RPZ-1 and (b) ETS-4. | 66 |
| <i>Figure 4-2.</i> Nitrogen and methane adsorption isotherms at 298 K for Ba-RPZ-1 and Ba-ETS-4. Data displayed in terms of (a) gravimetric basis and (b) volumetric basis. | 68 |
| <i>Figure 4-3.</i> IGC profiles at 298 K by injecting a 50-50% N ₂ /CH ₄ mixture in a column of (a) Ba-RPZ-1 and (b) Ba-ETS-4. | 69 |
| <i>Figure 5-1.</i> Powder X-ray diffraction of as-synthesized (a) Na-RPZ-1 and (b) Na-ETS-4. | 78 |

| | |
|--|-----|
| Figure 5-2. Block diagram of the laboratory-scale PSA apparatus employed for O ₂ /Ar breakthrough experiments. | 79 |
| Figure 5-3. IGC profiles at 303 K by injecting (a) 50-50% O ₂ /Ar, (b) 90-10% O ₂ /Ar, (c) pure argon, and (d) pure oxygen in a column of Ba-RPZ-1 and (e) 50-50% O ₂ /Ar in a column of Ba-ETS-4. | 81 |
| Figure 5-4. Compositional analysis (mole fraction) as a function of time at the outlet of the Ba-RPZ-1 adsorbent bed with a continuous inlet mixture of 50-50% O ₂ /Ar. | 82 |
| Figure 5-5. Compositional analysis (mole fraction) as a function of time at the outlet of the Ba-RPZ-1 adsorbent bed with a continuous inlet mixture of 95-5% O ₂ /Ar. | 82 |
| Figure 5-6. Oxygen and argon adsorption isotherms at 303 K for Ba-RPZ-1. | 83 |
| Figure 5-7. Fractional uptake curves for oxygen and argon at 303 K from 70-100 kPa. | 85 |
| Figure 6-1. IGC profiles at 323 K for (a) Zn-, (b) Ca/H-, (c) Sr-, and (d) Ba-ETS-4. | 98 |
| Figure 6-2. IGC profiles at 343 K for (a) Zn-, (b) Ca/H-, (c) Sr-, and (d) Ba-RPZ-1. | 99 |
| Figure 6-3. Ethylene (white circles) and ethane (black circles) adsorption isotherms at 298 K for (a) Zn-, (b) Ca/H-, (c) Sr-, and (d) Ba-ETS-4. | 101 |
| Figure 6-4. Ethylene (white circles) and ethane (black circles) adsorption isotherms at 298 K for (a) Zn-, (b) Ca/H-, (c) Sr-, and (d) Ba-RPZ-1. | 102 |
| Figure 6-5. IAST model for C ₂ H ₄ /C ₂ H ₆ selectivity at 298 K for (a) Zn-, (b) Ca/H-, (c) Sr-, and (d) Ba-ETS-4. | 103 |
| Figure 6-6. IAST model for C ₂ H ₄ /C ₂ H ₆ selectivity at 298 K for (a) Zn-, (b) Ca/H-, (c) Sr-, and (d) Ba-RPZ-1. | 104 |

- Figure 7-1.** Ethylene (white circles) and ethane (black circles) adsorption isotherms at 298 K for selected cation-exchanged ETS-10 materials. Dotted lines represent the constrained Tóth model isotherms. 116
- Figure 7-2.** C_2H_4/C_2H_6 selectivity (from IAST) as a function of the total pressure for selected cation-exchanged ETS-10 materials at 298 K ($y = 0.5$). 118
- Figure 7-3.** IAST plot of x_{ethylene} (molar fraction of ethylene in the adsorbed phase) vs. y_{ethylene} (molar fraction of ethylene in the gas phase) at 298 K and 150 kPa (total pressure) for (a) Na-, (b) K-, (c) Li-, (d) Cu- and Ba-, (e) Ba/H-, and (f) La/H-ETS-10. 119
- Figure 8-1.** Carbon dioxide, ethane, and methane adsorption isotherms for (a) BPL activated carbon at 301 K, (b) 13X zeolite at 305 K, (c) ALPO-5 at 305 K, and (d) ZSM-5 at 298 K. 125
- Figure 8-2.** Carbon dioxide, ethane, and methane adsorption isotherms (up to 100 kPa) at 298 K for (a) Na-ETS-10, (b) Ba-ETS-10, and (c) Ba/H-ETS-10 (1 meq Ba/g). Equivalent data (up to 1 kPa) for (d) Na-ETS-10, (e) Ba-ETS-10, and (f) Ba/H-ETS-10 (1 meq Ba/g) are also presented. 129
- Figure 8-3.** Carbon dioxide adsorption isotherms for (a) Ba/H-ETS-4 (6 meq Ba/g) activated at 473 K, (b) fully-exchanged Ba-ETS-4 activated at 473 K, (c) Ba/H-ETS-4 (4 meq Ba/g) activated at 423 K, (d) Ba/H-ETS-4 (1 meq Ba/g) activated at 373 K, (e) Ba/H-ETS-4 (1 meq Ba/g) activated at 393 K, and (f) Ba/H-ETS-4 (1 meq Ba/g) activated at 473 K. 132
- Figure 8-4.** Carbon dioxide, ethane, and methane adsorption isotherms at 298 K for (a) Ba-ETS-4, (b) Ca/H-ETS-4 (4 meq Ca/g), and (c) Zn-ETS-4. 133
- Figure 8-5.** Carbon dioxide, ethane, and methane adsorption isotherms at 298 K for (a) Ba-RPZ-1, (b) Ca/H-RPZ-1 (4 meq Ca/g), and (c) Zn-RPZ-1. 134
- Figure 9-1.** IGC profiles obtained at 303 K with 30 cm³/min of helium carrier flow for argon, oxygen, and a 50-50% mixture of O₂/Ar on (a) Ag-ETS-10 and (b) Ag-mordenite. 145

Figure 9-2. Nitrogen, argon, and oxygen adsorption isotherms at 303 K on (a) Ag-ETS-10 and (b) Ag-mordenite, with Langmuir fitting curves up to a pressure of 120 kPa. The inserts expand the lower pressure regimes. 146

Nomenclature

Abbreviations

| | |
|----------|---|
| ALPO-5 | Aluminophosphate-5 |
| AST | Adsorbed solution theory |
| BEA | Beta zeolite |
| BET | Brunauer, Emmett, Teller |
| CMS | Carbon molecular sieve |
| CTS | Contracted titanium silicate |
| ETS-4 | Engelhard titanosilicate-4 |
| ETS-10 | Engelhard titanosilicate-10 |
| GC | Gas chromatograph |
| GHP | Gravimetric high pressure |
| HFZ | Halogen free zorite |
| IAST | Ideal adsorbed solution theory |
| IGC | Inverse-phase gas chromatography |
| INAA | Instrumental neutron activation analysis |
| IUPAC | International union of pure and applied chemistry |
| JCPDS | Joint committee on powder diffraction standards |
| LSX | Low silica X |
| MFC | Mass flow controller |
| NMR | Nuclear magnetic resonance |
| OD | Outer diameter |
| PSA | Pressure swing adsorption |
| psi | Pound per square inch |
| RPZ | Reduced pore zorite |
| SAPO-5 | Silicoaluminophosphate-5 |
| SLOWPOKE | Safe low-power critical experiment |
| STP | Standard temperature and pressure |

| | |
|--------|----------------------------------|
| TCD | Thermal conductivity detector |
| TSA | Temperature swing adsorption |
| UNILAN | Uniform Langmuir |
| VPSA | Vacuum-pressure swing adsorption |
| VSA | Vacuum swing adsorption |
| WDX | Wavelength dispersive X-ray |
| XRD | X-ray diffraction |
| ZSM-5 | Zeolite socony mobil-5 |
| ZSM-15 | Zeolite socony mobil-15 |

Greek Letters

| | |
|-------------------------|--|
| α | Adsorption rate constant Limiting selectivity Polarizability Sticking probability |
| β | Desorption rate constant |
| γ | Activity coefficient |
| ΔG | Free energy change |
| ΔH | Enthalpy change Heat of adsorption |
| ΔS | Entropy change |
| ΔH_{iso} | Isosteric heat of adsorption |
| ε | Monolayer volume of the adsorbent Potential field |
| θ | Angle Diffraction angle Fractional coverage |
| θ_{T} | Total surface coverage |
| μ | Chemical potential Permanent dipole moment |
| π | Pi (constant) Spreading pressure |
| σ | Effective kinetic diameter Interfacial tension of the monolayer-covered surface |

| | |
|-------------|--|
| | Standard deviation |
| σ^0 | Interfacial tension of the clean surface |
| ϕ | Interaction energy Potential function |
| ϕ_D | Dispersion energy |
| ϕ_F | Field-dipole interaction energy |
| ϕ_{FQ} | Field-quadrupole interaction energy |
| ϕ_P | Polarization energy |
| ϕ_R | Close-range repulsion energy |
| φ | Potential energy |

Notations

| | |
|----------|---|
| $^\circ$ | Degree |
| A | Pre-exponential factor Surface area |
| Å | Angstrom |
| B | Empirical constant for the Lennard-Jones 6-12 potential Langmuir adsorption constant |
| b | Tóth equation parameter |
| C | Dispersion constant |
| c | BET constant UNILAN equation parameter |
| D | Diffusivity |
| D/r^2 | Rate constant |
| E | Constant pair interaction energy |
| E_d | Activation energy for desorption |
| F | Field gradient Field strength |
| G | Gibbs free energy |
| g^m | Molar Gibbs free energy |
| <i>i</i> | Component |

| | |
|-----------------------------|---|
| K | Henry's law constant Kelvin (temperature unit) |
| k | Boltzmann constant Freundlich adsorption constant |
| K- β | Diffraction wavelength |
| K _L | Langmuir equation parameter |
| L | Liquefaction |
| M | Molar concentration |
| m | Mass Number of fitting parameters |
| meq | Milliequivalent |
| MIN-1 | Size parameter (smallest cross section of the gas molecule) |
| MIN-2 | Size parameter (next largest dimension of the gas molecule) |
| N | Number of experimental points |
| n | Adsorbate concentration (gravimetric basis) Freundlich exponent Number of moles |
| n _{calc} | Calculated adsorbate concentration |
| n _{exp} | Experimental adsorbate concentration |
| n _i ⁰ | Number of moles of <i>i</i> adsorbed from the pure-gas |
| n _m | Monolayer capacity (gravimetric basis) |
| n _T | Total number of moles of the adsorbed mixture |
| O7 | Oxygen-7 |
| P, p | Total pressure |
| P ₀ | Saturation pressure |
| pH | Potential of hydrogen |
| P _i | Partial pressure of <i>i</i> |
| P _i ⁰ | Equilibrium vapor pressure of pure component <i>i</i> |
| P _s | Saturation pressure |
| Q | Heat of adsorption for physically adsorbed species Quadrupole moment |
| R | Gas constant |
| r | Rate of condensation |

| | |
|--------------------|---|
| | Separation distance |
| r_{\min} | Minimum separation distance |
| S | Entropy |
| s | UNILAN equation parameter |
| S_{ext} | External surface |
| S_{int} | Internal surface |
| S_{total} | Equivalent specific surface |
| T | Temperature |
| t | Tóth equation parameter |
| $Ti1$ | Titanium-1 |
| $Ti2$ | Titanium-2 |
| $Ti=O$ | Titanyl |
| $Ti-OH$ | Titanol |
| U | Internal energy |
| V | Volume |
| v | Adsorbate concentration (volumetric basis) |
| | Collision frequency |
| v_m | Monolayer capacity (volumetric basis) |
| V_{mic} | Micropore volume |
| V^* | Molar volume |
| W | Gas volume |
| w_0 | Adsorbate loading at time zero |
| w_{eq} | Adsorbate loading at equilibrium |
| w_t | Adsorbate loading at time t |
| wt % | Weight percent |
| X_i, x_i | Composition of i in the adsorbed phase |
| Y_i, y_i | Composition of i in the gas phase |
| z | Number of occupied sites adjacent to an adsorbate |
| | Separation distance |

INTRODUCTION

1.1 Overview

Zeolite molecular sieves form an important class of inorganic materials that is widely employed in the chemical processing industry for applications ranging from adsorption to catalysis and ion-exchange.¹⁻³ Since zeolites were first discovered by Axel Cronstedt in 1756,⁴ 190 unique structures of zeolites have been identified and more than 40 natural zeolite frameworks have been characterized.⁵ These microporous materials, best represented by aluminum or titanium silicates, have reshaped the chemical processing industry and continue to offer many potential new applications, particularly in adsorptive gas separation technology.

Adsorption is a spontaneous thermodynamic process that occurs when a gas (or liquid) accumulates on the surface of a solid adsorbent, forming a film of atoms or molecules known as the adsorbate. In gas adsorption on porous solids such as zeolite molecular sieves, the gas phase is predominantly concentrated in the interior channels of the porous framework, although some surface adsorption may also occur. Adsorption occurs in many natural physical, chemical, and biological systems, and is widely employed in the chemical processing industry for the separation and purification of gases and liquids (Table 1-1).⁶ Typical solid adsorbents employed in the field of gas adsorption include zeolite molecular sieves, silica gels, activated carbons, activated alumina, and synthetic resins. Adsorptive separation of gas mixtures on porous solids is generally achieved by one of three fundamental mechanisms: steric, kinetic, or equilibrium-based separation.⁷

This work centers on developing new molecular sieve materials and applying them to adsorptive gas separation processes. Chapter two reviews the fundamentals of adsorption and adsorptive gas separation processes. In chapter three, a novel mechanism for pore size control using framework anions is introduced,^{8,9} and its applications in the separation of N₂/CH₄ and O₂/Ar are detailed in chapters four and five, respectively. While chapters three to five focus on steric separations of molecules, chapter six describes how C₂H₄/C₂H₆ can be separated by kinetic means. In chapter seven, a titanium silicate molecular sieve (ETS-10) is modified to alter its adsorptive properties in order to control

the equilibrium separation of ethylene and ethane.^{10,11} Chapter eight describes new molecular sieve materials that employ hybrid separation mechanisms designed to resolve target gas mixtures such as CO₂/C₂H₆ and CO₂/CH₄. Chapter nine shows that metallic nanoparticles (of silver) supported on molecular sieve templates can be used for molecular separation, such as Ar/O₂ and N₂/O₂.¹² Finally, chapter ten summarizes the key findings of this research program and recommends future work.

Table 1-1. Examples of Commercial Adsorptive Separation Processes

| Separation | Adsorbent |
|---|---|
| <i>Gas Purification</i> | |
| H ₂ O/olefin-containing cracked gas, natural gas, air, synthesis gas, etc. | Silica, alumina, zeolite (3A) |
| CO ₂ /C ₂ H ₄ , natural gas, etc. | Zeolite, carbon molecular sieve |
| Hydrocarbons, halogenated organics, solvents/vent streams | Activated carbon, silicalite, others |
| Sulfur compounds/natural gas, hydrogen, liquefied petroleum gas (LPG), etc. | Zeolite, activated alumina |
| SO ₂ /vent streams | Zeolite, activated carbon |
| Odors/air | Silicalite, others |
| Indoor air pollutants — VOCs | Activated carbon, silicalite, resins |
| Tank-vent emissions/air or nitrogen | Activated carbon, silicalite |
| Hg/chlor-alkali cell gas effluent | Zeolite |
| <i>Liquid Bulk Separations</i> | |
| Normal paraffins/isoparaffins, aromatics | Zeolite |
| <i>p</i> -xylene/ <i>o</i> -xylene, <i>m</i> -xylene | Zeolite |
| Detergent-range olefins/paraffins | Zeolite |
| <i>p</i> -Diethyl benzene/isomer mixture | Zeolite |
| Fructose/glucose | Zeolite |
| Chromatographic analytical separations | Wide range of inorganic, polymer, and affinity agents |
| <i>Liquid Purifications</i> | |
| H ₂ /organics, oxygenated organics, halogenated organics, etc., dehydration | Silica, alumina, zeolite, corn grits |
| Organics, halogenated organics, oxygenated organics, etc./H ₂ O — water purification | Activated carbon, silicalite, resins |
| Inorganics (As, Cd, Cr, Cu, Se, Pb, F, Cl, radionuclides, etc.)/H ₂ O — water purification | Activated carbon |
| Odor and taste bodies/H ₂ O | Activated carbon |
| Sulfur compounds/organics | Zeolite, alumina, others |
| Decolorizing petroleum fractions, syrups, vegetable oils, etc. | Activated carbon |
| Various fermentation products/fermentor effluent | Activated carbon, affinity agents |
| Drug detoxification in the body | Activated carbon |

1.2 Introduction

Zeolite molecular sieves are crystalline microporous metal oxides that derive their name, in part, from their ability to separate molecular species by size.¹³ Precise separations are possible because the three-dimensional network of uniformly-sized pores and channels within a molecular sieve can discriminate between molecules based on size. This distinctive property has resulted in the utilization of molecular sieves in many commercial adsorptive gas separation processes, especially hydrocarbon purification.¹⁴⁻¹⁸

Classical aluminosilicate molecular sieves have pore openings which range from 2.5 to 10 Å. The pore aperture of each sieve is determined by the 6-, 8-, 10-, or 12-membered rings inherent to its specific zeolitic structure.¹⁹ The pore size of these materials can be modified to some extent by cation substitution within the porous framework, but the control is incremental and restricted to certain structure types.¹⁹ This approach to pore size control only allows step-size changes in the pore aperture and, therefore, does not yield molecular sieves with a continuum of effective pore sizes. Since some important separations (such as CO/N₂ and O₂/Ar) require currently unachievable intermediate pore sizes, a new approach to channel aperture control would expand the possible applications of molecular sieves.

An evolution in pore size control for crystalline molecular sieves began when a unique property of Engelhard Titanosilicate-4 (ETS-4),^{20,21} the first synthetic zorite^{22,23} analog, was reported.²⁴ In most cation forms, the crystal lattice of ETS-4 systematically contracts upon structural dehydration at elevated temperatures and, through this mechanism, the lattice dimensions and, consequently, the channel apertures of ETS-4 can be controlled to “tune” the effective size of the pores. This phenomenon, known as the Molecular Gate[®] effect, has achieved commercial success in natural gas purification.^{14,15} Contracted Sr-ETS-4 (CTS) adsorbents, for example, have been applied to difficult size-based separations including N₂/CH₄ (3.64 Å vs. 3.76 Å, respectively²⁵) on an industrial scale. However, the contraction process inevitably damages the ETS-4 framework and introduces crystal lattice defects, eliminating some pore volume and reducing the

capacity of the adsorbent.^{26,27} Therefore, only certain cation-exchanged forms of ETS-4-based adsorbents are stable under thermal activation, limiting the practical usage of the Molecular Gate[®] technology.

Chapter three reports a novel mechanism to systematically control the pore size of zorite-based titanium silicate molecular sieves through halogen substitution of terminal hydroxyl groups.^{8,9} The quantity and type of halogen used determines the adsorptive properties of the molecular sieve. These halogen containing zorites represent a new class of size-selective adsorbents with readily tailored and highly specific pore sizes. This new approach to pore size control has promise in multiple areas of size-based separation, particularly light hydrocarbon purification and permanent gas separation.

To demonstrate the effectiveness of these new anion-controlled zorite analogs in light hydrocarbon purification, a small-pored, halogen containing titanium silicate molecular sieve adsorbent, Ba-RPZ-1, is synthesized and tested for use in the separation of N₂/CH₄ mixtures at room temperature. The results are detailed in chapter four.

Natural gas represents one of the most valuable energy resources in the world. In 2008, the production of natural gas in Alberta alone approached five trillion cubic feet.²⁸ Raw natural gas is a mixture composed primarily of methane that is contaminated with carbon dioxide, hydrogen sulfide, water, and nitrogen.²⁹ While constituents such as carbon dioxide and water are relatively simple to remove by selective adsorption, the separation of nitrogen from natural gas is more challenging because most adsorbents are selective toward methane instead of nitrogen.^{30,31} Size-selective separation is an alternative but it is tremendously difficult as nitrogen and methane differ in size by less than 0.15 Å.^{19,25}

At high concentrations, nitrogen lowers the heating value of natural gas due to reduced overall hydrocarbon content. While many natural gas deposits are contaminated with high levels of nitrogen (>20 wt %), the nitrogen content in natural gas must be reduced to less than 4 wt % in order to meet pipeline specifications for non-combustibles.²⁹ Many current natural gas nitrogen rejection processes employ cryogenic distillation in order to

achieve the required specifications. However, the combined costs of liquefaction and subsequent re-compression of the low pressure product make this an expensive process, economically unfeasible for use in the growing number of small, highly contaminated natural gas fields.³⁰ Therefore, an alternative technology such as pressure swing adsorption (PSA) utilizing molecular sieve adsorbents, which can operate at near ambient temperatures and maintain a high pressure product stream, is needed to provide a more economical process for the purification of natural gas.³²

Ba-RPZ-1 is a barium-stabilized, halogen containing reduced pore zorite (RPZ) whose pore size is controlled by the level of structural chloride anions.^{8,9} Chloride anions progressively and systematically constrict the RPZ-1 pore size as their concentration in the framework increases, enabling the preparation of thermally-stable, size-selective materials.^{8,9} In chapter four, Ba-RPZ-1 is used to demonstrate the most precise separation of N₂/CH₄ reported to date. With further development, Ba-RPZ-1 has the potential to replace the Molecular Gate[®] materials used for the adsorptive purification of natural gas.

Another potential application of anion-controlled Ba-RPZ-1 is in permanent gas separation, especially the size-selective separation of oxygen and argon. The separation of oxygen and argon is one of the most important processes in the industrial purification of the constituents of air, but is also one of the most difficult. The basic methods used for this separation include selective adsorption and cryogenic distillation. At cryogenic temperatures, the adsorptive selectivity of oxygen over argon on classical zeolites appears to be large enough for a viable separation.³³ However, under these conditions, an industrial process would be unrealistic because the energy requirements would be too high.³⁴ Unfortunately, at room temperature, little or no selectivity for oxygen over argon is found for common adsorbents, including zeolites. Isothermic heats of adsorption for oxygen and argon on typical adsorbents are nearly identical, the only exception being silver-exchanged molecular sieves, which have been reported to show a mild argon selectivity of 1.2-1.5.³⁵ Attempts have been made to exploit the mild thermodynamic selectivity of oxygen over argon by chromatographic separation of oxygen and argon

using columns containing 5A zeolite,³⁶ 13X zeolite,³⁷ or Ca-chabazite (one of the most polarizing adsorbents known),³⁸ but all of these processes require extremely dry adsorbents and are commercially impractical due to very low product yield.

Early attempts made to separate O₂/Ar mixtures by selective adsorption at ambient temperature used long chromatographic columns of zeolites and polymers.^{39,40} More recently, bulk industrial processes involving carbon molecular sieves (CMS) have been proposed, both for the purification of oxygen from O₂/Ar mixtures and to obtain an argon-enriched stream.^{41,42} The thermodynamic selectivity of oxygen over argon on CMS is too small to allow equilibrium-based pressure swing adsorption cycles, but the rate of oxygen uptake on CMS is much faster than the rate of argon uptake (25-30 times), opening the possibility of PSA processes based on kinetic selectivity.⁴¹⁻⁴³ However, the resolution of oxygen and argon over CMS is far from perfect and the maximum argon purity reported for a process utilizing CMS is on the order of 80-90%.^{41,42} Therefore, an inorganic molecular sieve with cleaner resolution of O₂/Ar and better predictability than current CMS materials could enable more efficient processes for the separation and purification of oxygen and argon. In chapter five, mixtures of oxygen and argon are cleanly resolved at room temperature using Ba-RPZ-1 as the adsorbent in a laboratory-scale demonstration unit.

The separation mechanism of the anion-controlled zorite analogs that are discussed in chapters three to five is primarily based on the steric effect. In chapter six, kinetic separations are performed following surface modifications of these anion-controlled materials. For instance, by manipulating the extra-framework cations in the structures of RPZ-1 and related materials, kinetic separation of ethylene and ethane is achieved.

The separation of ethylene and ethane is of key importance to the petrochemical sector. Annual global demand for ethylene, used to manufacture products such as plastic, rubber, and films, exceeds 100 million tonnes, making ethylene the largest product (by tonnage) of the petrochemical industry.⁴⁴ In Alberta, the petrochemical sector is one of the largest industries in the province, estimated at \$14 billion net sales per annum.⁴⁵ Clearly, the

economic impact of ethylene production plays a significant role in Alberta's energy-driven economy, and this success is supported by the abundant, competitively-priced supply of hydrocarbon feedstocks unique to Alberta's petroleum-rich environment.

In Alberta, ethylene production is primarily based on ethane. Through steam cracking and thermal decomposition, ethane is converted into ethylene. However, this process results in a complex mixture of ethylene (principal component) and other hydrocarbons, including un-cracked ethane. Economically, it is desirable to recycle the un-cracked ethane via a C_2H_4/C_2H_6 separation process. Currently, this separation involves repeated compression and refrigeration, which is energy-intensive and contributes roughly 75% to the overall cost of olefin production. Therefore, if the separation of ethylene from ethane could be achieved through an adsorptive approach, the cost of ethylene production could be significantly reduced.

Chapter six describes the kinetic separation of ethylene and ethane using surface-modified, small-pored titanium silicate molecular sieve adsorbents. While this method is promising, an alternative equilibrium-based process, which separates ethylene and ethane through electrostatic interactions and thermodynamic affinities, is detailed in chapter seven.¹⁰

In chapter seven, the adsorptive properties (selectivity and swing capacity) of modified Engelhard Titanosilicate-10 (ETS-10) are controlled by manipulating the type and quantity of its extra-framework cations. ETS-10 is a large-pored, mixed octahedral/tetrahedral titanium silicate molecular sieve possessing a three-dimensional network of interconnecting channels.⁴⁶⁻⁴⁸ The channels of ETS-10 are uniquely configured to display a surface charge that is both shielded and homogenous. ETS-10, with an average pore size of $\sim 8 \text{ \AA}$,⁴⁷ has been used extensively in ion-exchange, gas separation, and catalytic studies.⁴⁹⁻⁵¹

The adsorptive properties of most zeolite molecular sieves can be changed substantially by substituting different extra-framework cations. In ETS-10, different cationic species

can occupy different lattice sites within the crystal framework,⁵² altering the local electrostatic field that governs molecular adsorptive interactions. This phenomenon makes it possible to tailor ETS-10 adsorbents to have precise adsorptive characteristics under a wide range of conditions. In chapter seven, the thermodynamic selectivities and swing capacities of ETS-10 materials are manipulated through cation-exchange in order to improve the separation of ethylene and ethane.¹⁰

Development of new molecular sieve materials can provide versatility and alternative approaches to industrial gas separation processes. The results in chapters six and seven show that the separation of ethylene and ethane can be performed by very different means, and that the effectiveness of each approach is system-dependent.

In chapter eight, all of these molecular sieve modification techniques are synergistically integrated to illustrate that multi-functional adsorbents can be designed and prepared for many target separations. This approach is demonstrated through the separations of CO₂/C₂H₆ and CO₂/CH₄, since the separation of carbon dioxide from light hydrocarbons is an important stage in the industrial production of ethane or methane from natural gas.⁵³ For some applications, such as the synthesis of ethylene by decomposition of ethane, the carbon dioxide content in the ethane stream must be reduced to trace levels. This can be accomplished by chemical absorption with amines, but the purification process is feasible only when the carbon dioxide content in the inlet stream is already moderately low (<3-5%).⁵⁴ The total or partial extraction of carbon dioxide from ethane or methane by pressure swing adsorption could reduce the chemical and energy costs of the purification process, while eliminating the need for environmental-unfriendly amine scrubbers.^{54,55}

In chapter eight, adsorbents employing hybrid separation mechanisms are investigated. For example, the anion-controlled framework of Ba-RPZ-1 is used to exclude ethane and methane by the steric effect, while cation-exchange and surface modifications are used to tune the equilibrium and kinetic properties of the adsorbent.

All of the new molecular sieve materials discussed in chapters three through eight are designed to separate gas mixtures by one of the three fundamental separation mechanisms. Chapter nine, however, is an introduction to gas adsorption and separation by interaction with nanometals.¹²

In chapter nine, nanometals, such as nanosilver, formed on the surfaces of molecular sieves are used as unique adsorbents to separate gas mixtures. Nanosilver, when formed on titanium silicate ETS-10, yields one of the most selective materials reported to date for the separation of Xe/N₂⁵⁶ and Ar/O₂.¹² While the interaction between nanosilver and inert gas species can be complex, the nature of this phenomenon may be related to the directional properties given by the d orbitals of the silver ions.⁵⁷ Ag⁺ in silver zeolites react, upon heating, to generate clusters with a wide range of compositions including metal nanoensembles and groupings which may be composed of a combination of silver ions and silver atom clusters. The clusters can occupy different sites in the zeolitic structure.⁵⁸ This variability in the composition and location of the clusters results in materials that may acquire unexpected adsorptive behaviors. Adsorptive gas separation through interaction with nanometals has a broad range of potential applications that will become an important focus for the development of new molecular sieve nanomaterials.

The dissertation concludes with chapter ten, which highlights the key discoveries of this work. The objective of this research program is to develop new molecular sieve materials and to examine their applications in adsorptive gas separation processes. New molecular sieve materials for adsorptive gas separation processes are generated by a variety of techniques, including pore size control by anion substitution, surface modification by cation-exchange, and the development of specialized, surface-supported metal nanoparticles. Continual development and characterization of new microporous materials are crucial to the chemical processing industry, and should be viewed as an avenue for the discovery of next-generation adsorptive gas separation technologies.

1.3 References

- (1) Keller II, G. E.; Anderson, R. A.; Yon, C. M. In *Handbook of Separation Process Technology*; Rousseau, R. W., Eds.; Adsorption; Wiley: Hoboken, 1987; pp 644-696.
- (2) Weitkamp, J. *Solid State Ionics* **2000**, *131*, 175.
- (3) Helfferich, F. G. *Ion Exchange*; Dover: New York, 1995.
- (4) Cronstedt, A. *Akad. Handl.* **1756**, *18*, 120.
- (5) Database of Zeolite Structures. <http://www.iza-structure.org/databases/> (accessed April 1, 2009).
- (6) Humphrey, J. L.; Keller II, G. E. *Separation Process Technology*; McGraw-Hill: New York, 1997.
- (7) Yang, R. T. *Gas Separation by Adsorption Processes*; Butterworths Publishers: Stoneham, 1987.
- (8) Lin, C. C. H.; Sawada, J. A.; Wu, L.; Haastrup, T.; Kuznicki, S. M. *J. Am. Chem. Soc.* **2009**, *131*, 609.
- (9) Kuznicki, S. M.; Sawada, J. A.; Rode, E. J.; Lin, C. C. H. Titanium Silicate Materials, Method for their Manufacture, and Method for Using Such Titanium Silicate Materials for Adsorptive Fluid Separations. World Patent No. WO/2008/002463, March 1, 2008.
- (10) Anson, A.; Wang, Y.; Lin, C. C. H.; Kuznicki, T. M.; Kuznicki, S. M. *Chem. Eng. Sci.* **2008**, *63*, 4171.
- (11) Kuznicki, S. M.; Anson, A.; Segin, T.; Lin, C. C. H. Modified ETS-10 Zeolites for Olefin Separation. Canadian Patent Application 2,618,267, Filed January 21, 2008.
- (12) Anson, A.; Kuznicki, S. M.; Kuznicki, T.; Haastrup, T.; Wang, Y.; Lin, C. C. H.; Sawada, J. A.; Eyring, E. M.; Hunter, D. *Microporous Mesoporous Mater.* **2008**, *109*, 577.
- (13) Cundy, C. S.; Cox, P. A. *Chem. Rev.* **2003**, *103*, 663.
- (14) Butwell, K. F.; Dolan, W. B.; Kuznicki, S. M. Selective Removal of Nitrogen from Natural Gas by Pressure Swing Adsorption. U.S. Patent 6,197,092, March 6, 2001.

- (15) Kuznicki, S. M.; Bell, V. A.; Petrovic, I.; Desai, B. T. Small-Pored Crystalline Titanium Molecular Sieve Zeolites and their Use in Gas Separation Processes. U.S. Patent 6,068,682, May 30, 2000.
- (16) Kuznicki, S. M.; Bell, V. A. Olefin Separations Employing CTS Molecular Sieves. U.S. Patent 6,517,611, February 11, 2003.
- (17) Roeseler, C. M.; Kulprathipanja, S.; Rekoske, J. E. Adsorptive Separation Process for Recovery of Para-xylene. U.S. Patent 6,706,938, March 16, 2004.
- (18) Choi, S.; Lee, S.-J.; Kang, S.-C.; Kim, S.-W.; Ku, M.-S.; Choi, A.-S.; Chang, B.-M. Process for Separating Normal Paraffins from Hydrocarbons and Applications for the Separated Hydrocarbons. U.S. Patent 6,870,073, March 22, 2005.
- (19) Breck, D. W. *Zeolite Molecular Sieves: Structure, Chemistry and Use*; Wiley: New York, 1974.
- (20) Yilmaz, B.; Miraglia, P. Q.; Warzywoda, J.; Sacco Jr. A. *Microporous Mesoporous Mater.* **2004**, *71*, 167.
- (21) Kuznicki, S. M. Preparation of Small-Pored Crystalline Titanium Molecular Sieve Zeolites. U.S. Patent 4,938,939, July 3, 1990.
- (22) Sandomirskii, P. A.; Belov, N. V. *Sov. Phys. Crystallogr.* **1979**, *24*, 686.
- (23) Mer'kov, A. N.; Bussen, I. V.; Goiko, E. A.; Kul'chitskaya, E. A.; Men'shikov, Y. P.; Nedorezova, A. P. *Zap. Vses. Mineral. Obshchest.* **1973**, *102*, 54.
- (24) Kuznicki, S. M.; Bell, V. A.; Nair, S.; Hillhouse, H. W.; Jacubinas, R. M.; Braunbarth, C. M.; Toby, B. H.; Tsapatsis, M. *Nature* **2001**, *412*, 720.
- (25) Sircar, S.; Myers, A. L. In *Handbook of Zeolite Science and Technology*; Auerbach, S. M.; Carrado, K. A.; Dutta, P. K., Eds.; Gas Separation by Zeolites; Marcel Dekker Inc.: New York, 2003; pp 1063-1104.
- (26) Marathe, R. P.; Farooq, S.; Srinivasan, M. P. *Langmuir* **2005**, *21*, 4532.
- (27) Marathe, R. P.; Mantri, K.; Srinivasan, M. P.; Farooq, S. *Ind. Eng. Chem. Res.* **2004**, *43*, 5281.
- (28) About Natural Gas. <http://www.energy.gov.ab.ca/NaturalGas/940.asp> (accessed April 1, 2009).
- (29) Dolan, W. B.; Butwell, K. F. Selective Removal of Nitrogen from Natural Gas by Pressure Swing Adsorption. U.S. Patent 6,444,012, September 3, 2002.

- (30) Maple, M. J.; Williams, C. D. *Microporous Mesoporous Mater.* **2008**, *111*, 627.
- (31) Li, P.; Tezel, F. H. *J. Chem. Eng. Data* **2009**, *54*, 8.
- (32) Jasra, R. V.; Choudary, N. V.; Bhat, S. G. T. *Sep. Sci. Technol.* **1991**, *26*, 885.
- (33) Barrer, R. M.; Robins, A. B. *Trans. Faraday Soc.* **1953**, *49*, 807.
- (34) Kovak, K. W.; Agrawal, R.; Peterson, J.C. Method of Purifying Argon through Cryogenic Adsorption. U.S. Patent 5,159,816, November 3, 1992.
- (35) Sebastian, J.; Jasra, R. V. *Ind. Eng. Chem. Res.* **2005**, *44*, 8014.
- (36) Walker, J. A. J. *Nature* **1966**, *209*, 197.
- (37) Karlsson, B.-M. *Anal. Chem.* **1966**, *38*, 668.
- (38) Maroulis, P. J.; Coe, C. G. *Anal. Chem.* **1989**, *61*, 1112.
- (39) Pollock, G. E.; O'Hara, D.; Hollis, O. L. *J. Chromatogr. Sci.* **1984**, *22*, 343.
- (40) Pollock, G. E. *J. Chromatogr. Sci.* **1986**, *24*, 173.
- (41) Rege, S. U.; Yang, R. T. *Adsorption* **2000**, *6*, 15.
- (42) Jin, X.; Malek, A.; Farooq, S. *Ind. Eng. Chem. Res.* **2006**, *45*, 5775.
- (43) Ma, Y. H.; Sun, W.; Bhandakar, M.; Wang, J.; Miller, G. W. *Sep. Technol.* **1991**, *1*, 90.
- (44) Storck, W. J. *Chem. Eng. News* **2006**, *84*, 59.
- (45) Alberta Industries. <http://www.albertacanada.com/industries/861.html> (accessed April 1, 2009).
- (46) Al-Baghli, N. A.; Loughlin, K. F. *J. Chem. Eng. Data* **2006**, *51*, 248.
- (47) Kuznicki, S. M. Large-Pored Crystalline Titanium Molecular Sieve Zeolites. U.S. Patent 5,011,591, April 30, 1991.
- (48) Anderson, M. W.; Terasaki, O.; Ohsuna, T.; Philippou, A.; Mackay, S. P.; Ferreira, A.; Rocha, J.; Lidin, S. *Nature* **1994**, *367*, 347.
- (49) Pavel, C. C.; Vuono, D.; Nastro, A.; Nagy, J. B.; Bilba, N. *Stud. Surf. Sci. Catal.* **2002**, *142 A*, 295.
- (50) Kuznicki, S. M.; Thrush, K. A.; Allen, F. M.; Levine, S. M.; Hamil, M. M.; Hayhurst, D. T.; Mansour, M. In *Synthesis of Microporous Materials: Molecular Sieves, Vol. 1*; Occelli, M. L.; Robson, H. E., Eds.; Synthesis and Adsorptive Properties of Titanium Silicate Molecular Sieves; Van Nostrand Reinhold: New York, 1992; pp 427-456.

- (51) Gervasini, A.; Picciau, C.; Auroux, A. *Microporous Mesoporous Mater.* **2000**, *35-36*, 457.
- (52) Anderson, M. W.; Agger, J. R.; Luigi, D.-P.; Baggaley, A. K.; Rocha, J. *PCCP* **1999**, *1*, 2287.
- (53) Cavenati, S.; Grande, C. A.; Rodrigues, A. E. *Energy Fuels* **2006**, *20*, 2648.
- (54) Rao, A. B.; Rubin, E. S.; *Environ. Sci. Technol.* **2002**, *36*, 4467.
- (55) Collie, J.; Hlavinka, M.; Ashworth, A. In Proceedings of the 48th Annual Laurence Reid Gas Conditioning Conference, Norman, OK, March 1-4, 1998; pp 175-193.
- (56) Kuznicki, S. M.; Anson, A.; Kuznicki, T. M.; Haastrup, T.; Eyring, E. M.; Hunter, D. *J. Phys. Chem. C* **2007**, *111*, 1560.
- (57) Habgood, H. W. *Can. J. Chem.* **1964**, *42*, 2340.
- (58) Sun, T.; Seff, K. *Chem. Rev.* **1994**, *94*, 857.

**FUNDAMENTALS OF ADSORPTION AND ADSORPTIVE
GAS SEPARATION PROCESSES**

2.1 The Concept of Adsorption

Adsorption is a spontaneous thermodynamic process that occurs when a gas (or liquid) accumulates on the surface of a solid adsorbent, forming a film of atoms or molecules known as the adsorbate. In gas adsorption on porous solids such as zeolite molecular sieves, the gas phase is predominately concentrated in the interior channels of the porous framework, although some surface adsorption may also occur. Adsorption occurs in many natural physical, chemical, and biological systems. Gas adsorption is widely employed in the chemical processing industry for the separation and purification of gases (Table 2-1).¹ Typical solid adsorbents employed in the field of gas adsorption include zeolite molecular sieves, silica gels, activated carbons, activated alumina, and synthetic resins.

Adsorption, which differs from absorption (associated with the diffusion of a substance into the parent material), is a consequence of surface energy.² In the bulk phase of a material, all of the bonding requirements of the constituent atoms are filled by surrounding atoms in the material. However, atoms located at the surface of the adsorbent are not completely surrounded by other atoms and, therefore, can attract adsorbates from the gas phase. A gas molecule near a solid surface experiences a reduction in potential energy as a consequence of interaction with other atoms (or molecules) from the solid. The result is that gas molecules tend to concentrate in this region so that the molecular density in the vicinity of the surface is substantially greater than in the gas phase. The strength of the surface forces depends on the nature of the adsorbate and the adsorbent. If the forces are relatively weak, involving only Van der Waals interactions supplemented with polar or quadrupolar species by electrostatic forces (dipole or quadrupole interactions), the type of interaction is called physical adsorption.² If the interaction forces are strong, involving a significant degree of electron transfer, it is known as chemical adsorption, which is limited to a monolayer whereas in physical adsorption, multiple molecular layers can be formed.²

Table 2-1. Examples of Industrial Adsorptive Gas Separation Processes

| Separation ^a | Adsorbent |
|--|---------------------------|
| <i>gas bulk separations</i> | |
| normal paraffins, isoparaffins, aromatics | zeolite |
| N ₂ /O ₂ | zeolite |
| O ₂ /N ₂ | carbon molecular sieve |
| CO, CH ₄ , CO ₂ , N ₂ , Ar, NH ₃ /H ₂ | zeolite, activated carbon |
| acetone/vent streams | activated carbon |
| C ₂ H ₄ /vent streams | activated carbon |
| H ₂ O/ethanol | zeolite |
| <i>gas purifications</i> | |
| H ₂ O/olefin-containing cracked gas, natural gas, air, synthesis gas, etc. | silica, alumina, zeolite |
| CO ₂ /C ₂ H ₄ , natural gas, etc. | zeolite |
| organics/vent streams | activated carbon, others |
| sulfur compounds/natural gas, hydrogen, liquefied petroleum gas (LPG), etc. | zeolite |
| solvents/air | activated carbon |
| odors/air | activated carbon |
| NO _x /N ₂ | zeolite |
| SO ₂ /vent streams | zeolite |
| Hg/chlor-alkali cell gas effluent | zeolite |

2.2 Fundamental Forces of Adsorption

The forces of adsorption within a zeolitic framework arise from electrostatic interactions. The total potential energy of the adsorption process can be divided into parts representing contributions from the different types of interactions between the adsorbate and the adsorbent.

It has been suggested that the total energy of interaction, $\phi(z)$, is the sum of contributions from the dispersion energy (ϕ_D), close-range repulsion (ϕ_R), polarization (ϕ_P), field-dipole interaction (ϕ_F), and field gradient-quadrupole interaction (ϕ_{FQ}).² Together, these interactions make up the fundamental forces of adsorption. The interaction energy, which determines the adsorption strength between the adsorbate and the adsorbent, is system-dependent.

The dispersion force, first characterized by London,³ is a force that arises from rapid fluctuations of electron density in an atom, which induces an electrical moment in its neighboring atom, hence creating an attraction between them. In adsorption, these forces always exist between the adsorbate and the adsorbent. The potential energy, φ , between two atoms separated by a distance, r , can be approximated by:⁴

$$\varphi(r) = -Cr^{-6} \quad (2-1)$$

Where C is one of the dispersion constants associated with the dipole-dipole interactions. The negative sign implies attraction.

A theoretical expression was derived for the close-range repulsive potential, an exponential function of r , $\exp(-kr)$, which can be approximated by:

$$\varphi(r) = Br^{-12} \quad (2-2)$$

Therefore, the total potential energy is the sum:

$$\varphi(r) = -Cr^{-6} + Br^{-12} \quad (2-3)$$

This is the familiar Lennard-Jones 6-12 potential as depicted in Figure 2-1.⁵ The parameter B is an empirical constant, and C can be theoretically calculated. Some well-known relationships, including those by London,³ Kirkwood and Müller,^{4,6} and Slater and Kirkwood,⁷ have been derived for calculating the value of C .

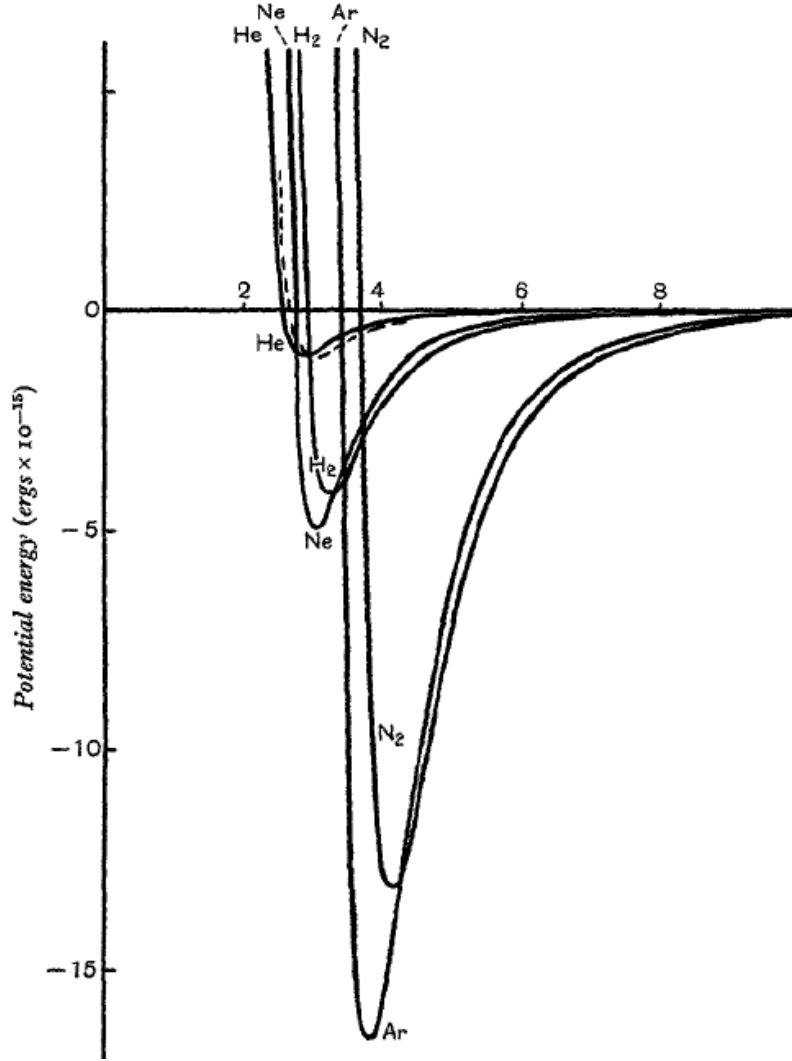


Figure 2-1. The potential energy of selected gas pairs as a function of their distance apart in Å.

For a gas molecule on a solid surface separated by a distance z (measured between the center of the molecule and the plane going through the centers of the surface atoms), the potential function, $\phi(z)$, can be calculated by summing over all interacting pairs of atoms:

$$\phi(z) = \phi_D + \phi_R = -\sum_i \left(C_{ij} \sum_j r_{ij}^{-6} \right) + \sum_i \left(B_{ij} \sum_j r_{ij}^{-12} \right) \quad (2-4)$$

For a polar surface that induces a dipole in the adsorbate molecule, the interaction energy is:⁴

$$\phi_P = -\frac{1}{2}\alpha^2 F \quad (2-5)$$

Where F is the field strength at the center of the adsorbate and α is the polarizability. If the adsorbate molecule has a permanent dipole, μ , an additional energy, due to the field-dipole interaction, is required:

$$\phi_F = -F\mu \cos\theta \quad (2-6)$$

Where θ is the angle between the field and the axis of the dipole. For adsorbate molecules possessing a quadrupolar moment (Q), another contribution, ϕ_{FQ} , results from the interaction with the field gradient F.

It is clear that, for a given adsorbate molecule, the bond strength is a function of the polarity, and that for the same surface the bond strength is higher for gas molecules with permanent dipoles and quadrupoles.

By summing up all components, the total potential between the adsorbate molecules and the adsorbent surface is:

$$\phi(z) = \phi_D + \phi_R + \phi_P + \phi_F + \phi_{FQ} \quad (2-7)$$

2.3 Single-Component Gas Adsorption

For a given gas-solid pair, the amount adsorbed at equilibrium is described by:

$$v = f(P, T) \quad (2-8)$$

Where v may be expressed in STP cc/g or STP cc/cc. At a fixed temperature T , v is only a function of the pressure P . This relationship forms the basis of an equilibrium adsorption isotherm.

2.3.1 Isotherm Models

The majority of the isotherms observed to date can be classified into five types, according to the IUPAC classification system (Figure 2-2).⁸

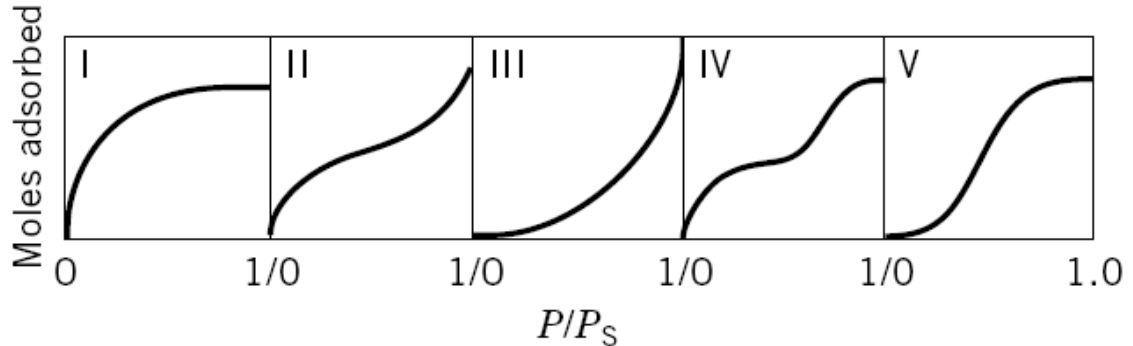


Figure 2-2. The IUPAC classification for adsorption isotherms.

Type I isotherm is characterized by the Langmuir isotherm for monolayer coverage, typical of adsorption in microporous solids. Type II isotherm illustrates the BET mechanism for multi-layer adsorption at sub-critical temperatures. Type III isotherm can be exemplified by water adsorption on charcoal where the adsorption is not favorable at low pressures because of the hydrophobic nature of the charcoal surface. At sufficiently high pressures, the adsorption is due to capillary condensation in the mesopores of charcoal. Types IV and V are the same as Types II and III with the exception that they

have finite limits as P approaches the saturation pressure (P_0) due to the finite pore volume of the porous solids. Some examples of the five types of isotherms include:

Type I: Adsorption of oxygen on charcoal at 90 K

Type II: Adsorption of nitrogen on zeolite X at 77 K

Type III: Adsorption of bromine on silica gel at 352 K

Type IV: Adsorption of benzene on ferric oxide gel at 323 K

Type V: Adsorption of water on charcoal at 373 K

Numerous adsorption theories and models have been developed to interpret these different types of isotherms.⁹ Isotherm equations can be used to predict and extrapolate the adsorption behavior of selected systems using only a limited number of experiments. In gas separation, Type I and Type II isotherms are the most frequently encountered. Most of the isotherm models developed to date are based on the following approaches:¹⁰

1. The Langmuir Approach: This well-known approach, developed by Irving Langmuir in 1918,¹¹ was originally a kinetic one, assuming that the adsorption system is in dynamic equilibrium, where the rate of evaporation is equal to the rate of condensation. The Langmuir isotherm remains to be the most useful correlation for describing gas adsorption on porous solids.
2. The Gibbs approach: This approach employs the Gibbs adsorption isotherm:¹²

$$-Ad\pi + nd\mu = 0 \quad (2-9)$$

It assumes a two-dimensional equation of state for the adsorbed film, relating π -A-T, where π is the spreading pressure, A is the surface area, n is the number of moles, and μ is the chemical potential. An integration of the Gibbs equation results in the desired isotherm. There are as many isotherms as the number of assumed equations of state, ranging from the ideal gas law to the virial equation.¹³

3. The potential theory: First formalized by Polanyi in 1914,¹⁴ the adsorption system is viewed as a gradual concentration of gas molecules toward the solid surface due to a potential field. There is a relationship between the potential field, ε , and the volume above the surface, W , for a given gas-solid system. This relationship, empirically obtained for the system, is called the “characteristic curve,” which is assumed to be temperature-independent. The adsorption potential is related to the work of isothermally compressing a gas from the gas pressure (P) to the saturation pressure (P_0) for liquefaction. An isotherm is obtained when the volume (W) is converted to the amount adsorbed by assuming that the adsorbed phase is a liquid.

2.3.2 Langmuir Isotherm

The Langmuir isotherm is the simplest yet one of the most useful isotherms for both physical and chemical adsorption on porous solids. Although Langmuir originally considered seven cases,¹¹ including multi-layer adsorption, adsorption on heterogeneous surfaces, and adsorption with dissociation, the Langmuir isotherm in its usual form is based on the following implicit assumptions:¹¹

1. The adsorbed atom or molecule is held at definite, localized sites.
2. Each site can only accommodate one atom or molecule.
3. The energy of adsorption is constant across all sites, and there is no lateral interaction, for example, via Van der Waals interaction, between neighboring adsorbate atoms or molecules.

The Langmuir isotherm is derived based on the concept of dynamic equilibrium between the rates of condensation (adsorption) and evaporation (desorption). Since the sites already occupied are no longer available for adsorption, the rate of adsorption per unit surface area is equal to $\alpha v(1-\theta)$,¹⁰ where v is the collision frequency of gas molecules striking the surface, α is the sticking probability or accommodation coefficient for adsorption, and θ is the fractional coverage. According to the kinetic theory of gases:¹⁵

$$v = \frac{P}{(2\pi mkT)^{1/2}} \quad (2-10)$$

The rate of desorption per unit surface area for physically adsorbed species is:

$$\beta\theta e^{-E_d/RT} = \beta\theta e^{-Q/RT} \quad (2-11)$$

Where β is the rate constant for desorption, and E_d is the activation energy for desorption which equals the heat of adsorption for physically adsorbed species, Q .

At dynamic equilibrium,

$$\theta = \frac{v}{v_m} = \frac{BP}{1 + BP} \quad (2-12)$$

And,

$$B = \frac{\alpha}{\beta(2\pi mkT)^{1/2}} e^{Q/RT} \quad (2-13)$$

This is the Langmuir isotherm and B is the Langmuir adsorption constant. θ is the fractional monolayer coverage. The Langmuir isotherm is useful for practical purposes because it fits the Type I isotherm and the initial region of the Type II isotherm.

The isotherm reduces to a linear form ($\theta = BP$), or Henry's law form, for small P . For this reason, B is also known as the Henry's law constant. For large P , θ approaches unity where condensation begins.

The temperature dependence of B is $e^{Q/RT} T^{-1/2}$,¹⁰ thus its value decreases rapidly with increasing temperature because Q is always positive, i.e. physical adsorption is always

exothermic. The latter is true because the free energy (G) must decrease for the adsorption process to occur, i.e. ΔG is negative. Since the entropy change, ΔS , for the adsorption process is also negative due to an ordering of molecules on the adsorbent surface, ΔH must be negative according to the Gibbs free energy equation, $\Delta G = \Delta H - T\Delta S$.¹⁶

2.3.3 Langmuir Isotherm with Lateral Interactions

The Langmuir isotherm assumes that the energy of adsorption is constant across all sites, and that there are no lateral interactions between adjacent adsorbate molecules. By using more realistic assumptions, many modifications have been made to the Langmuir isotherm. A simple modification can be made by considering lateral interactions between neighboring adsorbate atoms and molecules.¹⁷ Such an interaction is largely due to the attractive Van der Waals forces and therefore increases physical adsorption. By assuming that the lateral interaction energy is constant, the following Langmuir constant can be obtained:¹⁸

$$B = \frac{\alpha}{\beta(2\pi mkT)^{1/2}} e^{(Q+zE)/RT} \quad (2-14)$$

Where z = the number of occupied sites adjacent to an adsorbate

E = the constant pair interaction energy

2.3.4 Freundlich Isotherm

In Langmuir's original paper,¹¹ adsorption on non-uniform surfaces was considered and the amount adsorbed was summed over all types of sites, each having its corresponding value of B , bond energy, and heat of adsorption. Zeldowitsch, by assuming an exponentially decaying function of site density with respect to Q , derived the classical empirical isotherm known as the Freundlich isotherm.¹⁹

$$v = kP^{1/n} \quad (2-15)$$

2.3.5 BET Isotherm

In situations where the temperature is below the critical temperature of the adsorbate gas, the Type II isotherm predominates over Type I. In this case, there is a multi-layer of adsorbate buildup well before a complete monolayer is formed. To account for this, a two-parameter isotherm was developed by Brunauer, Emmett, and Teller,²⁰ which was essentially an extension of the Langmuir model for multi-layer adsorption.

In the BET model, each site can accommodate 0 to i (i approaches infinity) adsorbate molecules that are non-mobile on the surface. On the first layer, the rate of condensation on the bare sites is equal to the rate of evaporation from the sites that are covered by only one adsorbate molecule. Following this approach, i equations are generated when equilibrium is established for all layers.

The important assumption is then made that the heat of adsorption beyond the first layer is constant and equals the heat of liquefaction. In addition, the ratio of the adsorption and desorption constants, α/β , is also assumed constant for layers beyond the first one. By summing over all layers, the BET equation is obtained:

$$\frac{P}{v(P_0 - P)} = \frac{1}{v_m c} + \frac{c-1}{v_m c} \left(\frac{P}{P_0} \right) \quad (2-16)$$

Where the value of c is given by:

$$c = \frac{\alpha_1 \beta_2}{\alpha_2 \beta_1} \exp\left(\frac{Q_1 - Q_L}{RT}\right) \cong \exp\left(\frac{Q_1 - Q_L}{RT}\right) \quad (2-17)$$

In equation 2-17, the numerical subscripts indicate the number of layers from the surface, and L denotes liquefaction. The values of c and v_m are determined experimentally.

The constant c is usually large and is always greater than unity. The BET equation continues to be the major tool for measuring the surface area of porous solids. Using experimental data in the range of $P/P_0 = 0.05$ to 0.3 , the left-hand side of equation 2-16 can be plotted against the relative pressure, and the values of v_m and c are determined from the slope and intercept of the plot. Knowing the molecular area of the adsorbate (e.g. $16.2 \text{ \AA}^2/\text{molecule}$ of nitrogen at 77K), the value of the surface area can be calculated directly from v_m .

The BET equation is rarely used for correlating adsorption data. The reason for this is that the equation is not applicable to adsorption under supercritical conditions (i.e. at temperatures above the critical temperature). Under these conditions, the BET model reverts to the Langmuir isotherm.

2.4 Multi-Component Gas Adsorption

The isotherm models described thus far all pertain to single-component gas adsorption. Realistically, models or correlations for multi-component gas adsorption are crucial to the design of adsorptive gas separation processes. Ideally, these models should be capable of predicting the equilibrium parameters from the pure-gas isotherms of each constituent in the mixture, within a range of operating pressures and temperatures.

The measurement of multi-component gas adsorption is not necessarily difficult, but it is certainly tedious. Fortunately, significant progress in the theoretical aspects of multi-component gas adsorption has been made, allowing accurate predictions of multi-component systems to be much more attainable.

2.4.1 Multi-Component Langmuir Isotherm

The Langmuir isotherm for single-component gas adsorption can be extended for a mixture containing n-components.²¹ The same assumption of an ideal, localized monolayer is made. The system is defined as containing partial pressures P_1 and P_2 in the gas phase, which is in equilibrium with coverages θ_1 and θ_2 on the surface. The rate of condensation for gas 1, r_1 , is given by:

$$r_1 = \alpha_1 v_1 (1 - \theta_1 - \theta_2) = \alpha_1' P_1 (1 - \theta_1 - \theta_2) \quad (2-18)$$

Where α is the sticking probability and v is given by equation 2-10. The rate of evaporation for gas 1 is $\beta_1' \theta_1$, which is given by equation 2-11.

At equilibrium,

$$\alpha_1' P_1 (1 - \theta_1 - \theta_2) = \beta_1' \theta_1 \quad (2-19)$$

By rearranging, we can obtain an expression in terms of θ_1 :

$$\theta_1 = \frac{B_1 P_1 (1 - \theta_2)}{1 + B_1 P_1} \quad (2-20)$$

With the corresponding equation for θ_2 , we can obtain:

$$\theta_1 = \frac{B_1 P_1}{1 + B_1 P_1 + B_2 P_2} \quad (2-21)$$

Therefore, for an n-component mixture:

$$\theta_i = \frac{B_i P_i}{1 + \sum_{j=1}^n B_j P_j} \quad (2-22)$$

This is known as the multi-component Langmuir isotherm, and the total surface coverage is the sum of all fractional coverages for each i^{th} species:

$$\theta_T = \sum_{i=1}^n \theta_i \quad (2-23)$$

2.4.2 Ideal Adsorbed Solution Theory

The ideal adsorbed solution theory (IAST) is the most successful approach to the prediction of multi-component equilibria from single-component isotherm data.²² In essence, the theory is based on the assumption that the adsorbed phase is thermodynamically ideal, and that the equilibrium pressure for each component is the product of its mole fraction in the adsorbed phase and the equilibrium pressure for the pure component at the same spreading pressure.

The derivation of IAST begins by applying the fundamental thermodynamic equations for liquids to the adsorbed phase. The total internal energy, U , and the total Gibbs free energy, G , of the adsorbed phase are given by:

$$dU = TdS - \pi dA + \sum \mu_i dn_i \quad (2-24)$$

$$dG = -SdT + Ad\pi + \sum \mu_i dn_i \quad (2-25)$$

Where π and A , respectively, replace P and V , and the adsorbed mixture is treated as a two-dimensional phase that is not necessarily a monolayer. The quantity A is the surface area and π is the spreading pressure, which plays a central role in applying solution

equilibria to mixture adsorption. The physical meaning of spreading pressure is analogous to a monomolecular film at the gas-liquid interface:

$$\pi = \sigma^0 - \sigma \quad (2-26)$$

Where σ^0 and σ are the surface or interfacial tensions of the clean and monolayer-covered surfaces, respectively. In other words, π defines the lowering of the surface tension at the gas-solid interface upon adsorption.

Using equation 2-24, the spreading pressure π can be defined by:

$$\pi = -\left(\frac{\partial U}{\partial A}\right)_{S,ni} \quad (2-27)$$

Alternatively, it can also be calculated from measurable quantities. From equation 2-9, the Gibbs adsorption isotherm is:

$$Ad\pi = \sum n_i d\mu_i \quad (2-28)$$

Equation 2-28 is analogous to the Gibbs-Duhem equation. For pure-gas adsorption and assuming ideal gas behavior:

$$Ad\pi = nRTd \ln P \quad (2-29)$$

After rearranging, the spreading pressure can be calculated by:

$$\frac{\pi A}{RT} = \int_0^P \frac{n}{P} dP \quad (2-30)$$

In equation 2-25, the intensive variables are π , T, and composition. Myers and Prausnitz proposed that the activity coefficients for the mixed adsorbates should be defined in the same way as for solutions. Following their approach, the molar Gibbs free energy for mixing the adsorbates at constant T and π is:

$$g^m(T, \pi, X_i) = RT \sum X_i \ln(\gamma_i X_i) \quad (2-31)$$

Where γ_i is the activity coefficient of the i^{th} species in the mixed adsorbates. Utilizing the activity coefficient defined in equation 2-31 along with the equilibrium criterion, which states that the chemical potential for each component in the adsorbed phase is equal to that in the gas phase, it can be shown that:

$$PY_i = P_i^0(\pi)X_i\gamma_i \quad (2-32)$$

Where P_i^0 is the equilibrium vapor pressure for pure component i adsorbed at the same π and T as the adsorbed mixture. In the ideal situation (γ_i is unity), equation 2-32 reduces to Raoult's law.¹³

Using the same proposition based on equation 2-31, the molar area of the mixed adsorbates is:

$$\frac{1}{n_T} = \sum \frac{X_i}{n_i^0} + \frac{RT}{A} \sum X_i \left(\frac{\partial \ln \gamma_i}{\partial \pi} \right)_{X_i} \quad (2-33)$$

Here, n_T is the total number of moles of the adsorbed mixture, whereas n_i^0 is the number of moles of i adsorbed from the pure-gas at the same π and T as the adsorbed mixture.

Furthermore, the number of moles of each component adsorbed is defined as:

$$n_i = n_T X_i \quad (2-34)$$

Equations 2-32, 2-33, and 2-34 are needed for predicting mixture adsorption from single-component isotherms, whereas equation 2-30 is used to evaluate P_i^0 . Together, these equations form the basis of the adsorbed solution theory (AST). In the case where the gas phase is non-ideal, simply replace the pressure with fugacity.

For the special case of ideal solution, the activity coefficients are unity. Therefore, equation 2-32 becomes:

$$PY_i = P_i^0 (\pi) X_i \quad (2-35)$$

And equation 2-33 simplifies to:

$$\frac{1}{n_T} = \sum \frac{X_i}{n_i^0} \quad (2-36)$$

Equations 2-30, 2-34, 2-35, and 2-36 form the ideal adsorbed solution theory, by which multi-component adsorption can be predicted from single-component isotherms.

2.5 Henry's Law

The adsorbed layer at the surface of a solid may be regarded as a distinct phase from a thermodynamic sense. Equilibrium with the surrounding gas (or liquid) is governed by the laws of thermodynamics. Physical adsorption from the gas phase (onto a solid adsorbent) is an exothermic process, therefore equilibrium favors adsorption at low temperatures and desorption at high temperatures. At sufficiently low pressures, the equilibrium relationship generally approaches a linear form, known as the Henry's law:¹³

$$v = KP \quad (2-37)$$

Where the proportionality constant (K) is the Henry's law constant. The Henry's law constant is simply the adsorption equilibrium constant, and it decreases with increasing temperature. The temperature dependence of the Henry's law constant can be described in terms of the Van't Hoff relationship:¹³

$$K = A \exp\left(-\frac{\Delta H}{RT}\right) \quad (2-38)$$

Where A is the pre-exponential factor, ΔH is the heat of adsorption, R is the gas constant, and T is the absolute temperature.

2.6 Selectivity

The selectivity, or separation factor, is a concept in gas adsorption and separation that describes the adsorbent's preference toward competing adsorbates. The selectivity is a function of pressure and temperature. The selectivity of gas A over gas B in the Henry's law region, or the limiting selectivity (α), is defined as the ratio of the Henry's law constants of gas A and gas B:

$$\alpha(A/B) = \frac{K_A}{K_B} \quad (2-39)$$

2.7 Heat of Adsorption

Physical adsorption processes are exothermic in nature. This is because the entropy change (ΔS) and the free energy change (ΔG) are both negative during the adsorption process. Accordingly, thermodynamics require the enthalpy change (ΔH), or the heat of

adsorption, to be negative (exothermic). This implies that adsorption strength decreases with increasing temperature.

The isosteric heat of adsorption, δH_{iso} , may be determined from the slope of the adsorption isostere (line of constant adsorbate loading) on the graph of $\ln P$ vs. $1/T$ using the Clausius-Clapeyron equation:¹³

$$\frac{d \ln P}{d(1/T)} = -\frac{\delta H_{\text{iso}}}{R} \quad (2-40)$$

Here, R is the gas constant, P is the adsorbate absolute pressure, and T is the absolute temperature.

Other associated quantities include the integral heat of adsorption, which is the total heat released when the adsorbate loading is increased from zero to some final value at isothermal conditions.¹⁶ The differential heat of adsorption is the incremental change in the heat of adsorption with a differential change in the adsorbate loading.¹⁶

In most zeolites, at low adsorbate loadings, the differential heats of adsorption decrease with increasing adsorbate loading. This is direct evidence that the adsorbent surface is energetically heterogeneous, i.e. some adsorption sites interact more strongly with the adsorbate molecules. These sites, consequently, are filled first so that adsorption of additional molecules involves progressively lower heats of adsorption.

2.8 Fundamental Mechanisms of Gas Separation

Adsorptive separation of gas mixtures on porous solids is typically achieved by one of the three fundamental separation mechanisms or a combination thereof.²³

1. Equilibrium Separation
2. Kinetic Separation
3. Steric Separation

2.8.1 Equilibrium Separation

Equilibrium separation is the most common mechanism of adsorptive gas separation. It is driven by the laws of electrostatics and thermodynamics, based on the differences in the interaction energies between the competitive adsorbates and the adsorbent.

The main concepts associated with equilibrium separation are equilibrium selectivity and capacity. While the equilibrium selectivity is simply the separation factor at equilibrium conditions, the capacity of the adsorbent (at equilibrium) depends on two complementary factors: surface area and porosity.

An example of equilibrium separation is oxygen generation from air using Li-LSX zeolite.²⁴ Li-LSX has a much higher affinity for nitrogen than oxygen at equilibrium conditions. Therefore, when air is passed through the adsorbent bed, a pure stream of oxygen could be collected at the outlet.

2.8.2 Kinetic Separation

Kinetic separation is based on the concept that one adsorbate species adsorbs faster than the competition. Although a kinetic selectivity may not exist at equilibrium, the difference in the rate of adsorption, rather than equilibrium affinities, can be utilized to design a separation system. The rate of physical adsorption is generally controlled by

diffusion limitations rather than the actual rate of equilibration on a surface. Therefore, many equilibrium gas separation processes are not truly equilibrium-based, but contain a kinetic component (associated with mass transfer), making them “quasi-equilibrium” in nature.

Carbon molecular sieves (CMS) represent a class of adsorbents that can separate molecular species by the kinetic phenomenon. Kinetic separation is possible with CMS because it has a distribution of pore sizes. Such a distribution of pores allows different gases to diffuse at different rates while totally avoiding exclusion of any gases in the mixture.

An example of kinetic separation using carbon molecular sieves is the production of nitrogen from air.²⁴ The diffusion of oxygen is approximately 30 times faster than nitrogen diffusion in CMS and, although the capacity of CMS is only a fraction of most zeolites, it is more economical to use CMS for the production of nitrogen from air.

2.8.3 Steric Separation

The steric effect is derived from the molecular sieving property of zeolites. Steric separation is based on the concept that only small and properly-oriented molecules can diffuse into the pores of the adsorbent, whereas other molecules, either due to size or geometry, are completely excluded. This is a characteristic feature of zeolitic adsorbents since these materials are crystalline and the dimensions of the micropores are determined by the crystal structure. Control of pore size can be achieved by cation-exchange, silanation, structural contraction,²⁵ and the recently discovered, framework anion substitution.²⁶

One of the largest applications of steric separation is the separation of normal paraffins from iso-paraffins and cyclic hydrocarbons using 5A zeolites.²⁴ More recently, nitrogen rejection from natural gas has also been performed through the steric separation mechanism, using a synthetic titanium silicate known as ETS-4.²⁷

2.9 Adsorptive Gas Separation Processes

Adsorptive gas separation processes are widely employed in the chemical industry for the large-scale separation and purification of gas mixtures.²⁸ These processes are generally classified by their method of regeneration. Pressure swing adsorption (PSA) and temperature swing adsorption (TSA) are the most frequently applied processes for gas separation. However, other processes utilizing purge swing cycles and reactive sorption are also possible. Most adsorptive processes employ fixed beds, but some use moving or fluidized beds, or rotary wheels.

2.9.1 Adsorbent Design

The role of the adsorbent in adsorptive gas separation processes is to provide a specialized surface required for the selective adsorption of certain gas molecules.²⁴ A high selectivity is the primary requirement, but a high capacity is also desirable since it determines the size of the adsorbent bed and the regeneration frequency. Since the overall performance of an adsorptive gas separation process depends on both equilibrium and kinetic factors, adsorbent design must consider not only equilibrium properties (such as selectivity and capacity), but also kinetic characteristics (such as diffusion rates).

2.9.2 Pressure Swing Adsorption

A pressure swing adsorption cycle (Figure 2-3)² is one in which desorption takes place at a pressure much lower than adsorption (since thermodynamics favor adsorption at high pressures). Its principal application is for bulk separations where contaminants are present at high concentrations. Systems with weakly-adsorbed species are especially suited for PSA cycles. The applications of PSA separation include air separation and upgrading of fuel gases.²

In a PSA cycle, two processes occur during regeneration: depressurizing and purging. Depressurization must provide adequate reduction in the partial pressure of the adsorbate

to allow desorption. Then, enough purge gas must flow through the adsorbent bed to sweep the desorbed materials away. Equilibrium determines the maximum capacity of the adsorbed gas and dictates when regeneration is required. These cycles operate under near-isothermal conditions and require no heating or cooling steps, thus they are very efficient and cost-effective.

Pressure swing adsorption can be further classified into three categories: classical PSA, VSA (vacuum swing adsorption), and VPSA (vacuum-pressure swing adsorption). The main difference between these three processes is the operating pressure range. A classical PSA cycle swings between a high super-atmospheric (above 1 atm) and a lower super-atmospheric pressure. A VSA cycle swings from a super-atmospheric pressure to a sub-atmospheric (below 1 atm) pressure. VPSA cycles swing rapidly just above and below atmospheric pressure thus it is the most efficient of the three PSA variants. The type of process utilized is system-dependent, i.e. it depends on the characteristics of the adsorbates and the adsorbent.

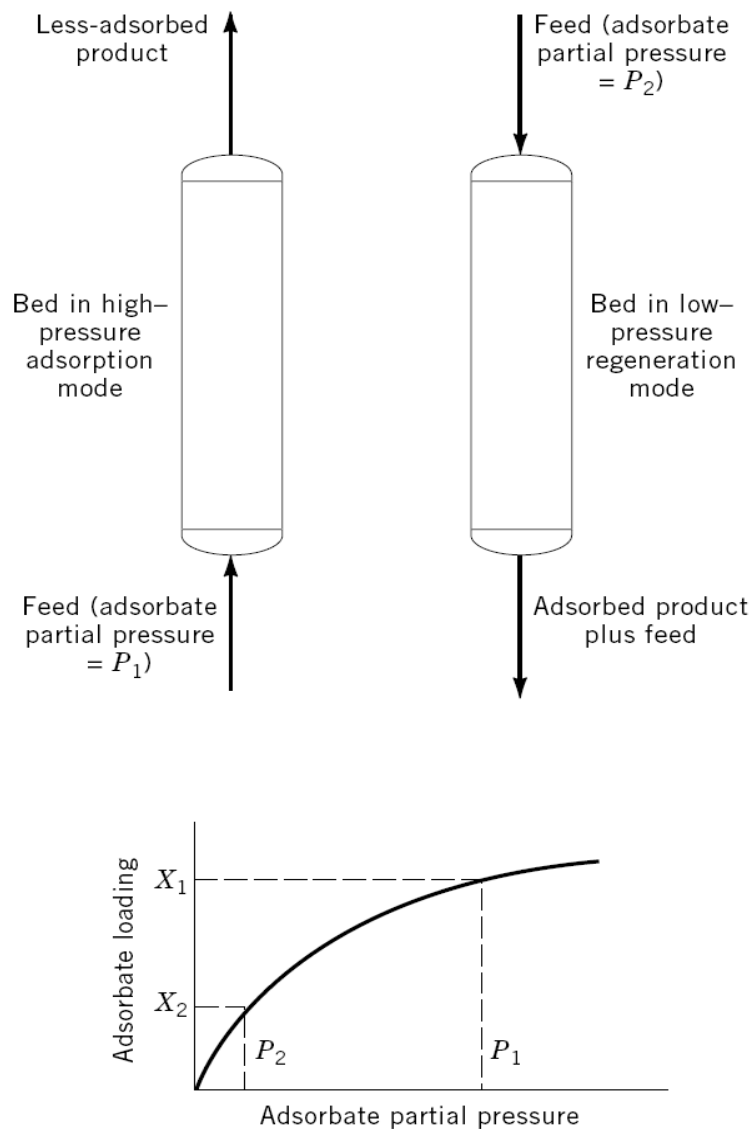


Figure 2-3. Schematic of a pressure swing adsorption cycle.

2.9.3 Temperature Swing Adsorption

A temperature swing adsorption cycle (Figure 2-4)² is one in which desorption takes place at a temperature much higher than adsorption (since thermodynamics favor adsorption at low temperatures). Its principal application is for trace separations where contaminants are present at low concentrations. Systems with strongly-adsorbed species are especially suited for TSA cycles. The applications of TSA separation include desiccation, sweetening, carbon dioxide removal, and pollution control.²

In a TSA cycle, three processes occur during regeneration: heating, purging, and cooling. Heating must provide adequate thermal energy to allow desorption. Then, a purge gas must flow through the adsorbent bed to sweep the desorbed components away. Equilibrium determines the maximum capacity of the adsorbed gas and dictates when regeneration is required. The last stage of regeneration is cooling the bed, as the adsorbent must return to its original temperature (and condition) designed for adsorption.

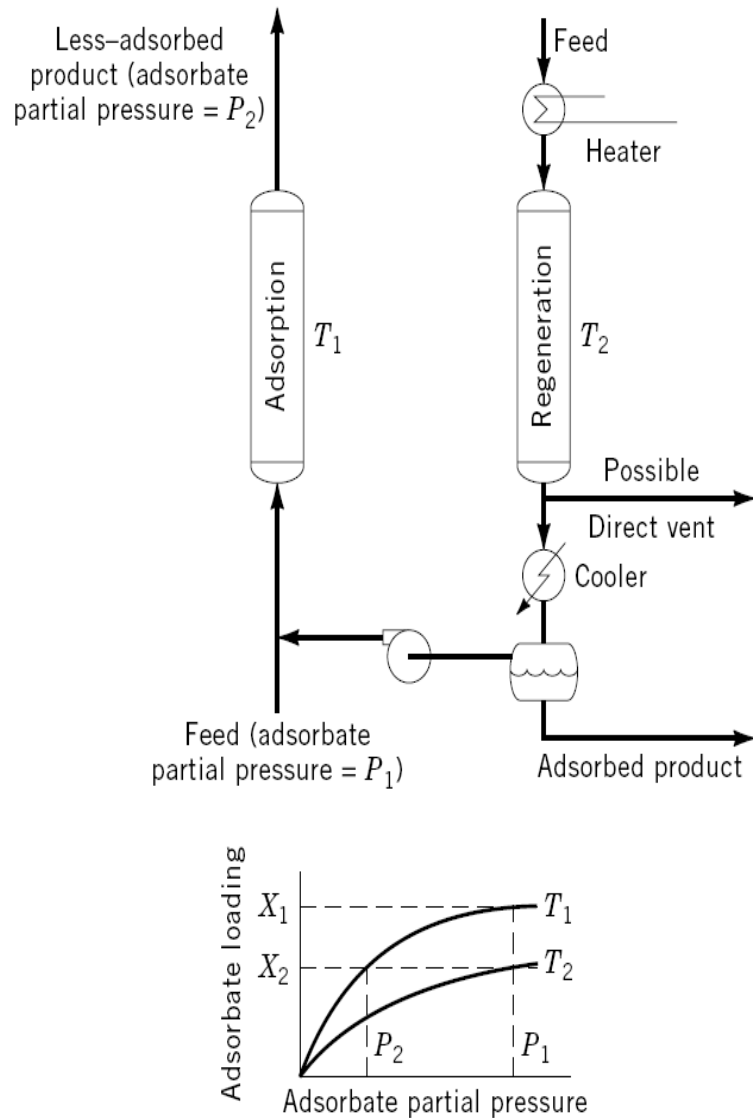


Figure 2-4. Schematic of a temperature swing adsorption cycle.

2.10 Conclusions

The overall performance of an adsorptive gas separation process depends on both materials development (with specific adsorptive properties) and process optimization. Continual research and development of new microporous materials is crucial to the chemical processing industry, and should be viewed as an avenue for the discovery of next-generation adsorptive gas separation technologies.

2.11 References

- (1) Keller II, G. E. In *Industrial Gas Separations*, ACS Symposium Ser. No. 223: Whyte Jr., T. E.; Yon, C. M., Wagener, E. H., Eds.; American Chemical Society: Washington, D.C., 1983; pp 145.
- (2) Adsorption, Gas Separation. *Kirk-Othmer Encyclopedia of Chemical Technology* [Online]; Wiley & Sons, Posted April 18, 2003. (accessed March 25, 2009).
- (3) London, F. Z. *Physik* **1930**, 63, 245.
- (4) Kirkwood, J. G. *Phys. Zeits.* **1932**, 33, 57.
- (5) Lennard-Jones, J. E. *Proc. Phys. Soc.* **1931**, 43, 461.
- (6) Müller, A. *Proc. Roy. Soc.* **1936**, 154A, 624.
- (7) Slater, J. C.; Kirkwood, J. G. *Phys. Rev.* **1931**, 37, 682.
- (8) Adsorption, Fundamentals. *Kirk-Othmer Encyclopedia of Chemical Technology* [Online]; Wiley & Sons, Posted April 16, 2001. (accessed March 25, 2009).
- (9) Gregg, S. J.; Sing, K. S. W. *Adsorption, Surface Area and Porosity*; Academic Press: London and New York, 1982.
- (10) Yang, R. T. *Gas Separation by Adsorption Processes*; Butterworths Publishers: Stoneham, 1987.
- (11) Langmuir, I. *J. Am. Chem. Soc.* **1918**, 40, 1361.
- (12) Chatteraj, D. K.; Birdi, K. S. *Adsorption and the Gibbs Surface Excess*; Plenum Publishing Company: New York, 1984.
- (13) Gaskell, D. R. *Introduction to the Thermodynamics of Materials Fourth Edition*; Taylor and Francis Books Inc.: London, 2003.
- (14) Polanyi, M. *Verh. Deut. Phys. Ges.* **1914**, 16, 1012.
- (15) Present, R. D. *Kinetic Theory of Gases*; McGraw-Hill: California, 1958.
- (16) Breck, D. W. *Zeolite Molecular Sieves: Structure, Chemistry and Use*; Wiley: New York, 1974.
- (17) Fowler, R. H.; Guggenheim, E. A. *Statistical Thermodynamics*; Cambridge University Press: Cambridge, 1952.
- (18) Ross, S.; Winkler, W. J. *Colloid Sci.* **1955**, 10, 319.

- (19) Freundlich, H. *The Elements of Colloidal Chemistry*, translated by George Barger; Dutton and Company Publishers: New York, 1924.
- (20) Brunauer, S.; Emmett, P. H.; Teller, E. *J. Am. Chem. Soc.* **1938**, *60*, 309.
- (21) Markham, E. C.; Benton, A. F. *J. Am. Chem. Soc.* **1931**, *53*, 497.
- (22) Myers, A. L.; Prausnitz, J. M. *AIChE J.* **1965**, *11*, 121.
- (23) Sircar, S.; Myers, A. L. In *Handbook of Zeolite Science and Technology*; Auerbach, S. M.; Carrado, K. A.; Dutta, P. K., Eds.; Gas Separation by Zeolites; Marcel Dekker Inc.: New York, 2003; pp 1063-1104.
- (24) Yang, R. T. *Adsorbents: Fundamentals and Applications*; Wiley: Hoboken, 2003.
- (25) Kuznicki, S. M.; Bell, V. A.; Nair, S.; Hillhouse, H. W.; Jacubinas, R. M.; Braunbarth, C. M.; Toby, B. H.; Tsapatsis, M. *Nature* **2001**, *412*, 720.
- (26) Lin, C. C. H.; Sawada, J. A.; Wu, L.; Haastrup, T.; Kuznicki, S. M. *J. Am. Chem. Soc.* **2009**, *131*, 609.
- (27) Kuznicki, S. M.; Bell, V. A.; Petrovic, I.; Desai, B. T. Small-Pored Crystalline Titanium Molecular Sieve Zeolites and their Use in Gas Separation Processes. U.S. Patent 6,068,682, May 30, 2000.
- (28) Keller II, G. E.; Anderson, R. A.; Yon, C. M. In *Handbook of Separation Process Technology*; Rousseau, R. W., Eds.; Adsorption; Wiley: Hoboken, 1987; pp 644-696.

ANION-CONTROLLED PORE SIZE OF TITANIUM SILICATE MOLECULAR SIEVES[†]

[†] A version of this chapter has been published. Reproduced with permission from Lin, C. C. H.; Sawada, J. A.; Wu, L.; Hastrup, T.; Kuznicki, S. M. *J. Am. Chem. Soc.* **2009**, *131*, 609. Copyright 2009 American Chemical Society.

3.1 Summary

Titanium silicate molecular sieves contain structural units that are fundamentally different from classical aluminosilicates. In addition to ordered octahedral titanium chains, members of the zorite family contain pentagonal titanium units which project into the main adsorption channels of the framework. We report that the effective pore size of these materials can be controlled by substituting halogens at the O7 sites that cap the pentagonal pyramids projecting into the channels. The quantity and type of halogen used determines the adsorptive properties of the molecular sieve. Barium-exchange stabilizes these materials over a wide temperature range (nominally 473-673 K). The barium-exchanged materials do not contract appreciably with calcination, as is observed in related Molecular Gate[®] materials, and thus halogen content can control the pore size of the materials. This new approach to pore size control may have important implications for the purification of multiple classes of compounds, including light hydrocarbons and permanent gases.

3.2 Introduction

Zeolite molecular sieves form an important class of inorganic materials that is widely employed in the chemical processing industry for applications ranging from adsorption to catalysis and ion-exchange.¹⁻³ Molecular sieves are crystalline microporous metal oxides that derive their name, in part, from their ability to separate molecular species by size.⁴ Precise separations are possible because the three-dimensional network of uniformly-sized pores and channels within a molecular sieve can discriminate between molecules based on size. This distinctive property has resulted in the utilization of molecular sieves in many commercial adsorptive gas separation processes, especially hydrocarbon purification.⁵⁻⁹

Classical aluminosilicate molecular sieves have pore openings which range from 2.5 to 10 Å. The pore aperture of each sieve is determined by the 6-, 8-, 10-, or 12-membered rings inherent to its specific zeolitic structure.¹⁰ The pore size of these materials can be modified to some extent by cation substitution within the porous framework, but the control is incremental and restricted to certain structure types.¹⁰ For example, potassium ion-exchange with zeolite Na-A (pore size of ~3.8 Å) reduces its effective pore size to ~3.3 Å, because potassium, being a larger monovalent cation than sodium, blocks the pore openings more effectively. This reduction does not occur gradually with increasing ion-exchange, but changes suddenly at a threshold of approximately 25% potassium-exchange.¹⁰ Similarly, the effective pore size of Na-A increases abruptly to ~4.3 Å after ~30% calcium-exchange. This approach to pore size control allows step-size changes in the pore aperture, but does not yield molecular sieves with a continuum of effective pore sizes. Since some important separations (such as CO/N₂ and O₂/Ar) require currently unachievable intermediate pore sizes, a new approach to channel aperture control would expand the possible applications of molecular sieves.

An evolution in pore size control for crystalline molecular sieves began when a unique property of Engelhard Titanosilicate-4 (ETS-4),^{11,12} the first synthetic zorite^{13,14} analog, was reported.¹⁵ In most cation forms, the crystal lattice of ETS-4 systematically contracts

upon structural dehydration at elevated temperatures and, through this mechanism, the lattice dimensions and, consequently, the channel apertures of ETS-4 can be controlled to “tune” the effective size of the pores. This phenomenon, known as the Molecular Gate[®] effect, has achieved commercial success in natural gas purification.^{5,6} Contracted Sr-ETS-4 (CTS) adsorbents, for example, have been applied to difficult size-based separations including N₂/CH₄ (3.64 Å vs. 3.76 Å, respectively¹⁶) on an industrial scale. However, the contraction process inevitably damages the ETS-4 framework and introduces crystal lattice defects, eliminating some pore volume and reducing the capacity of the adsorbent.^{17,18} Therefore, only certain cation-exchanged forms of ETS-4-based adsorbents are stable under thermal activation, limiting the practical usage of the Molecular Gate[®] technology.

3.3 Experimental Methods

Synthesis of Halogen Free Zorite (HFZ-1) and 3 members of a new class of titanium silicate materials, the Halogen Containing Zorites (ETS-4, RPZ-1, and RPZ-2), was performed hydrothermally in 125 mL Teflon-lined autoclaves (PARR Instruments) using the compositions, synthesis temperatures, and reaction times outlined below. All mixtures were stirred in a Waring blender for 1 h prior to charging the autoclaves. The typical procedure for HFZ-1 synthesis (molar ratio of SiO₂:TiO₂:Na₂O:K₂O:H₂O:F:Cl:I = 6.82:1:4.46:0.76:205.25:0:0:0) involved mixing 1.32 g of potassium hydroxide (85+% KOH, Fisher) with 3.00 g of sodium hydroxide (97+% NaOH, Fisher) in 15.00 g of de-ionized water (resistivity >18 MΩcm). This mixture was then added to 22.00 g of sodium silicate (28.80% SiO₂, 9.14% Na₂O, Fisher), followed by the addition of 32.22 g of titanium oxysulfate solution (4.27% Ti, Aldrich). Unlike monovalent anions, divalent anions (such as SO₄) cannot be linked to the chain-bridging titanium units, thus will not be incorporated into the HFZ-1 framework. The reaction mixture for HFZ-1 was autoclaved at 488 K for 48 h. ETS-4 (molar ratio of SiO₂:TiO₂:Na₂O:K₂O:H₂O:F:Cl:I = 5.75:1:4.45:1.55:40.97:3.10:4.27:0) was synthesized at 423 K for 168 h in a mixed F/Cl system as described in the patent literature.¹² RPZ-1 synthesis (molar ratio of

$\text{SiO}_2:\text{TiO}_2:\text{Na}_2\text{O}:\text{K}_2\text{O}:\text{H}_2\text{O}:\text{F}:\text{Cl}:\text{I} = 5.75:1:4.45:0.95:40.97:0:6.18:0$) involved mixing 25.10 g of sodium silicate, 4.60 g of sodium hydroxide, 3.00 g of potassium chloride (99% KCl, Fisher), and 16.30 g of titanium trichloride (20% TiCl_3 , 6% HCl, Fisher), and was autoclaved at 473 K for 40 h. RPZ-2 (molar ratio of $\text{SiO}_2:\text{TiO}_2:\text{Na}_2\text{O}:\text{K}_2\text{O}:\text{H}_2\text{O}:\text{F}:\text{Cl}:\text{I} = 5.75:1:4.45:1.55:61.92:0:4.27:3.10$) was synthesized by mixing 25.10 g of sodium silicate, 4.60 g of sodium hydroxide, 10.88 g of potassium iodide (99% KI, Fisher), and 16.30 g of titanium trichloride. The reaction mixture for RPZ-2 was autoclaved at 488 K for 16 h. All materials were thoroughly washed and filtered prior to cation-exchange. Ion-exchange for barium was carried out by refluxing at 373 K in aqueous barium chloride (0.82 M) for 2-24 h. The pelletization of the barium-exchanged materials involved mixing 6.00 g of the molecular sieves (equilibrated at 373 K) with 2.50 g of Ludox HS-40 colloidal silica (Aldrich). The mixture was homogenized using a mortar and pestle, then compressed in a pellet press to 10,000 psi. The resulting cakes were crushed and sieved to obtain 16-50 mesh particles that were utilized for inverse-phase gas chromatographic analysis.

HFZ-1, ETS-4, RPZ-1, and RPZ-2 were characterized by instrumental neutron activation analysis (INAA), wavelength dispersive X-ray spectroscopy (WDX), powder X-ray diffraction (XRD), inverse-phase gas chromatography (IGC), and equilibrium adsorption isotherm analysis. INAA was conducted using the SLOWPOKE Nuclear Reactor Facility located at the University of Alberta. WDX data were collected using a JEOL JZA-8900R WD/ED Combined Microanalyzer. Signals were obtained from secondary electrons at an accelerating voltage of 15 kV. Phase identification of the as-synthesized materials was conducted through XRD using a Rigaku Geigerflex 2173 with a vertical goniometer equipped with a graphite monochromator for filtration of $\text{K}\text{-}\beta$ wavelengths. IGC analysis was performed on a Varian 3800 gas chromatograph (GC) equipped with a thermal conductivity detector (TCD). Test adsorbents were packed into 10" long copper columns with an OD of 0.25" using a plastic funnel. The columns were filled with approximately 4 g of pelletized adsorbents (16-50 mesh), which were activated at 523 K and 0.5 psig for 10 h under a helium flow of $30 \text{ cm}^3/\text{min}$. Characterization gas (single-phase or mixture) was introduced by a 1 mL pulse injection into the column. Equilibrium

adsorption isotherms were measured volumetrically at 298 K up to 100 kPa using an AUTOSORB-1-MP from Quantachrome Instruments (Boynton Beach, FL) on crystalline powders (no binders or diluents were added to the samples). All samples were activated at 523 K for 10 h under vacuum (<0.0005 Torr).

Unit cell representations of anion-controlled zorite analogs, viewed along the $[0\ 1\ 0]$ direction (b-axis), were generated and modified using the CCDC software Mercury¹⁹ with crystallographic data obtained from the literature.²⁰ The model portrays the statistical occupancies of Si and Ti in the unit cell. Titanium and silicon atoms are depicted as black and gray, respectively. Other species include O (red), F (green), Cl (blue), and I (violet). Van der Waals radii were used to depict the size of all framework elements.²¹ Extra-framework cations and water molecules were omitted for clarity.

3.4 Results and Discussion

We have developed a novel mechanism to precisely control the effective pore size of synthetic titanium silicate zorite analogs. The new control mechanism does not rely on cation substitution or structural contraction; instead, the channel dimensions are manipulated by controlling the size and concentration of framework anions projecting into the channels. ETS-4 and zorite analogs contain chains of octahedrally coordinated titanium propagating in the $[0\ 1\ 0]$ direction that are connected by silicate tetrahedra in the $[0\ 0\ 1]$ crystal plane.^{22,23} Relative to these six-coordinated titanium atoms (Ti1) of occupancy factor 1, the unit cell also contains chain-bridging units consisting of five-coordinated titanium atoms (Ti2) having a fractional occupancy of ~ 0.25 .^{20,24,25} This model is statistically portrayed by the Rietveld-refined crystal structure of zorite analogs presented in Figure 3-1. Based on this proposed structure, an atom at the terminal position of the five-coordinated square-pyramid, designated as the O7 crystallographic site (Figure 3-1a), will project into the $[0\ 1\ 0]$ channel system (b-axis) and act as a physical barrier restricting the effective pore size of the molecular sieve. It has been proposed that the O7 sites are occupied by hydroxyl groups²³ or related species such as

structural water,²⁶ and we propose that these groups can be substituted through synthesis with monovalent anions, particularly halogens. Halogen substitution is not uncommon in nature, especially in rock-forming silicates such as topaz²⁷ and tremolite.²⁸ Our model suggests that large halogens such as Cl or I (Figures 3-1c and 3-1d, respectively), when positioned at the O7 sites, create a steric effect that reduces the effective pore size of titanium silicate zorite analogs.

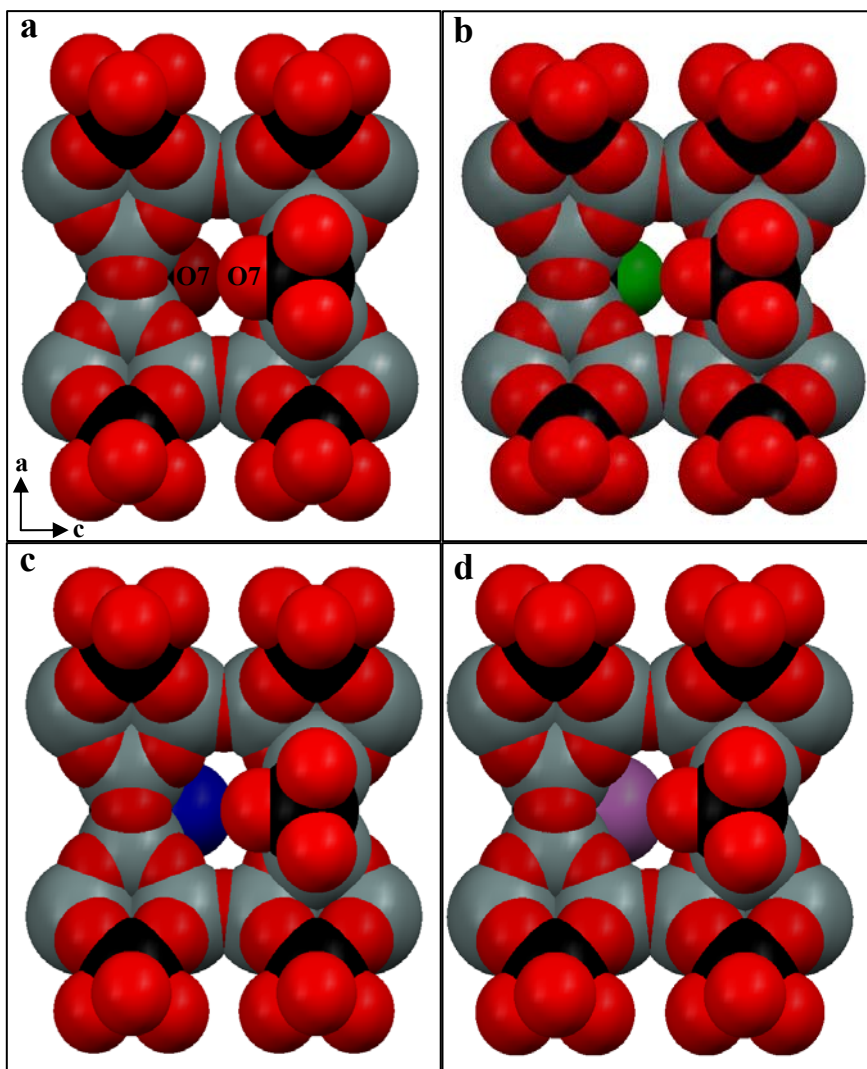


Figure 3-1. Unit cell representations of anion-controlled zorite analogs. (a) The zorite framework with OH occupying the O7 sites, viewed along the [0 1 0] direction (b-axis). Halogen free zorite has the largest effective pore size and channel accessibility of the series. Titanium, silicon, and oxygen atoms are depicted as black, gray, and red, respectively. (b) Fractional substitution of F (green) for O (red) at an O7 site. This substitution does not substantially change the effective pore size since F (1.35 Å) and O (1.40 Å) are nearly identical in size. (c) Halogen containing zorite with Cl (blue) substitution at an O7 site. Pore size reduction, through a steric effect, is evident when (c) is compared to (a) and (b). (d) Iodine (violet) substitution at an O7 site. This zorite analog has the smallest effective pore size of the series.

Certain cations, such as barium, stabilize the pore size of zorite analogs against contraction over a large temperature regime.²⁹ In our current approach, the pore size of the barium-stabilized materials is then controlled by manipulating the type and quantity of anions along the channel walls. This new approach may allow greater precision and flexibility than other methods of pore size control reported to date, and has potential applications in multiple areas of size-based separation, including light hydrocarbon purification and permanent gas separation.

The results of quantitative bulk elemental analyses of synthetic Halogen Free Zorite (HFZ-1) and 3 members of a new class of titanium silicate materials, the Halogen Containing Zorites (ETS-4¹² and the Reduced Pore Zorites³⁰ RPZ-1 and RPZ-2), by INAA and WDX, are shown in Table 3-1. The analyses confirm that the halogen content of the four materials reflects the molar composition of the synthesis mixtures from which the materials were prepared. These results indicate that halogens can be incorporated directly into the framework of titanium silicate zorite analogs through the synthesis process. Partial, rather than total, replacement with halogens at the O7 sites was observed in all cases (except HFZ-1). The highest level of halogen incorporation at the O7 sites was observed in ETS-4, with almost 30% replacement by halogen species, predominantly fluorine. In other mixed halogen systems, substitution was always dominated by the smaller of the halogen species. The data suggest that these titanium silicate frameworks prefer hydroxyl groups and appear to be selective toward halogens with smaller atomic radii, preferentially incorporating halogens in the sequence of F > Cl > I (Van der Waals radii: 1.35 Å, 1.80 Å, and 2.15 Å, respectively²¹).

Table 3-1. Quantitative Bulk Elemental Analyses of Anion-Controlled Zorite Analogs

| INAA (Mass Percent) Composition Data | | | | | | |
|--------------------------------------|------|------|------|----|-------|------|
| Sample | Si | Ti | Ba | F* | Cl | I |
| Ba-HFZ-1 | 18.7 | 11.8 | 27.9 | - | <0.02 | ND |
| Ba-ETS-4 | 18.3 | 11.4 | 28.7 | - | 0.15 | ND |
| Ba-RPZ-1 | 18.5 | 12.0 | 29.5 | - | 0.22 | ND |
| Ba-RPZ-2 | 18.1 | 11.1 | 28.9 | - | 0.28 | 0.20 |

*Fluorine cannot be quantified by INAA
ND = not detectable (below detection limit)

| WDX (Mass Percent) Composition Data | | | | | | |
|-------------------------------------|------|------|------|------|-------|------|
| Sample | Si | Ti | Ba | F | Cl | I |
| Ba-HFZ-1 | 18.6 | 11.8 | 27.7 | ND | <0.01 | ND |
| Ba-ETS-4 | 18.3 | 11.8 | 27.8 | 0.20 | 0.14 | ND |
| Ba-RPZ-1 | 18.0 | 11.7 | 28.9 | ND | 0.23 | ND |
| Ba-RPZ-2 | 18.1 | 11.9 | 28.8 | ND | 0.24 | 0.19 |

ND = not detectable (below detection limit)

Phase identification for the four zorite analogs was conducted through powder X-ray diffraction analysis. The XRD patterns (Figure 3-2) indicate that the as-synthesized materials are highly crystalline with unit cell parameters closely resembling those of mineral zorite.^{13,14} The data also demonstrate that the unit cell size does not change with the type or quantity of halogen incorporated. Within the framework, only an isomorphic substitution at the O7 position can account for this observation, as substitutions at any other position would create either a distortion or a change in the lattice parameters. The inversion in the relative intensities of the two dominant peaks observed at 2θ angles of 8.8° and 14.7° (for HFZ-1 and ETS-4 compared to RPZ-1 and RPZ-2) is likely an effect of preferred orientation, and not indicative of a change in the overall lattice structure.

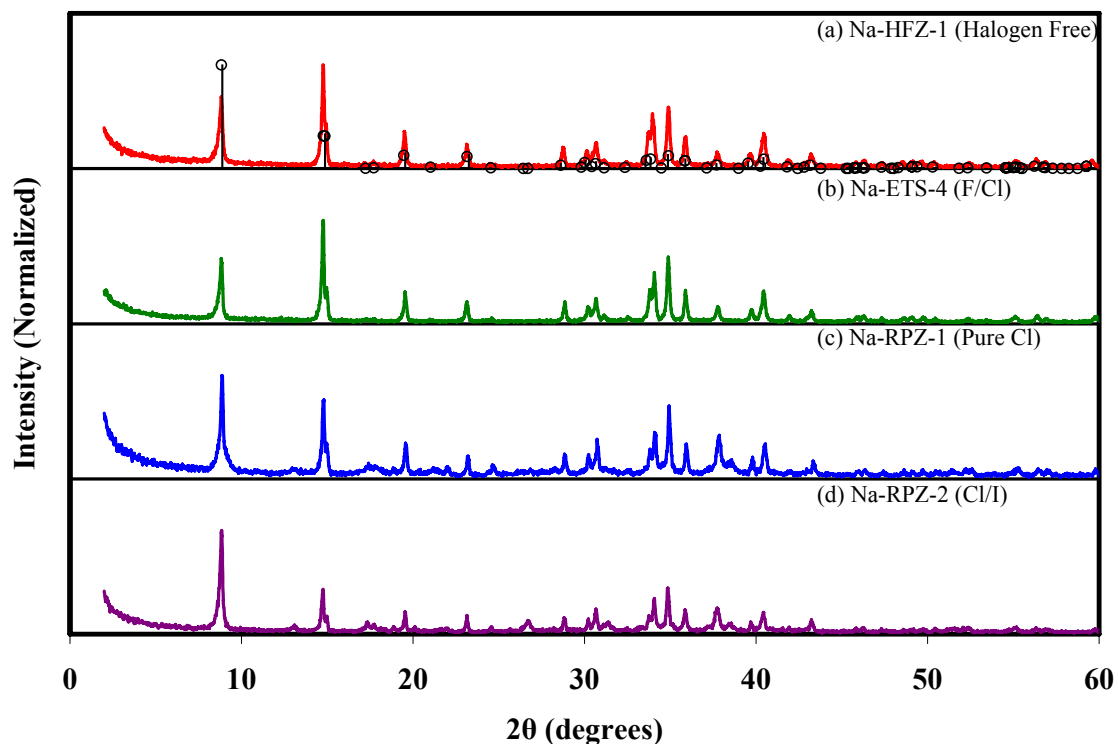


Figure 3-2. Powder X-ray diffraction of as-synthesized anion-controlled zorite analogs. (a) XRD pattern for HFZ-1. All of the zorite analogs have unit cell parameters that closely resemble those of mineral zorite. The JCPDS reference for zorite (PDF#01-084-0144) is superimposed on the HFZ-1 XRD pattern for comparison (black circles). (b) XRD pattern for ETS-4. Fractional substitution of F and Cl for O has no discernable effect on the unit cell parameters. (c) XRD pattern for RPZ-1. Inversion in the relative intensities at 2θ angles of 8.8° and 14.7° , as compared to HFZ-1 and ETS-4, is likely due to preferred orientation effects in HFZ-1 and ETS-4, and not structural differences between the zorite analogs. (d) XRD pattern for RPZ-2. Mixed Cl/I incorporation increases the observed peak inversion.

According to our model, the effective pore size of halogen containing zorites should decrease as the number of framework halogens increases, since the halogen atoms will act as physical barriers and reduce channel accessibility for adsorbate molecules. Figure 3-1 indicates that the effective pore size should be influenced not only by the type (size) of halogens occupying the O7 positions, but also by the quantity of halogen atoms that line the channel walls. A large population of halogens in the channel should result in pores that appear smaller to the diffusing gas species, and restrict the rate of mass transfer. Conversely, if halogens are absent from the channels, as in the structure of HFZ-1, channel accessibility should be maximized, creating the largest possible effective pore diameter.

Both inverse-phase gas chromatography and equilibrium adsorption isotherm analysis (Figures 3-3 and 3-4, respectively) support this model. The data illustrate that, despite their limited crystallographic differences, the adsorptive properties and effective pore size of barium-exchanged HFZ-1, ETS-4, RPZ-1, and RPZ-2 differ significantly, and that the differences correlate to composition. HFZ-1 contains no halogens, while ETS-4, RPZ-1, and RPZ-2 have been substituted (relative to HFZ-1) with F/Cl, Cl, and Cl/I, respectively (Van der Waals radii: F = 1.35 Å, Cl = 1.80 Å, and I = 2.15 Å²¹). The adsorptive characteristics of barium-exchanged HFZ-1, ETS-4, RPZ-1, and RPZ-2 were examined by chromatographic separation of O₂/Ar. The O₂/Ar (3.47 Å and 3.54 Å, respectively¹⁶) pair was chosen because subtle changes in the pore size (<0.1 Å resolution) of the adsorbents should significantly affect the separation of these probe molecules. Separation of oxygen and argon was not observed on either Ba-HFZ-1 or Ba-ETS-4 (Figure 3-3a). Comparison with the pure-gas chromatograms of oxygen and argon indicates that both oxygen and argon molecules are free to enter the channels of Ba-HFZ-1 and Ba-ETS-4. Since the isosteric heats of adsorption for oxygen and argon are similar,³¹ thermodynamic selectivity is not expected if both species are fully adsorbed. However, when the pore size is systematically restricted by increasing the halogen content, as in Ba-RPZ-1 and Ba-RPZ-2, the marginally larger argon molecules are excluded based on size. Water adsorption capacities of the samples (~10% at saturation) are nearly identical in all cases, indicating that the intracrystalline void spaces are comparable. The degree of halogen substitution is apparently too small to substantially change the internal pore volume.

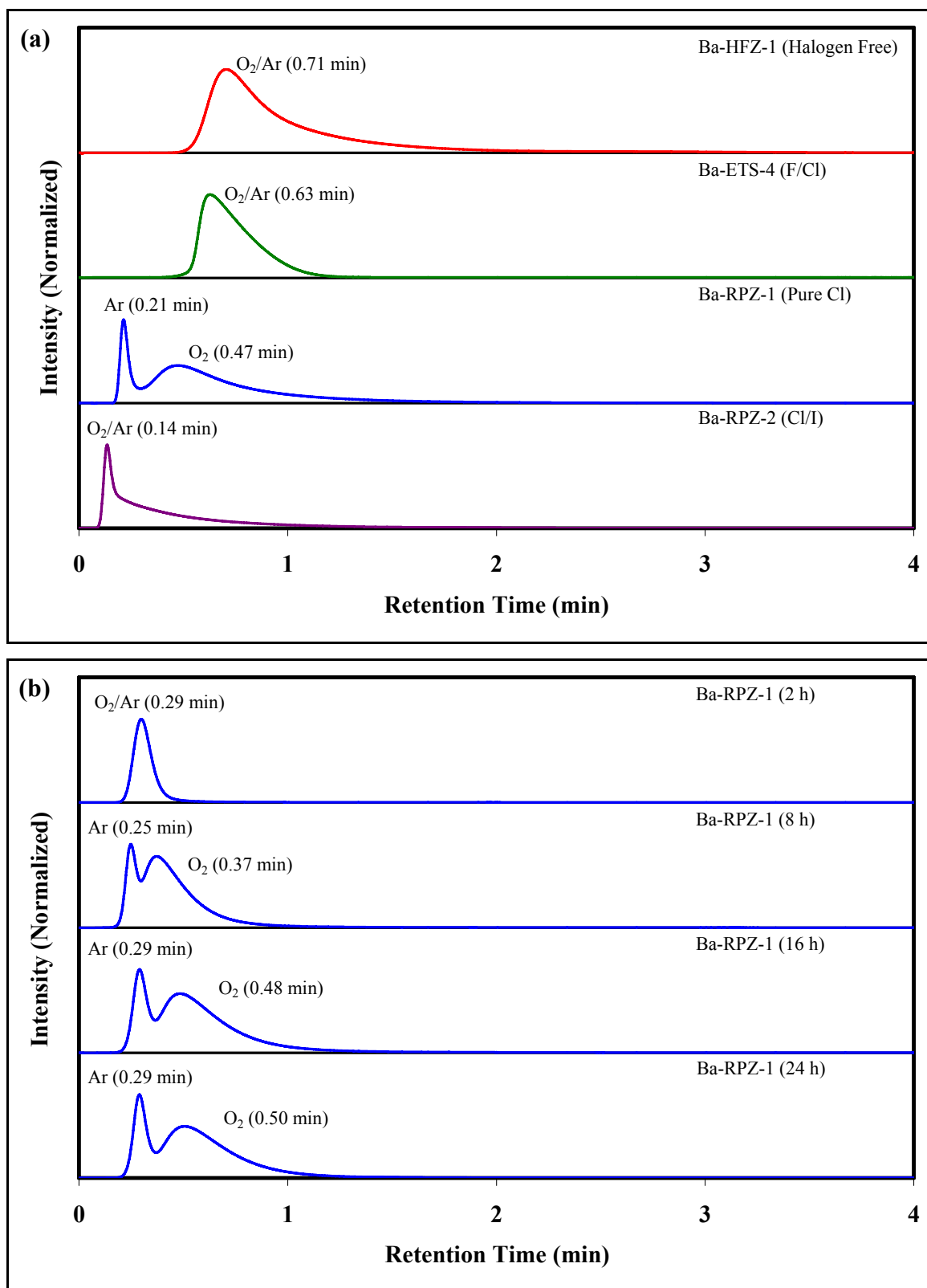


Figure 3-3. Chromatographic separation of O₂/Ar on anion-controlled zorite analogs. (a) Chromatographic separation of O₂/Ar (3.47 Å and 3.54 Å, respectively) on Ba-HFZ-1, Ba-ETS-4,

Ba-RPZ-1, and Ba-RPZ-2. As framework halogen incorporation increases in the synthetic zorite series, argon is selectively size-excluded, facilitating the kinetic separation of oxygen from argon, as seen in Ba-RPZ-1. At the highest level of halogen incorporation, Ba-RPZ-2 excludes both oxygen and argon at a zero-time (minimum time for gas molecules to diffuse through the void space of the column) of 0.14 min. (b) Chromatographic separation of O₂/Ar (3.47 Å and 3.54 Å, respectively) on four samples of Ba-RPZ-1 that have been ion-exchanged for increasing time periods. As the exchange time increases, the Cl atoms within the Ba-RPZ-1 framework are replaced by smaller hydroxyl groups (OH), increasing the effective pore size of the zorite analog. Systematic enlargement of effective pore size facilitates the kinetic separation of oxygen from argon.

It appears that synthetically incorporated halogens can be replaced by hydroxyl groups during prolonged reflux in an aqueous solution. IGC analysis of O₂/Ar separation in Figure 3-3b indicates that the effective pore size of Ba-RPZ-1 systematically increases as a function of ion-exchange time during reflux in a barium chloride solution. At short exchange times (2 h), high quantities of framework Cl in Ba-RPZ-1 restrict the diffusion of both oxygen and argon. As the exchange time is extended (up to 24 h), an increasing number of framework Cl atoms are selectively replaced with OH. Reducing the framework Cl in Ba-RPZ-1 increases the effective pore size and channel accessibility, allowing oxygen to diffuse into the molecular sieve and facilitating the kinetic separation of oxygen from argon. The data suggest that materials with a continuum of pore sizes can be derived from a parent material (such as Na-RPZ-1) simply by controlling the ion-exchange times and conditions.

This new, finely-controlled mechanism allows for the design of adsorbents with highly specific pore sizes and adsorptive characteristics. The data presented in Figure 3-4 illustrate the adsorption or exclusion of three selected gas molecules: ethane (4.44 Å), methane (3.76 Å), and nitrogen (3.64 Å),¹⁶ based on kinetic diameter. Ba-HFZ-1, which is synthesized in the absence of halogens, has the largest channel accessibility and is the only material of the series that can adsorb ethane. Methane, having a smaller diameter than ethane, can enter the pores of both Ba-HFZ-1 and Ba-ETS-4, but is excluded from the Ba-RPZ materials. The exclusion of methane is the result of halogens in both the Ba-RPZ-1 and Ba-RPZ-2 frameworks restricting pore size and channel accessibility. In the case of nitrogen (the smallest molecule of the three examined), all of the materials except Ba-RPZ-2 show substantial adsorption, confirming that Ba-RPZ-2, which contains the

highest level of framework halogens, has the smallest effective pore size of the series. The small capacities for ethane and methane on Ba-RPZ-2 can be attributed to the adsorption of C_2H_6 and CH_4 molecules on the external surfaces of the adsorbent. Surface adsorption of nitrogen is not observed, as it is a less polar species. The correlation between framework anion concentration and functional pore size validates the model that the pore size of these titanium silicate molecular sieves can be controlled by manipulating the anions in the framework structure. The quantity and type of O7 substituted halogens directly control the effective pore size of these titanium silicate zorite analogs.

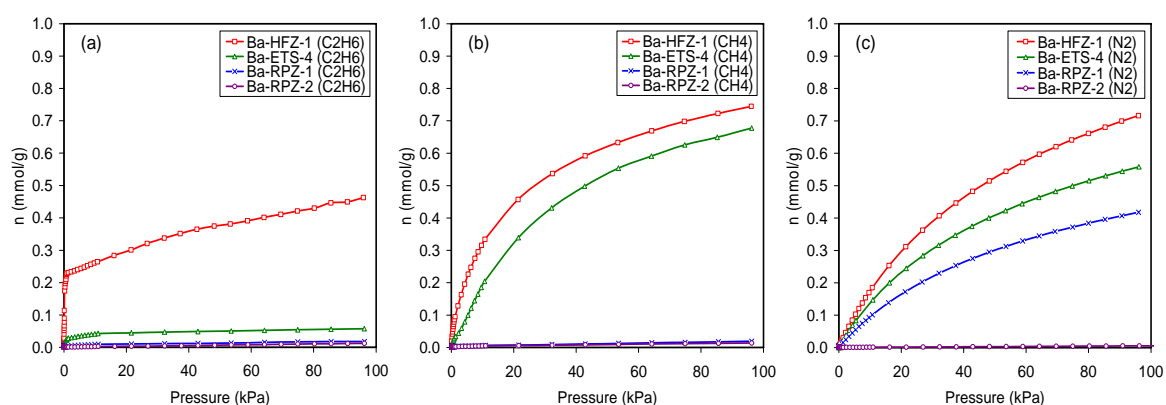


Figure 3-4. Equilibrium adsorption isotherms of anion-controlled zorite analogs. (a) Ethane (C_2H_6) isotherms for the series Ba-HFZ-1, Ba-ETS-4, Ba-RPZ-1, and Ba-RPZ-2. Ba-HFZ-1, which contains no framework halogens, is the only material that adsorbs ethane (4.44 Å). Ethane is excluded from all three halogen containing zorites. (b) Methane (CH_4) isotherms for the series Ba-HFZ-1, Ba-ETS-4, Ba-RPZ-1, and Ba-RPZ-2. Ba-RPZ-1 and Ba-RPZ-2, which have high concentrations of framework halogens, completely exclude methane (3.76 Å). Both Ba-HFZ-1 and Ba-ETS-4 adsorb methane, indicating a larger effective pore size than the Ba-RPZ materials. (c) Nitrogen (N_2) isotherms for the series Ba-HFZ-1, Ba-ETS-4, Ba-RPZ-1, and Ba-RPZ-2 indicate that Ba-RPZ-2, which contains the highest level of framework halogens and is the only zorite analog to exclude nitrogen (3.64 Å), has the smallest effective pore size of the series.

It should be noted that the coordination state of the chain-bridging titanium atom (Ti2) in zorite analogs remains a subject of active debate in the literature.^{20,23-26} Some studies have concluded that the O7 site is a titanyl group, with a Ti=O linkage to the apical oxygen,²⁰ while the results of other work indicate that the site is occupied by a titanol group (Ti-OH)²³ or a linkage to structural water.²⁶ In this work, location of the halogens was assigned to the O7 position because this is the position that is most strongly supported by the structural and functional data. Based on these data, the only location for

the halogens that could have such a profound impact on the effective pore size and the observed adsorptive properties is the O7 position, as indicated in Figure 3-1. Further research will be required to definitively determine the coordination state of the chain-bridging titanium atom (Ti2) in titanium silicate molecular sieves and its implication for this proposed model of a novel mechanism for rational pore size control in a molecular sieve.

3.5 Conclusions

We have established a novel mechanism to systematically control the pore size of titanium silicate molecular sieves through halogen substitution of terminal hydroxyl groups. These halogen containing zorites represent a new class of size-selective adsorbents with readily tailored and highly specific pore sizes. Anion-controlled titanium silicate molecular sieves have promise in multiple areas of size-based separation, particularly light hydrocarbon purification and permanent gas separation.

3.6 References

- (1) Keller II, G. E.; Anderson, R. A.; Yon, C. M. In *Handbook of Separation Process Technology*; Rousseau, R. W., Eds.; Adsorption; Wiley: Hoboken, 1987; pp 644-696.
- (2) Weitkamp, J. *Solid State Ionics* **2000**, *131*, 175.
- (3) Helfferich, F. G. *Ion Exchange*; Dover: New York, 1995.
- (4) Cundy, C. S.; Cox, P. A. *Chem. Rev.* **2003**, *103*, 663.
- (5) Butwell, K. F.; Dolan, W. B.; Kuznicki, S. M. Selective Removal of Nitrogen from Natural Gas by Pressure Swing Adsorption. U.S. Patent 6,197,092, March 6, 2001.
- (6) Kuznicki, S. M.; Bell, V. A.; Petrovic, I.; Desai, B. T. Small-Pored Crystalline Titanium Molecular Sieve Zeolites and their Use in Gas Separation Processes. U.S. Patent 6,068,682, May 30, 2000.
- (7) Kuznicki, S. M.; Bell, V. A. Olefin Separations Employing CTS Molecular Sieves. U.S. Patent 6,517,611, February 11, 2003.
- (8) Roeseler, C. M.; Kulprathipanja, S.; Rekoske, J. E. Adsorptive Separation Process for Recovery of Para-xylene. U.S. Patent 6,706,938, March 16, 2004.
- (9) Choi, S.; Lee, S.-J.; Kang, S.-C.; Kim, S.-W.; Ku, M.-S.; Choi, A.-S.; Chang, B.-M. Process for Separating Normal Paraffins from Hydrocarbons and Applications for the Separated Hydrocarbons. U.S. Patent 6,870,073, March 22, 2005.
- (10) Breck, D. W. *Zeolite Molecular Sieves: Structure, Chemistry and Use*; Wiley: New York, 1974.
- (11) Yilmaz, B.; Miraglia, P. Q.; Warzywoda, J.; Sacco Jr. A. *Microporous Mesoporous Mater.* **2004**, *71*, 167.
- (12) Kuznicki, S. M. Preparation of Small-Pored Crystalline Titanium Molecular Sieve Zeolites. U.S. Patent 4,938,939, July 3, 1990.
- (13) Sandomirskii, P. A.; Belov, N. V. *Sov. Phys. Crystallogr.* **1979**, *24*, 686.
- (14) Mer'kov, A. N.; Bussen, I. V.; Goiko, E. A.; Kul'chitskaya, E. A.; Men'shikov, Y. P.; Nedorezova, A. P. *Zap. Vses. Mineral. Obshchest.* **1973**, *102*, 54.
- (15) Kuznicki, S. M.; Bell, V. A.; Nair, S.; Hillhouse, H. W.; Jacubinas, R. M.; Braunbarth, C. M.; Toby, B. H.; Tsapatsis, M. *Nature* **2001**, *412*, 720.

- (16) Sircar, S.; Myers, A. L. In *Handbook of Zeolite Science and Technology*; Auerbach, S. M.; Carrado, K. A.; Dutta, P. K., Eds.; Gas Separation by Zeolites; Marcel Dekker Inc.: New York, 2003; pp 1063-1104.
- (17) Marathe, R. P.; Farooq, S.; Srinivasan, M. P. *Langmuir* **2005**, *21*, 4532.
- (18) Marathe, R. P.; Mantri, K.; Srinivasan, M. P.; Farooq, S. *Ind. Eng. Chem. Res.* **2004**, *43*, 5281.
- (19) Cambridge Crystallographic Data Center. Mercury 1.4.2 – Structure Modeling Software. <http://www.ccdc.cam.ac.uk/products/mercury/> (accessed June 15, 2008).
- (20) Nair, S.; Jeong H.-K.; Chandrasekaran, A.; Braunbarth, C. M.; Tsapatsis, M.; Kuznicki, S. M. *Chem. Mater.* **2001**, *13*, 4247.
- (21) Pauling, L. *The Nature of the Chemical Bond and the Structure of Molecules and Crystals: An Introduction to Modern Structural Chemistry*; Cornell University Press: New York, 1960.
- (22) Philippou, A.; Anderson, M. W. *Zeolites* **1996**, *16*, 98.
- (23) Cruciani, G.; De Luca, P.; Nastro, A.; Pattison, P. *Microporous Mesoporous Mater.* **1998**, *21*, 143.
- (24) Braunbarth, C.; Hillhouse, H. W.; Nair, S.; Tsapatsis, M.; Burton, A.; Lobo, R. F. *Chem. Mater.* **2000**, *12*, 1857.
- (25) Nair, S.; Tsapatsis, M.; Toby, B. H.; Kuznicki, S. M. *J. Am. Chem. Soc.* **2001**, *123*, 12781.
- (26) Usseglio, S.; Calza, P.; Damin, A.; Minero, C.; Bordiga S.; Lamberti, C.; Pelizzetti, E.; Zecchina, A. *Chem. Mater.* **2006**, *18*, 3412.
- (27) Alberico, A.; Ferrando, S.; Ivaldi, G.; Ferraris, G. *Eur. J. Mineral.* **2003**, *15*, 875.
- (28) Cameron, M.; Gibbs, G. V. *Am. Mineral.* **1973**, *58*, 879.
- (29) Kuznicki, S. M.; Bell, V. A.; Petrovic, I.; Blosser, P. W. Separation of Nitrogen from Mixtures thereof with Methane Utilizing Barium Exchanged ETS-4. U.S. Patent 5,989,316, November 23, 1999.
- (30) Kuznicki, S. M.; Sawada, J. A.; Rode, E. J.; Lin, C. C. H. Titanium Silicate Materials, Method for their Manufacture, and Method for Using Such Titanium Silicate Materials for Adsorptive Fluid Separations. World Patent No. WO/2008/002463, March 1, 2008.

(31) Peter, S. A.; Sebastian, J.; Jasra, R. V. *Ind. Eng. Chem. Res.* **2005**, *44*, 6856.

**SEPARATION OF NITROGEN AND METHANE BY
ADSORPTION ON HALOGEN CONTAINING REDUCED
PORE ZORITE**

4.1 Summary

A small-pored, halogen containing titanium silicate molecular sieve adsorbent, Ba-RPZ-1, was synthesized and tested for use in the separation of N₂/CH₄ mixtures at room temperature. Both equilibrium adsorption isotherm analyses and inverse-phase gas chromatographic experiments indicate substantial improvements in the separation of nitrogen from methane using Ba-RPZ-1, as compared to the commercial Molecular Gate[®] adsorbent ETS-4. Ba-RPZ-1 has been used to demonstrate the most precise separation of N₂/CH₄ reported to date and can potentially improve current adsorptive natural gas purification systems. These results have broad implications in all areas of molecular purification, including the separation of N₂/CH₄, O₂/Ar, olefin/paraffin, CO₂/HC, O₂/N₂, and other economically important light hydrocarbons.

4.2 Introduction

Natural gas represents one of the most valuable energy resources in the world. In 2008, the production of natural gas in Alberta alone approached five trillion cubic feet.¹ Raw natural gas is a mixture composed primarily of methane (CH₄) that is contaminated with carbon dioxide (CO₂), hydrogen sulfide (H₂S), water (H₂O), and nitrogen (N₂).² While constituents such as carbon dioxide and water are relatively simple to remove by selective adsorption, the separation of nitrogen from natural gas is more challenging because most adsorbents are selective toward methane instead of nitrogen.^{3,4} Size-selective separation is an alternative but it is tremendously difficult as nitrogen and methane differ in size by less than 0.15 Å.⁵ Removing contaminant such as nitrogen from methane is increasing important for natural gas production because many natural gas deposits are contaminated with high levels of nitrogen (>20 wt %), rendering them un-useable.

Nitrogen, at high concentrations, lowers the heating value of natural gas due to reduced overall hydrocarbon content. In order to meet pipeline specifications for non-combustibles, the nitrogen content in natural gas must be reduced to less than 4 wt %.² Many current natural gas nitrogen rejection processes employ cryogenic distillation in order to achieve the required specifications. However, the combined costs of liquefaction and subsequent re-compression of the low pressure product make this an expensive process, economic only for large, highly contaminated fields.³ For small natural gas fields, there is an increased demand for recovering the methane but cryogenic separation is not economically feasible. Therefore, an alternative technology such as pressure swing adsorption (PSA) utilizing molecular sieve adsorbents, which can operate at near ambient temperatures and maintain a high pressure product stream, is needed to provide a more economical process for the purification of natural gas.⁶

The commercialization of PSA processes for N₂/CH₄ separation has been slow due to the difficulty in developing satisfactory adsorbents. Microporous materials, such as aluminosilicate zeolites, have been examined as potential adsorbents for N₂/CH₄

separation. For example, clinoptilolite can achieve the separation quite effectively, but only if its extra-framework cations are selected appropriately.⁷ The synthetic form is difficult to prepare,⁸ and while the natural mineral is abundant, its commercial utility has been hindered by the variability in the extra-framework cation composition with source deposit,⁹ and the tendency of impurities present to lead to its conversion to mordenite during service. Alternative synthetic materials that can be manufactured controllably, are therefore required if a commercially viable adsorbent is to be utilized.

Engelhard Titanosilicate-4 (ETS-4)¹⁰ is a small-pored, mixed coordination titanium silicate molecular sieve related to the mineral zorite.^{11,12} The pores of ETS-4 contract upon dehydration at elevated temperatures, tuning the effective size of the pores and precisely altering the separation characteristics of the material.¹³ This phenomenon, known as the Molecular Gate[®] effect, has already achieved commercial success in natural gas purification.^{14,15} However, the contraction process inevitably damages the ETS-4 framework and introduces crystal lattice defects, both of which limit the potentials of the Molecular Gate[®] technology.

Recently, we discovered that the pore size of a new ETS-4 analog, Reduced Pore Zorite (RPZ), can be systematically engineered with sub-molecular precision (<0.1 Å resolution) by controlling the framework halogen content.^{16,17} RPZ-1 is a structural analog of the mineral zorite and the synthetic titanium silicate ETS-4. RPZ-1 contains structural chlorides which constrict the pores progressively and systematically as their concentration increases. This new method of pore size control allows size-selective materials to be prepared in stable cationic forms (such as barium) without crystal shrinkage.¹⁷ This allows the preparation of even more precise size-exclusion adsorbents than the Molecular Gate[®] materials.

Utilizing inverse-phase gas chromatography (IGC) and equilibrium adsorption isotherm analysis, we compare the adsorption and separation of N₂/CH₄ on Ba-RPZ-1 and Ba-ETS-4. The results of this investigation and their implications on the commercial purification of natural gas are also discussed.

4.3 Experimental Methods

RPZ-1 was synthesized according to the literature.¹⁶ The as-synthesized RPZ-1 was barium-exchanged by exposure to an excess of aqueous barium chloride solution at 373 K with stirring for 24 h. Sodium (Na) was essentially quantitatively exchanged by barium (Ba) and the finished material typically contained nearly 30 wt % Ba and <1 wt % Na. Barium is known to stabilize titanium silicate molecular sieves thus maximum replacement of sodium is desired. The barium-exchanged RPZ-1 was thoroughly washed with de-ionized water, and dried at 373 K in a forced-air oven. The average particle size produced for testing was found to be approximately 40 μm . For comparison, ETS-4 was synthesized according to the patent literature¹⁰ and barium-exchanged as above.

The as-synthesized RPZ-1 and ETS-4 was examined by powder X-ray diffraction (Figure 4-1) using a Rigaku Geigerflex 2173 with a vertical goniometer equipped with a graphite monochromator for filtration of K- β wavelengths. Peak positions in the RPZ-1 pattern are reminiscent of the mineral zorite and its closest synthetic analog, ETS-4, but with differing peak intensity ratios. It is evident that, like ETS-4 and its polymorphs, RPZ-1 is structurally related to the mineral zorite.

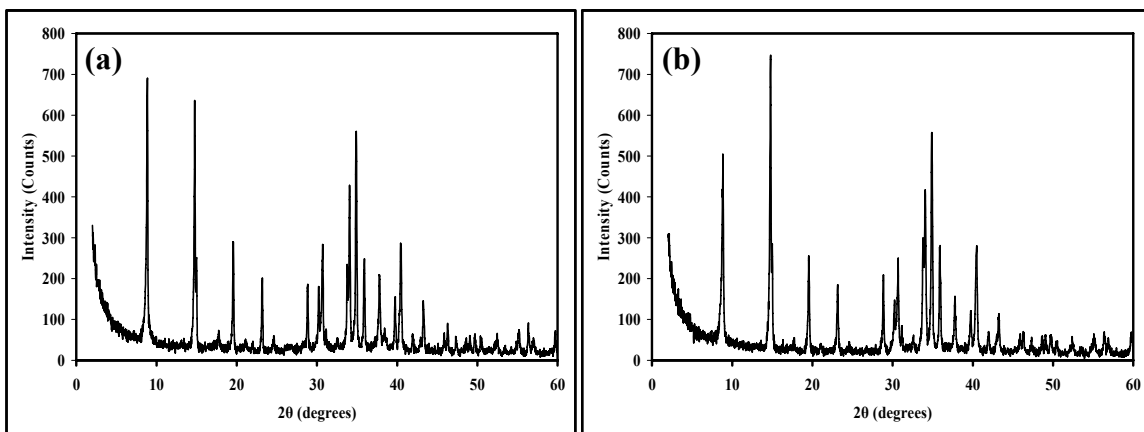


Figure 4-1. Powder X-ray diffraction of as-synthesized (a) RPZ-1 and (b) ETS-4.

Equilibrium adsorption isotherms were measured volumetrically at 298 K up to 100 kPa using an AUTOSORB-1-MP from Quantachrome Instruments (Boynton Beach, FL) on

crystalline powders (no binders or diluents were added to the samples). All samples were activated at 523 K for 10 h under vacuum (<0.0005 Torr).

IGC analysis was performed on a Varian 3800 gas chromatograph (GC) utilizing a thermal conductivity detector (TCD). Test adsorbents were packed into 10" long, 0.25" OD copper columns using a plastic funnel. The columns were filled with approximately 3.5 g of adsorbents. The adsorbents were activated at 523 K and 0.5 psig for 10 h under a helium flow of $30 \text{ cm}^3/\text{min}$. Characterization gases (nitrogen, methane, and mixtures thereof) were introduced by 1 mL pulse injections into the test columns.

4.4 Results and Discussion

Equilibrium adsorption isotherms (Figure 4-2) indicate that the separation factor of N_2/CH_4 is significantly higher on Ba-RPZ-1 than on Ba-ETS-4. The thermodynamic selectivity of nitrogen over methane can be calculated as the ratio of the respective Henry's law constants by applying the classical Langmuir equation.¹⁸ According to the values listed in Table 4-1, the thermodynamic selectivities of nitrogen over methane for Ba-RPZ-1 and Ba-ETS-4 at 298 K are 18.27 and 11.92, respectively.

The nitrogen capacity for Ba-RPZ-1, evaluated on a gravimetric basis (Figure 4-2a), is approximately 17% higher than for Ba-ETS-4. However, when compared on a volumetric basis (Figure 4-2b), the nitrogen capacity for Ba-RPZ-1 is 80% higher than for Ba-ETS-4. This is attributed to an increase in the density of Ba-RPZ-1 as compared to Ba-ETS-4. The substitution of Cl for F in the RPZ-1 preparation yields a denser material (Table 4-1). Such increase in N_2/CH_4 selectivity and, more importantly, volumetric nitrogen capacity allows new cycling conditions to generate greater yield and recovery of methane from a unit of any size.

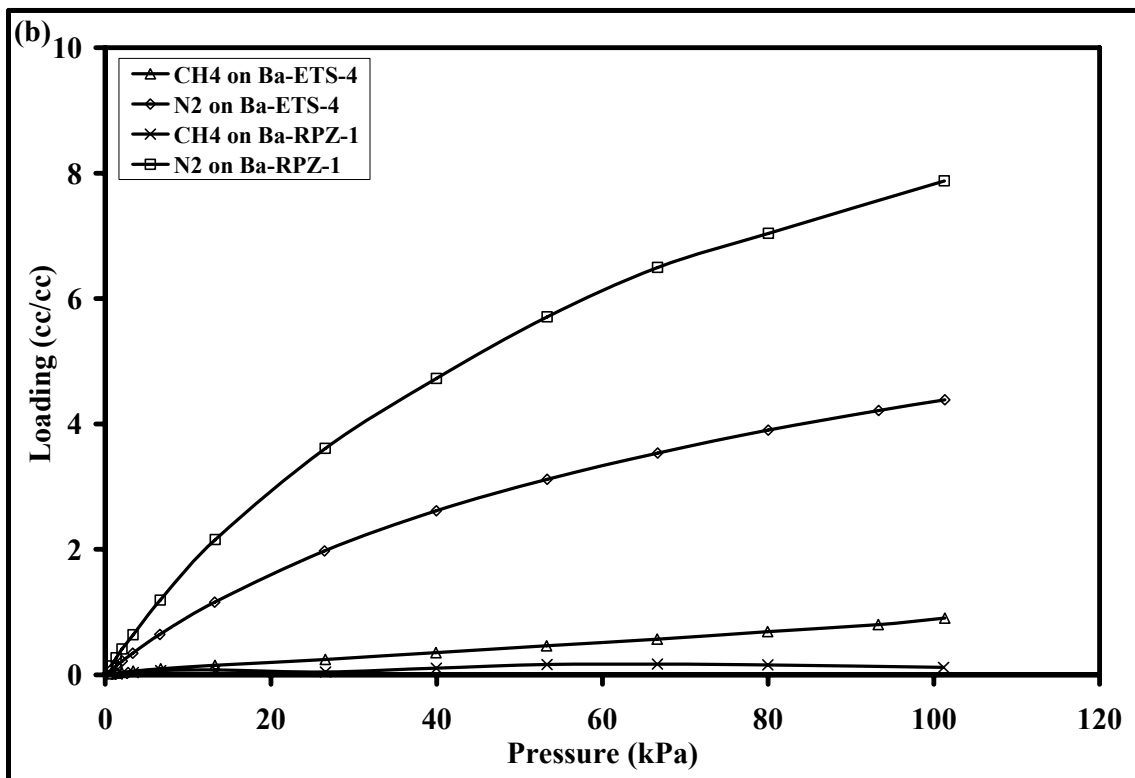
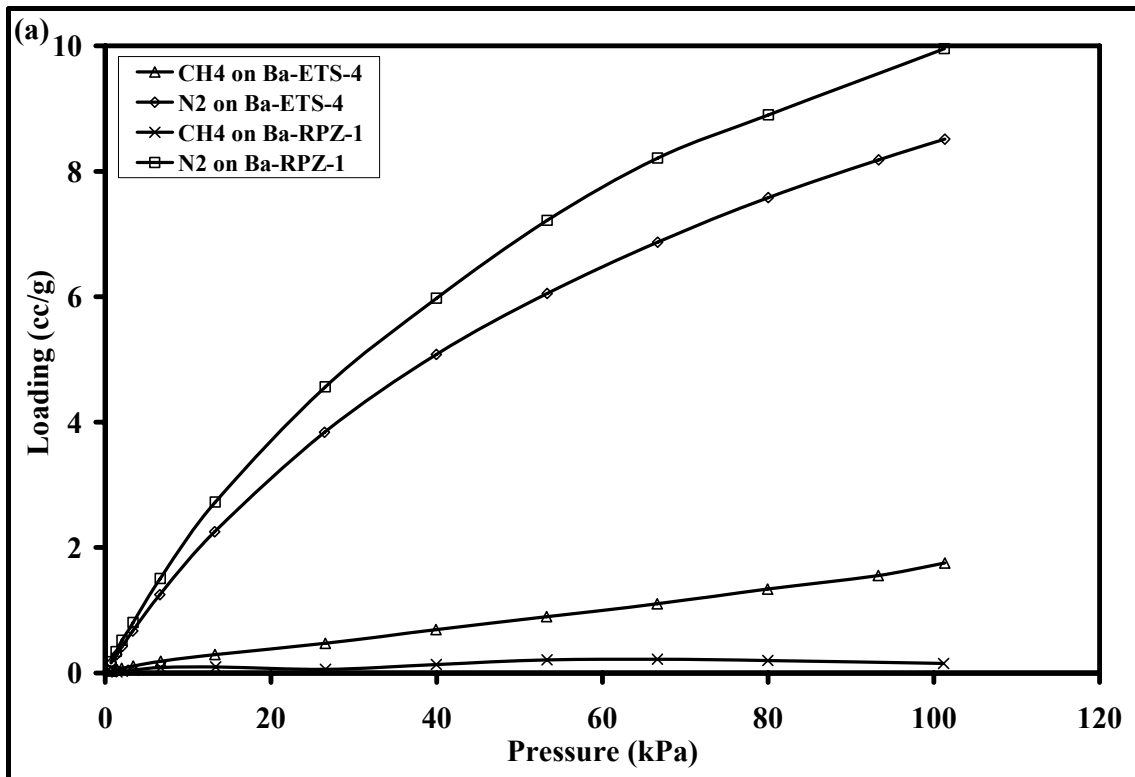


Figure 4-2. Nitrogen and methane adsorption isotherms at 298 K for Ba-RPZ-1 and Ba-ETS-4. Data displayed in terms of (a) gravimetric basis and (b) volumetric basis.

Table 4-1. Physical and Equilibrium Parameters for Ba-RPZ-1 and Ba-ETS-4

| Adsorbent | Density (g/cm ³) | K (mol/kg·kPa) | |
|-----------|------------------------------|----------------|---------|
| | | Nitrogen | Methane |
| Ba-RPZ-1 | 0.515 | 0.2302 | 0.0126 |
| Ba-ETS-4 | 0.791 | 0.1955 | 0.0164 |

The improved separation of N₂/CH₄ on Ba-RPZ-1, as compared to Ba-ETS-4, is further demonstrated by IGC experiments (Figure 4-3). In Figure 4-3a, methane is excluded at a near zero-time (minimum time for gas molecules to diffuse through the void space of the column) of 0.17 min. Compare this to a methane retention time of 0.35 min (Figure 4-3b), it is clear that Ba-RPZ-1 excludes methane much more effectively than Ba-ETS-4. The chromatographic selectivities of nitrogen over methane for Ba-RPZ-1 and Ba-ETS-4, utilizing a zero-time of 0.16 min, are 152.00 and 5.42, respectively.

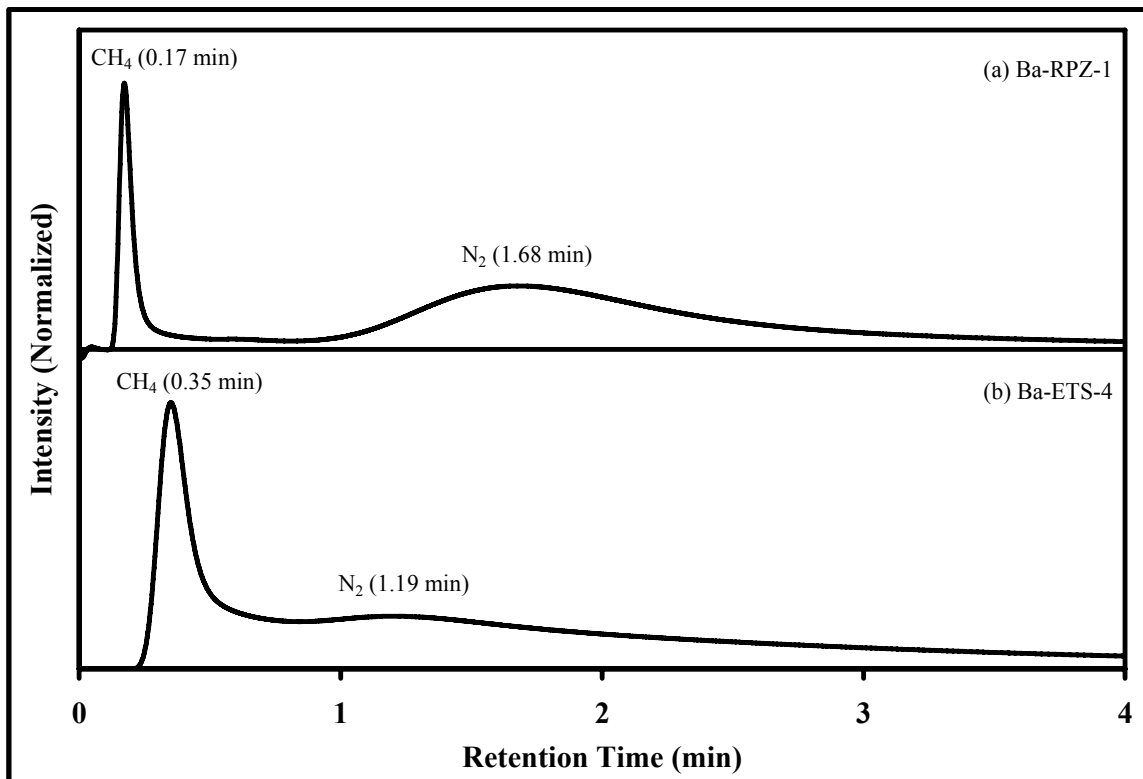


Figure 4-3. IGC profiles at 298 K by injecting a 50-50% N₂/CH₄ mixture in a column of (a) Ba-RPZ-1 and (b) Ba-ETS-4.

The shape of the nitrogen peak in Figure 4-3a is symmetrical and baseline-resolved, indicating good nitrogen diffusion in Ba-RPZ-1. Compared with the asymmetrical broadening of the nitrogen peak seen in Figure 4-3b, it is clear that the diffusion resistance of nitrogen is lower in Ba-RPZ-1 than Ba-ETS-4.

4.5 Conclusions

A small-pored, halogen containing titanium silicate molecular sieve adsorbent, Ba-RPZ-1, was shown to possess much improved nitrogen selectivity and volumetric nitrogen capacity in the separation of N_2/CH_4 than the commercial Molecular Gate[®] adsorbent ETS-4. This improvement is the direct result of a new mechanism of pore size control on titanium silicates using anionic halides as structural barriers to adsorption. The results of this investigation have broad implications in all areas of molecular purification, including the separation of N_2/CH_4 , O_2/Ar , olefin/paraffin, CO_2/HC , O_2/N_2 , and other economically important light hydrocarbons.

4.6 References

- (1) About Natural Gas. <http://www.energy.gov.ab.ca/NaturalGas/940.asp> (accessed April 1, 2009).
- (2) Dolan, W. B.; Butwell, K. F. Selective Removal of Nitrogen from Natural Gas by Pressure Swing Adsorption. U.S. Patent 6,444,012, September 3, 2002.
- (3) Maple, M. J.; Williams, C. D. *Microporous Mesoporous Mater.* **2008**, *111*, 627.
- (4) Li, P.; Tezel, F. H. *J. Chem. Eng. Data* **2009**, *54*, 8.
- (5) Breck, D. W. *Zeolite Molecular Sieves: Structure, Chemistry and Use*; Wiley: New York, 1974.
- (6) Jasra, R. V.; Choudary, N. V.; Bhat, S. G. T. *Sep. Sci. Technol.* **1991**, *26*, 885.
- (7) Ackley, M. W.; Giese, R. F.; Yang, R. T. *Zeolites* **1992**, *12*, 780.
- (8) Williams, C. D. *Chem. Commun.* **1997**, 2113.
- (9) Guest, J. E.; Williams, C. D. *Chem. Commun.* **2002**, 2870.
- (10) Kuznicki, S. M. Preparation of Small-Pored Crystalline Titanium Molecular Sieve Zeolites. U.S. Patent 4,938,939, July 3, 1990.
- (11) Sandomirskii, P. A.; Belov, N. V. *Sov. Phys. Crystallogr.* **1979**, *24*, 686.
- (12) Mer'kov, A. N.; Bussen, I. V.; Goiko, E. A.; Kul'chitskaya, E. A.; Men'shikov, Y. P.; Nedorezova, A. P. *Zap. Vses. Mineral. Obshchest.* **1973**, *102*, 54.
- (13) Kuznicki, S. M.; Bell, V. A.; Nair, S.; Hillhouse, H. W.; Jacubinas, R. M.; Braunbarth, C. M.; Toby, B. H.; Tsapatsis, M. *Nature* **2001**, *412*, 720.
- (14) Butwell, K. F.; Dolan, W. B.; Kuznicki, S. M. Selective Removal of Nitrogen from Natural Gas by Pressure Swing Adsorption. U.S. Patent 6,197,092, March 6, 2001.
- (15) Kuznicki, S. M.; Bell, V. A.; Petrovic, I.; Desai, B. T. Small-Pored Crystalline Titanium Molecular Sieve Zeolites and their Use in Gas Separation Processes. U.S. Patent 6,068,682, May 30, 2000.
- (16) Kuznicki, S. M.; Sawada, J. A.; Rode, E. J.; Lin, C. C. H. Titanium Silicate Materials, Method for their Manufacture, and Method for Using Such Titanium Silicate Materials for Adsorptive Fluid Separations. World Patent No. WO/2008/002463, March 1, 2008.

- (17) Lin, C. C. H.; Sawada, J. A.; Wu, L.; Haastrup, T.; Kuznicki, S. M. *J. Am. Chem. Soc.* **2009**, *131*, 609.
- (18) Langmuir, I. *J. Am. Chem. Soc.* **1918**, *40*, 1361.

**SEPARATION OF OXYGEN AND ARGON BY
ADSORPTION ON HALOGEN CONTAINING REDUCED
PORE ZORITE**

5.1 Summary

A small-pored, halogen containing titanium silicate molecular sieve adsorbent, Ba-RPZ-1, was synthesized and tested for use in the separation of O₂/Ar mixtures at room temperature. A clean resolution of both gases was achieved in the inverse-phase gas chromatographic experiments using a standard column containing 3.5 g of adsorbents, even when the argon content was only 10% of the mixture. In another experiment, using a column containing 30 g of adsorbents and a continuous O₂/Ar feed at 10 cm³/min, argon breakthrough was detected more than 5 minutes before oxygen breakthrough, even in the case of mixtures with low argon content (95-5% O₂/Ar). Equilibrium adsorption isotherms and isosteric heats of adsorption for oxygen and argon were found to be almost identical at room temperature. The thermodynamic selectivity was found to be mildly in favor of oxygen (approximately 1.1-1.2). However, the adsorption of oxygen was observed to be much faster than argon, indicating that the separation of the O₂/Ar mixtures was based on the sieving properties of the adsorbent and the size difference between the molecules of oxygen and argon.

5.2 Introduction

Separation of oxygen and argon is one of the most important processes in the industrial purification of the constituents of air, but is also one of the most difficult. The basic methods used for this separation include selective adsorption and cryogenic distillation. At cryogenic temperatures, the adsorptive selectivity of oxygen over argon on classical zeolites appears to be large enough for a viable separation. Barrer and Robins, investigating the ability of Na-mordenite to separate several binary gas mixtures, concluded that zeolite columns at 90 K can generate pure argon from O₂/Ar mixtures.¹ In these experiments, they detected wide differences in the adsorption rates of the pure gases (hydrogen, neon, oxygen, nitrogen, argon, and krypton), in which they attributed the resolution of the mixtures to both the affinity of the gases for the substrate and the adsorption kinetics. In the case of O₂/Ar mixtures at low temperatures, both factors tend to maximize the preferential binding of oxygen over argon. The chromatographic resolution of oxygen and argon can also be achieved in a column of zeolite 5A at dry ice/acetone bath temperatures (195 K).² Such separations of oxygen and argon on zeolites at cryogenic temperatures could be implemented as industrial processes, if they did not have high energy requirements.³

Unfortunately, at room temperature, little or no selectivity for oxygen over argon is found for common adsorbents, including zeolites. Isothermic heats of adsorption for oxygen and argon on typical adsorbents are nearly identical, the only exception being silver-exchanged molecular sieves, which have been reported to show a mild argon selectivity of 1.2-1.5.⁴ Attempts have been made to exploit the mild thermodynamic selectivity of oxygen over argon by chromatographic separation of oxygen and argon using columns containing 5A zeolite,⁵ 13X zeolite,⁶ or Ca-chabazite (one of the most polarizing adsorbents known),⁷ but all of these processes require extremely dry adsorbents and are commercially impractical due to very low product yield.

Early attempts made to separate O₂/Ar mixtures by selective adsorption at ambient temperature used long chromatographic columns of zeolites and polymers.^{8,9} More

recently, bulk industrial processes involving carbon molecular sieves (CMS) have been proposed, both for the purification of oxygen from O₂/Ar mixtures and to obtain an argon-enriched stream.^{10,11} The thermodynamic selectivity of oxygen over argon on CMS is too small to allow equilibrium-based pressure swing adsorption (PSA) cycles, but the rate of oxygen uptake on CMS is much faster than the rate of argon uptake (25-30 times), opening the possibility of PSA processes based on kinetic selectivity.¹⁰⁻¹² It is believed that the size of the gas molecules plays the major role in determining adsorption kinetics, but other factors whose relative contributions are difficult to determine may also play a role.^{13,14} However, the resolution of oxygen and argon over CMS is far from perfect and the maximum argon purity reported for a process utilizing CMS is on the order of 80-90%.^{10,11} In a model calculation of a five-step cycle designed for producing high purity argon using a Berghen-Forschung activated carbon at 303 K, the highest projected argon purity was 88% but that allowed the recovery of only 15% of the argon from the original stream.¹⁰ Calculations for a three-step PSA cycle using a Takeda carbon molecular sieve at 293 K projected a maximum argon purity of about 80% with recovery of 43%.¹¹ This report concluded that the Takeda carbon molecular sieve was better for O₂/Ar separation than both activated carbons (Berghen-Forschung) and modified 4A zeolites (RS-10). An inorganic molecular sieve with cleaner resolution of O₂/Ar and better predictability than current CMS materials could enable more efficient processes for the separation and purification of oxygen and argon.

Several titanium silicates, including ETS-4, ETS-10, and other structures based on octahedral titanium units, have been recognized for their adsorptive and molecular sieving properties.¹⁵⁻²⁰ ETS-4, in particular, has been noted for its ability to differentiate molecules by size, including the commercial separation of nitrogen from methane at high pressures.¹⁵⁻¹⁷ In this investigation, we examine the separation of oxygen and argon using Ba-RPZ-1, a new, zorite-like member of the titanium silicate family.²¹⁻²³

Reduced Pore Zorite (RPZ) is a structural analog of the mineral zorite and the synthetic titanium silicate ETS-4. RPZ-1 contains structural chlorides which constrict the pores progressively and systematically as their concentration increases.^{24,25} This new method

of pore size control allows size-selective materials to be prepared in stable cationic forms (such as barium) without crystal shrinkage.²⁴ This allows the preparation of even more precise size-exclusion adsorbents than the ETS-4 materials.

Using Ba-RPZ-1, clean chromatographic resolution can be obtained for O₂/Ar mixtures, even for those containing only 5% argon, which is the typical outlet argon composition of a primary PSA air separation unit. The sieving characteristics of this material are discussed in terms of a kinetic mechanism selective toward the adsorption of oxygen.

5.3 Experimental Methods

RPZ-1 was synthesized according to the literature.^{24,25} The as-synthesized RPZ-1 was barium-exchanged by exposure to an excess of aqueous barium chloride solution at 373 K with stirring for 24 h. Sodium (Na) was essentially quantitatively exchanged by barium (Ba) and the finished material typically contained nearly 30 wt % Ba and <1 wt % Na. Barium is known to stabilize titanium silicate molecular sieves thus maximum replacement of sodium is desired. The barium-exchanged RPZ-1 was thoroughly washed with de-ionized water, and dried at 373 K in a forced-air oven. The average particle size produced for testing was found to be approximately 40 μm. For comparison, ETS-4 was synthesized according to the patent literature²⁶ and barium-exchanged as above.

The as-synthesized RPZ-1 and ETS-4 was examined by powder X-ray diffraction (Figure 5-1) using a Rigaku Geigerflex 2173 with a vertical goniometer equipped with a graphite monochromator for filtration of K-β wavelengths. Peak positions in the RPZ-1 pattern are reminiscent of the mineral zorite²¹⁻²³ and its closest synthetic analog, ETS-4,²⁶ but with differing peak intensity ratios. It is clear that, like ETS-4 and its polymorphs,²⁶ RPZ-1 is structurally related to the mineral zorite.

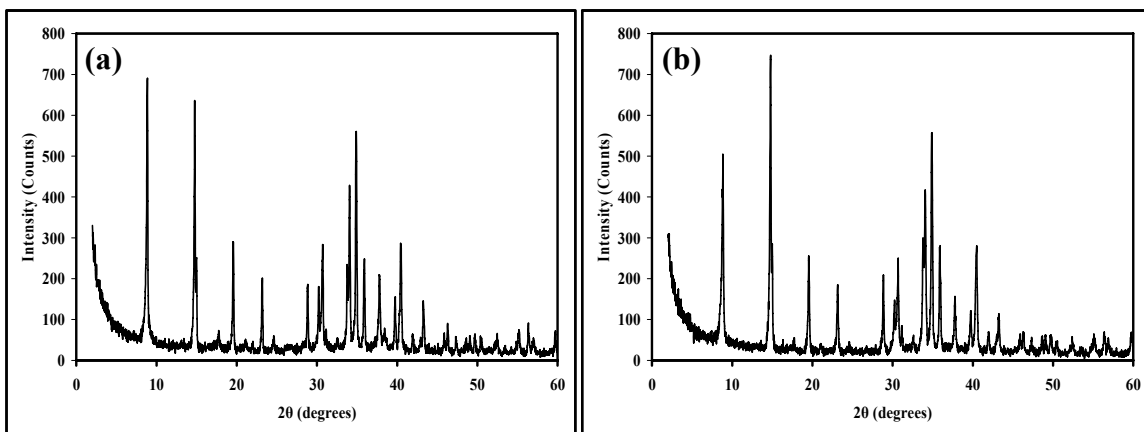


Figure 5-1. Powder X-ray diffraction of as-synthesized (a) Na-RPZ-1 and (b) Na-ETS-4.

Inverse-phase gas chromatography (IGC) was performed on a Varian 3800 gas chromatograph (GC) utilizing a thermal conductivity detector (TCD). Test adsorbents were packed into 10" long, 0.25" OD copper columns using a plastic funnel. The columns were filled with approximately 3.5 g of adsorbents. The adsorbents were activated at 523 K and 0.5 psig for 10 h under a helium flow of 30 cm³/min. Characterization gases (oxygen, argon, and mixtures thereof) were introduced by 1 mL pulse injections into the test columns.

The ability of RPZ-1 to produce a concentrated argon stream from an O₂/Ar mixture was further investigated using a continuous flow apparatus (Figure 5-2). The unit consisted of a single adsorbent bed equipped with a GC for the analysis of the outlet stream. The inlet stream was controlled by a four-port switching valve with two positions. One position connected a helium line to the adsorbent bed while the O₂/Ar line was connected to a pressure control needle valve. The second position connected the O₂/Ar line to the adsorbent bed. The flow rate of each gas (helium, oxygen, and argon) was adjusted by mass flow controllers (MFC). The experiments were conducted by first purging the bed with helium at a flow rate of 15 cm³/min. The flow of oxygen and argon was set at predetermined rates, and the pressure of the O₂/Ar stream was adjusted by the needle valve. Under optimal conditions, there was no pressure drop at the switching valve. After a complete purge of the adsorbents, the position of the switching valve was set so that the O₂/Ar mixture flowed through the adsorbent bed. Immediately after the

switching valve was set, the GC system was started and sampled the adsorbent bed outlet stream once per minute. The outlet stream was monitored until its composition was identical to the inlet stream composition. The bed was recycled by switching back to helium purge until no more oxygen or argon was detected in the outlet stream. The oxygen and argon composition of the outlet stream was analyzed by the GC. The molar fractions of oxygen and argon were calibrated independently using external standards.

The separation of oxygen and argon by adsorption on Ba-RPZ-1 was measured in a continuous flow system using both a 50-50% O₂/Ar mixture and a 95-5% O₂/Ar mixture. The bed dimensions were 0.5" OD and 17" in length. The chamber had a volume of 47 cm³, and contained slightly more than 30 g of the adsorbent. The total flow rate through the bed was 10 cm³/min, hence for the 50-50% O₂/Ar mixture, the flow rate of each gas was 5 cm³/min. Measurements were conducted with the bed at ambient temperature.

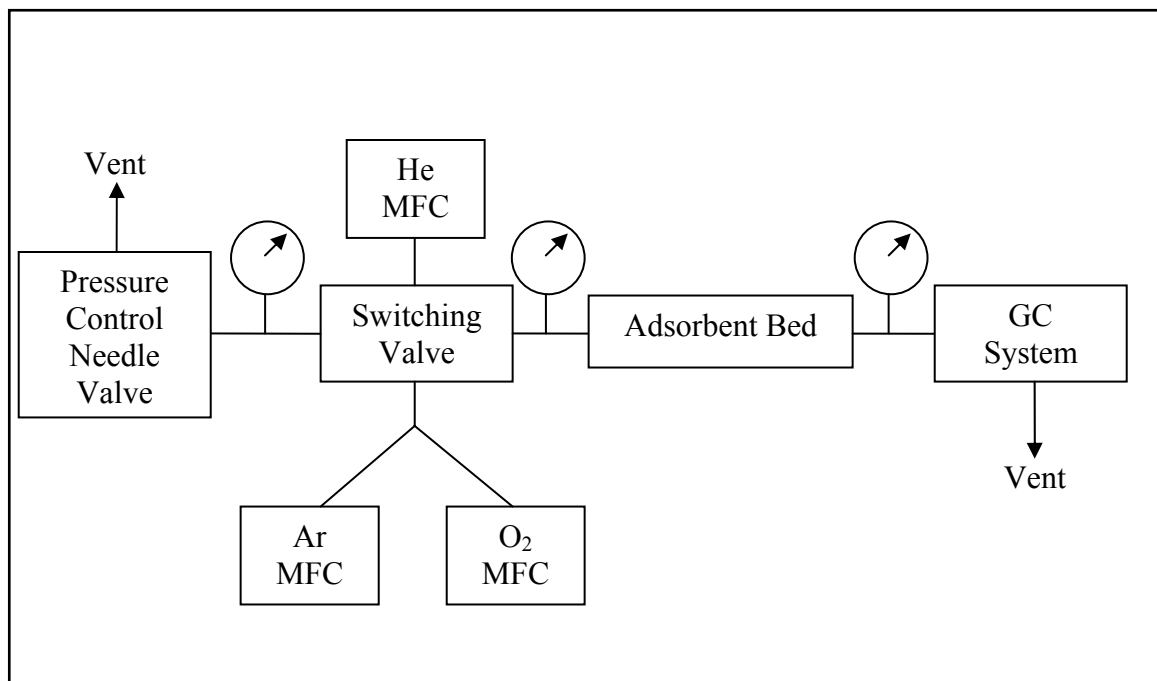


Figure 5-2. Block diagram of the laboratory-scale PSA apparatus employed for O₂/Ar breakthrough experiments.

Oxygen and argon adsorption isotherms were measured at 298, 303, and 308 K with a Rubotherm magnetic suspension balance (accuracy $\pm 1 \mu\text{g}$) that is integrated with a gravimetric high pressure (GHP) adsorption system constructed by VTI Corporation (Hialeah, FL). Test samples were activated at 473 K for 6 h under a vacuum of greater than 10^{-4} Torr. Buoyancy effects were corrected with a helium displacement isotherm taken at the same conditions as the oxygen and argon isotherms.

Kinetic experiments were also measured with the Rubotherm system. Weight change vs. time was measured in the pressure regimes of 40-70 and 70-100 kPa. Experimental conditions were identical to those used for collecting the equilibrium isotherms.

5.4 Results and Discussion

Figure 5-3a illustrates the chromatographic separation of a 1 mL mixture of 50-50% O₂/Ar on Ba-RPZ-1 at 303 K. Compared to the pure-gas chromatographic data (Figures 5-3c and 5-3d), it is clear that the first peak represents argon, while the second peak represents oxygen. The same peak identification can be assigned to Figure 5-3b, which illustrates the separation of a 1 mL mixture of 90-10% O₂/Ar on the same column. Ba-RPZ-1 clearly demonstrates a clean resolution of oxygen from argon under the experimental conditions. The oxygen and argon retention times (Figure 5-3) are almost identical regardless of the composition of the O₂/Ar mixtures. For comparison, an identically-sized column of Ba-ETS-4 was tested with a 1 mL mixture of 50-50% O₂/Ar and showed no resolution of these gases as seen in Figure 5-3e.

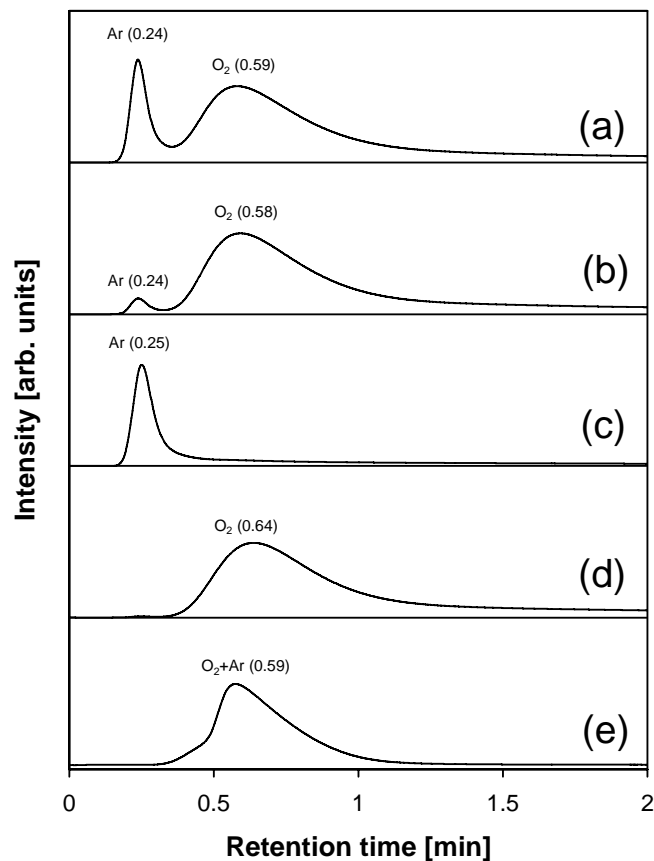


Figure 5-3. IGC profiles at 303 K by injecting (a) 50-50% O₂/Ar, (b) 90-10% O₂/Ar, (c) pure argon, and (d) pure oxygen in a column of Ba-RPZ-1 and (e) 50-50% O₂/Ar in a column of Ba-ETS-4.

The experimental results obtained from the continuous flow unit for a 50-50% O₂/Ar mixture and a 95-5% O₂/Ar mixture are presented in Figures 5-4 and 5-5, respectively. Figures 5-4 and 5-5 depict the relative oxygen and argon mole fractions at the outlet of the adsorbent bed. All data points in Figures 5-4 and 5-5 represent the mean values of triplicate chromatographic analyses.

For the 50-50% O₂/Ar mixture (Figure 5-4), oxygen was not detected at the outlet stream until the mixture had flowed for 8 minutes (the 4 minute offset was due to the analysis time). Only argon was noted in the product stream until the oxygen broke through after 8 minutes. For the 95-5% O₂/Ar mixture (Figure 5-5), the oxygen did not appear in the outlet stream until 7 minutes after the flow was initiated.

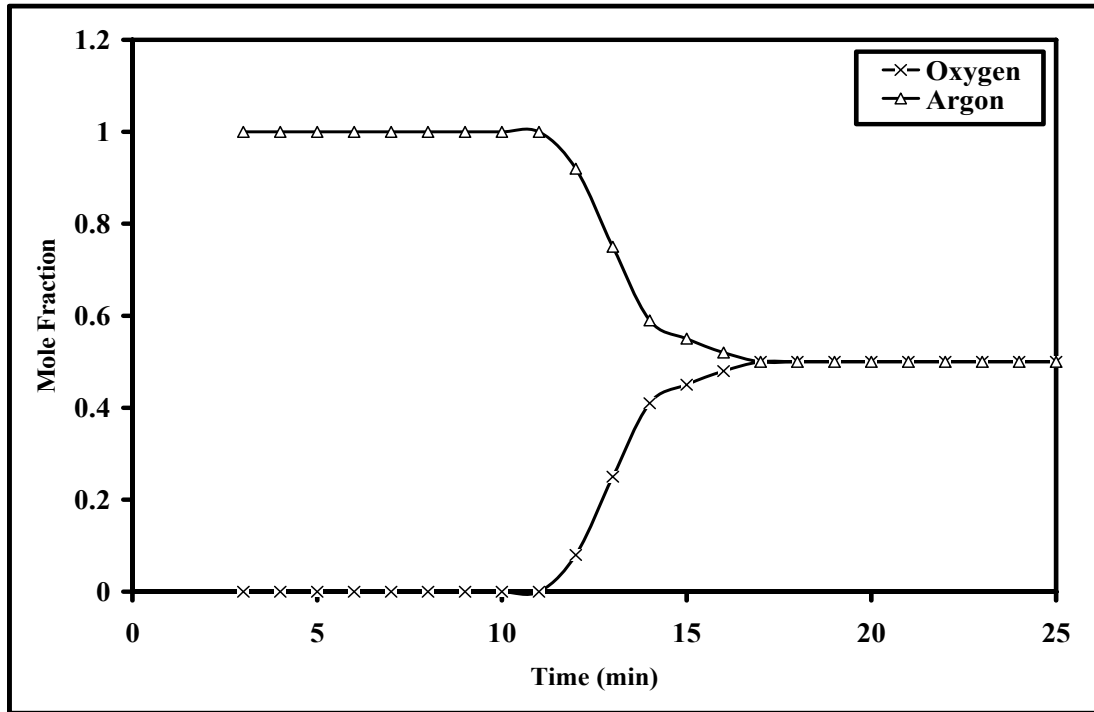


Figure 5-4. Compositional analysis (mole fraction) as a function of time at the outlet of the Ba-RPZ-1 adsorbent bed with a continuous inlet mixture of 50-50% O₂/Ar.

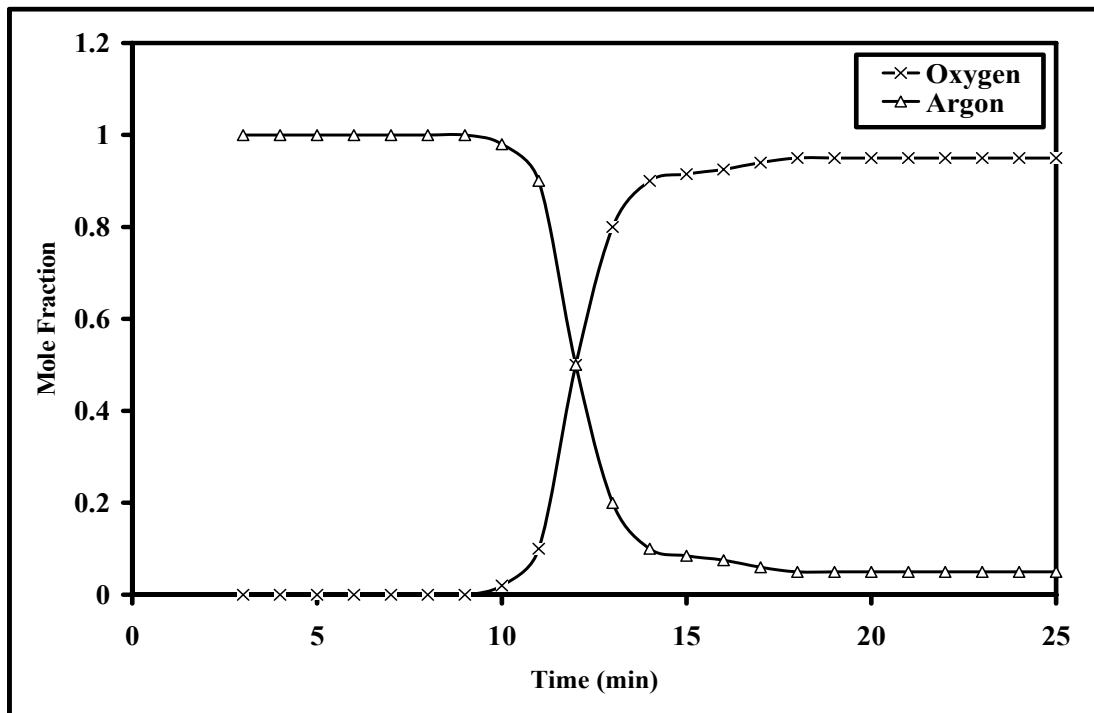


Figure 5-5. Compositional analysis (mole fraction) as a function of time at the outlet of the Ba-RPZ-1 adsorbent bed with a continuous inlet mixture of 95-5% O₂/Ar.

Figure 5-6 shows the oxygen and argon equilibrium adsorption isotherms at 303 K for Ba-RPZ-1. The total adsorption capacities for oxygen and argon are similar. At 298, 303, and 308 K, oxygen and argon isotherms in the range of 1-200 kPa can be described accurately by the classical Langmuir equation:

$$n = \frac{n_m \cdot K_L \cdot p}{1 + K_L \cdot p} \quad (5-1)$$

Where n is the adsorbate concentration (mol/kg) at the pressure p (kPa), and K_L and n_m are fitting parameters. The product $K_L \cdot n_m$ equals the Henry's law constant (K), observed at the low pressure linear region of the isotherm.

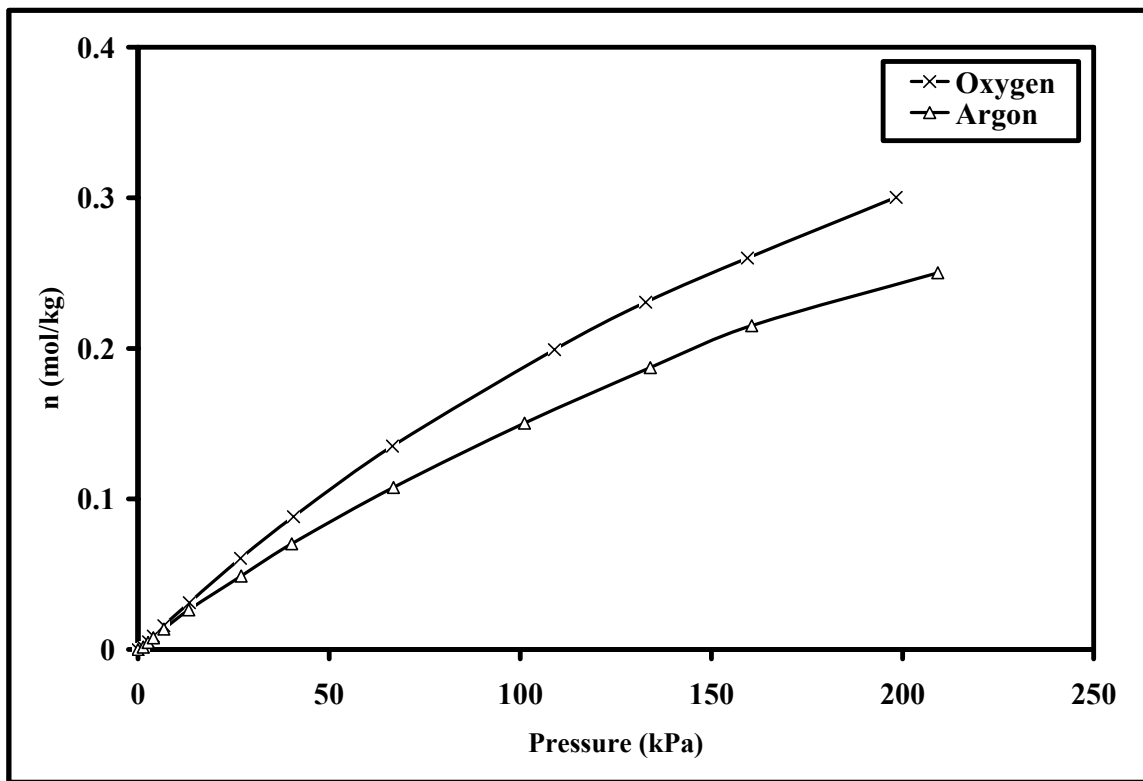


Figure 5-6. Oxygen and argon adsorption isotherms at 303 K for Ba-RPZ-1.

Statistical analysis began with a calculation of the parameters K_L and n_m for all the isotherms. We then obtained an average value for the monolayer capacity n_m (0.7031

mol/kg). For statistical reasons, the isotherms were fitted again by restricting n_m to the averaged value. Finally, the values of $K_L \cdot n_m$ are recalculated and are listed in Table 5-1, together with the estimated standard deviations (σ) for the fittings:

$$\sigma = \sqrt{\frac{\sum (n_{\text{exp}} - n_{\text{calc}})^2}{N - 2}} \quad (5-2)$$

Where n_{exp} is the experimental adsorbate concentration at pressure p , n_{calc} is the adsorbate concentration calculated from the Langmuir equation at the same pressure, and N is the number of experimental points.

Table 5-1. Equilibrium and Kinetic Parameters for the Adsorption of O₂/Ar on Ba-RPZ-1

| Gas | T (K) | 10 ³ ·K (mol/kg·kPa) | 10 ³ ·σ | 10 ³ ·D/r ² (s ⁻¹) | |
|--------|-------|---------------------------------|--------------------|--|------------|
| | | | | 40-70 kPa | 70-100 kPa |
| Oxygen | 298.5 | 2.542 | 2.1 | 2.129 | 2.502 |
| | 303.3 | 2.266 | 2.4 | 2.569 | 2.436 |
| | 308.2 | 1.903 | 0.9 | 2.250 | 2.398 |
| Argon | 298.5 | 2.164 | 2.2 | 0.280 | 0.346 |
| | 303.2 | 1.955 | 0.9 | 0.319 | 0.400 |
| | 308.2 | 1.670 | 1.8 | 0.424 | 0.502 |

The thermodynamic selectivity of oxygen over argon can be calculated as the ratio of the respective Henry's law constants. According to the values listed in Table 5-1, the thermodynamic selectivities of oxygen (over argon) are 1.17, 1.16, and 1.14 at 298, 303, and 308 K, respectively. The Henry's law constants were also used to estimate the limiting isosteric heats of adsorption by means of the Van't Hoff isobar. The heat of adsorption for oxygen (22.8 kJ/mol) is only slightly higher than for argon (20.5 kJ/mol). The heats of adsorption for oxygen and argon on Ba-RPZ-1 are slightly higher than those reported for carbon molecular sieves commercialized by Air Products and Chemicals Inc. (18.6±0.4 and 18.3±0.7 kJ/mol for oxygen and argon, respectively).¹³ With such similar values for thermodynamic selectivity and heat of adsorption, the separation of oxygen

and argon observed on Ba-RPZ-1 in the IGC experiments cannot be explained in terms of equilibrium parameters.

However, a substantial difference in the rate of adsorption for oxygen and argon on Ba-RPZ-1 is observed. As shown in the uptake curves of Figure 5-7 (fractional uptake vs. time), equilibrium capacity is achieved much faster in the case of oxygen than argon.

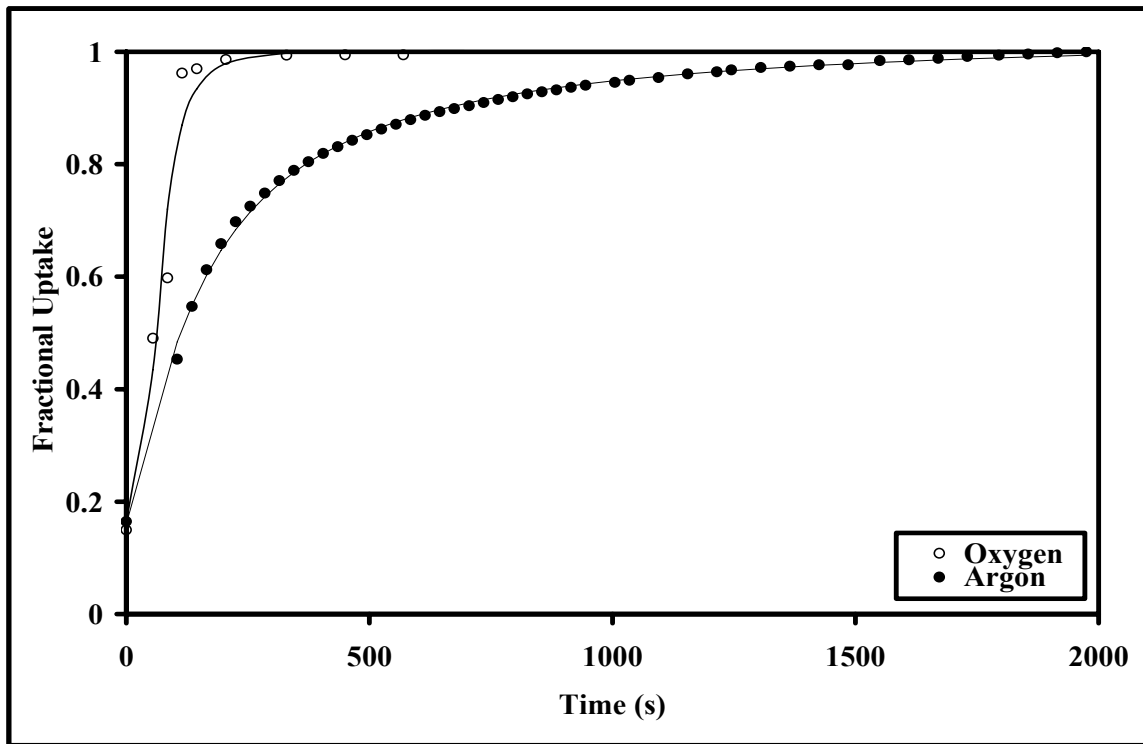


Figure 5-7. Fractional uptake curves for oxygen and argon at 303 K from 70-100 kPa.

The fractional uptake in Figure 5-7 is defined as $(w_t - w_0)/(w_{eq} - w_0)$, where w_0 is the adsorbate loading at the beginning of the pressure step (time zero), w_t is the adsorbate loading at time t (sec), and w_{eq} is the equilibrium adsorbate loading at the end of the pressure step. The experimental kinetic data were fitted to an expression describing the diffusion of gases inside the zeolite channels:¹¹

$$\frac{w_t}{w_{eq}} = 1 - \frac{6}{\pi} \sum_{n=1}^{\infty} \frac{\exp(-n^2 \pi^2 Dt / r^2)}{n^2} \quad (5-3)$$

Where D/r^2 is the rate constant for the process. The values of D/r^2 were calculated by fitting the experimental data to the expression above for oxygen and argon at 298, 303, and 308 K for the two pressure steps (40-70 and 70-100 kPa) that are listed in Table 5-1. The ratio of the diffusion rate constants for oxygen and argon are in the range of 5-8 under these conditions. The kinetic selectivity (α) of oxygen over argon can be calculated by applying the following expression:¹¹

$$\alpha = \frac{K_A}{K_B} \sqrt{\frac{D_A}{D_B}} \quad (5-4)$$

Where K is the Henry's law constants listed in Table 5-1. The kinetic selectivity of oxygen over argon for Ba-RPZ-1 is in the range of 2.5-3.3. This represents the minimal value because of experimental limitations. The rate of argon uptake is reasonably well-defined, but for oxygen, the beginning of the uptake curve is poorly-defined because the gas adsorption is faster than the balance equilibration time. Therefore, it is possible that the values of D/r^2 determined are too small in the case of oxygen and the true kinetic selectivity vs. argon may be even higher. The energy associated with the diffusion of argon into the adsorbent can be calculated by applying the Arrhenius equation. These calculations result in values of 32.0 and 28.8 kJ/mol in the pressure regimes of 40-70 and 70-100 kPa, respectively. These values are lower than the values calculated for a carbon molecular sieve commercialized by Air Products and Chemicals Inc., which was 41.4±3.8 and 43.3±2.9 kJ/mol for the pressure steps between 30-50 and 50-100 kPa, respectively.¹³

Our experimental data clearly indicate that the separation of O₂/Ar mixtures is due to kinetics rather than thermodynamics, presumably associated with the molecular sieve effect. However, most reference literatures indicate that the size difference between

oxygen and argon lies within 0.06 and 0.08 Å, which is too small to explain the observed molecular sieve effect.

The size of an adsorbable gas molecule is usually assessed by its effective kinetic diameter. The concept of effective kinetic diameter has become the most commonly accepted measure of a gas particle size interacting with molecular sieve type adsorbents.²⁷ Effective kinetic diameters have been reported by Breck,²⁷ Hirschfelder et al.,²⁸ as well as by Sircar and Myers.²⁹ Their values for oxygen, argon, and nitrogen are listed in Table 5-2.

Table 5-2. Effective Kinetic Diameters and Molecular Dimensions of Oxygen, Argon, and Nitrogen

| Gas | Effective Kinetic Diameter (Å) | | MIN-1 ³¹ | MIN-2 ³¹ | 3 rd Dimension ³¹ |
|----------|--------------------------------|----------------------|---------------------|---------------------|---|
| | Breck ²⁷ | Sircar ²⁹ | (Å) | (Å) | (Å) |
| Oxygen | 3.46 | 3.47 | 2.930 | 2.985 | 4.052 |
| Argon | 3.40 | 3.54 | 3.510 | 3.630 | N/A |
| Nitrogen | 3.64 | 3.64-3.80 | 2.991 | 3.054 | 4.046 |

Generally, the effective kinetic diameter of a gas is defined by a Lennard-Jones 6-12 type function describing the potential energy of two interacting objects $\phi(r)$ as a function of their distance, measured by the separation of their nuclei (r):

$$\phi(r) = 4\epsilon \left[\left(\frac{\sigma}{r} \right)^{12} - \left(\frac{\sigma}{r} \right)^6 \right] \quad (5-5)$$

The exponent of the attractive term expressed as a power of 6 of the function is well-defined in theory, accounting for induced dipole-dipole interactions between objects. The exponent of the repulsive term expressed as a power of 12 must be chosen empirically. This semi-empirical function works well for gas-gas interactions, describing the behavior of a number of gases when no adsorbent is present.

The effective kinetic diameter of interacting objects (σ) is the size parameter corresponding to zero potential energy, not the minimum of the potential energy, resulting from the interaction. The minimum of the potential energy, σ , is at r_{\min} , expressed as:

$$r_{\min} = 2^{1/6} \sigma \quad (5-6)$$

The factor $2^{1/6}$ is strictly a mathematical consequence of the Lennard-Jones 6-12 function chosen. The σ values can also be calculated from experimental second virial coefficients.²⁸

The Lennard-Jones model depicts atoms as soft spheres. If the interatomic distance is smaller than σ , the potential energy increases steeply. While a shorter distance of approach is not favored, it is not forbidden. The adsorbent framework is not a rigid structure. Molecular sieve frameworks are held together by strong covalent bonds, and these bonds vibrate. Within a molecule, the atom-to-atom distances and the bond angles can change with external conditions, especially in the presence of an adsorbent.³⁰ Therefore, the effective kinetic diameter of a molecule is not an absolute, universal size parameter for gas-adsorbent interactions under all conditions.

An alternative approach to the kinetic diameter was proposed by Webster et al.^{31,32} to address the problem of interaction between an adsorbate and a crystalline pore for non-spherical adsorbate molecules. This approach considers not only the size of the pore but its shape as well. Instead of a single size parameter, a set of parameters for each adsorbate is considered based on quantum chemistry and Van der Waals sizes. The first size parameter, MIN-1, is the smallest cross section of the gas molecule. The second size parameter, MIN-2, is the next largest dimension of the gas molecule. MIN-1 and MIN-2 are chosen to be perpendicular.

The MIN-2 size parameter for argon in Table 5-2 is reported as 3.63 Å, which is larger than its effective kinetic diameter. The MIN-2 values for oxygen and nitrogen are both much smaller than their corresponding effective kinetic diameters. According to this model, the observed adsorption of oxygen is explained by the oriented interaction between the zeolite window and the oxygen molecule. Instead of a randomly oriented molecule, this model anticipates oxygen approaching the pore along the diatomic axis of the molecule (head-on), exposing a much smaller molecular cross section than the effective kinetic diameter. Oxygen can pass through the window with this orientation. Eventually, many oxygen molecules interact with the window in this favored orientation. Argon, on the other hand, behaves as a solid sphere. Its orientation does not influence its apparent size. Because of this, oxygen, even with a larger effective kinetic diameter than argon, can enter the crystalline pores of a molecular sieve more rapidly than argon.

5.5 Conclusions

A halogen containing titanium silicate molecular sieve adsorbent, Ba-RPZ-1, was shown to have the ability to cleanly resolve mixtures of oxygen and argon at room temperature. This separation is the result of adsorption kinetics with oxygen penetrating the crystalline lattice of Ba-RPZ-1 much more readily than argon. Inorganic crystalline adsorbents with the ability to resolve oxygen and argon more rapidly and reproducibly than carbon molecular sieves could find wide spread applications in oxygen purification and argon generation, especially in newer rapid cycle PSA processes.

5.6 References

- (1) Barrer, R. M.; Robins, A. B. *Trans. Faraday Soc.* **1953**, *49*, 807.
- (2) Lard, E. W.; Horn, R. C. *Anal. Chem.* **1960**, *32*, 878.
- (3) Kovak, K. W.; Agrawal, R.; Peterson, J.C. Method of Purifying Argon through Cryogenic Adsorption. U.S. Patent 5,159,816, November 3, 1992.
- (4) Sebastian, J.; Jasra, R. V. *Ind. Eng. Chem. Res.* **2005**, *44*, 8014.
- (5) Walker, J. A. J. *Nature* **1966**, *209*, 197.
- (6) Karlsson, B.-M. *Anal. Chem.* **1966**, *38*, 668.
- (7) Maroulis, P. J.; Coe, C. G. *Anal. Chem.* **1989**, *61*, 1112.
- (8) Pollock, G. E.; O'Hara, D.; Hollis, O. L. *J. Chromatogr. Sci.* **1984**, *22*, 343.
- (9) Pollock, G. E. *J. Chromatogr. Sci.* **1986**, *24*, 173.
- (10) Rege, S. U.; Yang, R. T. *Adsorption* **2000**, *6*, 15.
- (11) Jin, X.; Malek, A.; Farooq, S. *Ind. Eng. Chem. Res.* **2006**, *45*, 5775.
- (12) Ma, Y. H.; Sun, W.; Bhandakar, M.; Wang, J.; Miller, G. W. *Sep. Technol.* **1991**, *1*, 90.
- (13) Reid, C. R.; O'koye, I. P.; Thomas, K. M. *Langmuir* **1998**, *14*, 2415.
- (14) Reid, C. R.; Thomas, K. M. *Langmuir* **1999**, *15*, 3206.
- (15) Kuznicki, S. M.; Bell, V. A.; Petrovic, I.; Blosser, P. W. Separation of Nitrogen from Mixtures thereof with Methane Utilizing Barium Exchanged ETS-4. U.S. Patent 5,989,316, November 23, 1999.
- (16) Kuznicki, S. M.; Bell, V. A.; Petrovic, I.; Desai, B. T. Small-Pored Crystalline Titanium Molecular Sieve Zeolites and their Use in Gas Separation Processes. U.S. Patent 6,068,682, May 30, 2000.
- (17) Kuznicki, S. M.; Bell, V. A.; Nair, S.; Hillhouse, H. W.; Jacobinas, R. M.; Braunbarth, C. M.; Toby, B. H.; Tsapatsis, M. *Nature* **2001**, *412*, 720.
- (18) Kuznicki, S. M.; Dang, D.; Hayhurst, D. T.; Thrush, K. A. Use of Crystalline Molecular Sieves Containing Charged Octahedral Sites in Removing Volatile Organic Compounds from a Mixture of the Same. U.S. Patent 5,346,535, September 13, 1994.

- (19) Sebastian, V.; Lin, Z.; Rocha, J.; Tellez, C.; Santamaria, J.; Coronas, J. *Chem. Commun.* **2005**, 3036.
- (20) Sebastian, V.; Lin, Z.; Rocha, J.; Tellez, C.; Santamaria, J.; Coronas, J. *Chem. Mater.* **2006**, *18*, 2472.
- (21) Sandomirskii, P. A.; Belov, N. V. *Sov. Phys. Crystallogr.* **1979**, *24*, 686.
- (22) Philippou, A.; Anderson, M. W.; *Zeolites* **1996**, *16*, 98.
- (23) Cruciani, G.; De Luca, P.; Nastro, A.; Pattison, P. *Microporous Mesoporous Mater.* **1998**, *21*, 143.
- (24) Lin, C. C. H.; Sawada, J. A.; Wu, L.; Haastrup, T.; Kuznicki, S. M. *J. Am. Chem. Soc.* **2009**, *131*, 609.
- (25) Kuznicki, S. M.; Sawada, J. A.; Rode, E. J.; Lin, C. C. H. Titanium Silicate Materials, Method for their Manufacture, and Method for Using Such Titanium Silicate Materials for Adsorptive Fluid Separations. World Patent No. WO/2008/002463, March 1, 2008.
- (26) Kuznicki, S. M. Preparation of Small-Pored Crystalline Titanium Molecular Sieve Zeolites. U.S. Patent 4,938,939, July 3, 1990.
- (27) Breck, D. W. *Zeolite Molecular Sieves: Structure, Chemistry and Use*; Wiley: New York, 1974.
- (28) Hirschfelder, J. O.; Curtiss, C. F.; Bird, R. B. *Molecular Theory of Gases and Liquids*; Wiley: New York, 1964.
- (29) Sircar, S.; Myers, A. L. In *Handbook of Zeolite Science and Technology*; Auerbach, S. M.; Carrado, K. A.; Dutta, P. K., Eds.; Gas Separation by Zeolites; Marcel Dekker Inc.: New York, 2003; pp 1063-1104.
- (30) Kopelevich, D. I.; Chang, H. C. *J. Chem. Phys.* **2001**, *115*, 9519.
- (31) Webster, C. E.; Drago, R. S.; Zerner, M. C. *J. Am. Chem. Soc.* **1998**, *120*, 5509.
- (32) Webster, C. E.; Drago, R. S.; Zerner, M. C. *J. Phys. Chem. B* **1999**, *103*, 1242.
- (33) Webster, C. E.; Cottone III, A.; Drago, R. S. *J. Am. Chem. Soc.* **1999**, *121*, 12127.

**SEPARATION OF ETHYLENE AND ETHANE BY
ADSORPTION ON SMALL-PORED TITANIUM SILICATE
MOLECULAR SIEVES[†]**

[†] A version of this chapter has been submitted for publication. Anson, A.; Lin, C. C. H.; Kuznicki, T. M.; Kuznicki, S. M. *Chem. Eng. Sci.* **2009**.

6.1 Summary

Adsorptive separation of ethylene and ethane represents a less energy-intensive alternative to current industrial separation practices done by sub-ambient distillation methods. In this approach, ethylene and ethane are separated by inverse-phase gas chromatographic and gravimetric isotherm techniques on cation-exchanged forms of ETS-4 and RPZ-1 titanium silicate molecular sieves. Inverse-phase gas chromatography reveals that kinetic separation of ethylene from ethane is possible using ETS-4 and RPZ-1 adsorbents exchanged with Zn or mixed Ca/H. Chromatographic selectivities of 4-40 for the adsorptive separation of ethylene and ethane were measured for these adsorbents, and the limiting selectivity calculated from the gravimetric adsorption isotherms was between 4 and 12. In accordance with the ideal adsorbed solution theory (IAST), C_2H_4/C_2H_6 selectivity increases with pressure in all of the cases studied, especially for Sr- and Ba-ETS-4. Due to the molecular sieving character of the adsorbents, size effects were observed for the adsorption of ethylene and ethane, and contact time between the adsorbent and the gas mixture was a key factor in the separation of the gases. ETS-4 and RPZ-1 exchanged with Zn or Ca/H are excellent candidates for the commercial adsorptive separation of ethylene and ethane.

6.2 Introduction

The industrial separation of ethylene and ethane is a key stage in the synthesis of ethylene-based polymers. The C_2H_4/C_2H_6 separation process is usually carried out by distillation at sub-ambient temperatures and requires intensive energy input. Adsorptive processes utilizing chemically-selective adsorbents, including pressure swing adsorption, have been proposed as alternatives to sub-ambient distillation.^{1,2} For example, adsorptive separation of ethylene and ethane on ETS-10, a large-pored titanium silicate, is highly favorable at ambient temperature.³ Size-selectivity does not contribute to the separation in this case, as ETS-10 is a synthetic molecular sieve with an average pore size of approximately 8 Å,⁴ which is larger than the kinetic diameters of both ethylene and ethane.

Alternately, size-selective separation of ethylene and ethane could be performed using ETS-4 or RPZ-1, two small-pored, synthetic analogs of the mineral zorite.⁵⁻⁷ ETS-4, a titanium silicate molecular sieve with an average pore size of 3-5 Å, is a proven size-selective adsorbent for small molecules of similar size.⁵ Following ion-exchange and thermal treatment, ETS-4 has been applied to multiple size-based separations, including O_2/Ar , N_2/CH_4 , and CH_4/C_2H_6 .⁸⁻¹¹ Reduced Pore Zorite (RPZ) is an analog of both ETS-4 and mineral zorite. The pore size of RPZ-1 is controlled by the level of structural chloride anions. Chloride anions progressively and systematically constrict the RPZ-1 pore size as their concentration in the framework increases, enabling the preparation of thermally-stable, size-selective materials.⁶ The isotherm profiles and adsorption strength for selected gases on both ETS-4 and RPZ-1 can be modified by ion-exchange of the extra-framework cations. Therefore, it may be possible to prepare an ideal adsorbent for the separation of ethylene and ethane by combining the size- and ion-selectivity of the adsorbents ETS-4 and RPZ-1.

In this investigation, we compare ethylene and ethane adsorption on ETS-4 and RPZ-1 by inverse-phase gas chromatography (IGC) and gravimetric isotherm measurements. The results are interpreted in terms of the physicochemical characteristics of the adsorbent

frameworks, the type of extra-framework cations, and the sieving effects that modify the adsorption kinetics for each gas.

6.3 Experimental Methods

ETS-4 was synthesized hydrothermally as previously described.^{5,11} In the as-synthesized form, sodium (Na) occupies most of the cationic sites within the framework. A typical sample of RPZ-1 titanium silicate was prepared by mixing 25.10 g of sodium silicate (28.80% SiO₂, 9.14% Na₂O, Fisher), 4.60 g of sodium hydroxide (97+% NaOH, Fisher), 3.00 g of potassium chloride (99% KCl, Fisher), and 16.30 g of titanium trichloride (20% TiCl₃, 6% HCl, Fisher). The mixture was stirred in a blender for 1 h, and then reacted in a 125 mL sealed autoclave (PARR Instruments) at 473 K for 48 h. The resultant material was washed with de-ionized water, and dried in a forced-air oven at 373 K.

Ion-exchanges were performed by exposing the as-synthesized molecular sieves (as <150 μm powders) to an excess of aqueous ionic solutions (i.e. BaCl₂, SrCl₂, or ZnCl₂) at 373 K with stirring for 24 h. The exchanged materials were washed with de-ionized water, and dried at 373 K.

Mixed cation forms of the titanium silicates (Ca/H-ETS-4 and Ca/H-RPZ-1) were prepared by first stirring the as-synthesized molecular sieves in concentration-controlled aqueous solutions of CaCl₂ (prepared by mixing 4 meq of CaCl₂ with 10 g of de-ionized water per gram of molecular sieve) at 373 K for 24 h. The partially-exchanged materials were then exposed to an HCl solution at pH 2 for 16 h at 293 K. The final products were washed with de-ionized water, and dried at 373 K.

IGC analysis was performed on a Varian 3800 gas chromatograph (GC) utilizing a thermal conductivity detector (TCD). Test adsorbents were packed into 10" long, 0.25" OD copper columns using a plastic funnel. The columns were filled with approximately 3 g of adsorbents, which were activated at 473 K and 0.5 psig for 10 h under 30 cm³/min

of helium flow. Mixtures of 50-50% C₂H₄/C₂H₆ were introduced into the test column by a 1 mL pulse injection under a helium flow of 15 cm³/min. Data were collected at 3 temperatures (303 K, 323 K, and 343 K) and a pressure of 0.5 psig.

Ethylene and ethane adsorption isotherms at 298 K were measured with a Rubotherm magnetic suspension balance (accuracy ±1 µg) that is integrated with a gravimetric high pressure (GHP) adsorption system constructed by VTI Corporation (Hialeah, FL). Test samples of approximately 130 mg were activated at 473 K for 6 h under a vacuum of greater than 10⁻⁴ Torr. Buoyancy effects were corrected with a helium displacement isotherm taken at the same conditions as the ethylene and ethane isotherms. The equilibration time was set at 1 h per data point.

6.4 Theoretical Background

Model analysis of the ethylene and ethane adsorption isotherms followed the procedures of Al-Baghli and Loughlin.³ Experimental isotherms were fitted by applying the UNILAN equation:

$$n = \frac{n_m}{2s} \ln \left(\frac{c + p \cdot \exp(s)}{c + p \cdot \exp(-s)} \right) \quad (6-1)$$

Where n is the amount adsorbed at the pressure p , and n_m , s , and c are model parameters. The parameter n_m is the theoretical monolayer capacity.³ Henry's law constant (K) can be calculated from the fitting parameters by the expression:

$$K = \frac{n_m}{c \cdot s} \sinh(s) \quad (6-2)$$

The selectivity of the adsorbent (α) in the Henry's law region (limiting selectivity) is defined as the ratio of the Henry's law constants of the pure-gas components:

$$\alpha = \frac{K_{\text{ethylene}}}{K_{\text{ethane}}} \quad (6-3)$$

The UNILAN equation is an empirical model used to characterize monolayer adsorption on heterogeneous surfaces. It is derived by assuming a patch-wise topography on the adsorbent surface and that each patch is ideal. The distribution of energy across each patch is assumed uniform. The UNILAN equation is a three-parameter isotherm suitable for describing hydrocarbon adsorption on activated carbons and zeolite molecular sieves.

In this investigation, the ideal adsorbed solution theory¹² was applied to model the binary adsorption of C₂H₄/C₂H₆. This theory has been successfully used to describe C₂H₄/C₂H₆ adsorption on titanium silicate ETS-10³ and on other related systems.^{12,13} The algorithm proposed by Valenzuela and Myers¹⁴ was applied for the IAST mathematical analysis. The UNILAN equation was used to model the pure compound isotherms for the IAST calculations. The selectivity of the adsorbent (α) for the adsorption of ethylene from a C₂H₄/C₂H₆ mixture at a given total pressure is calculated by:

$$\alpha_{ij} = \frac{y_i \cdot x_j}{y_j \cdot x_i} \quad (6-4)$$

Where x_i and y_i are the molar fractions of ethane in the adsorbed and gas phase, respectively, and x_j , y_j are the corresponding molar fractions of ethylene. At the limit of $p = 0$, the selectivity α_{ij} is equivalent to the Henry's law selectivity.

6.5 Results and Discussion

Figures 6-1 and 6-2 depict IGC profiles at optimal conditions obtained by the injection of C₂H₄/C₂H₆ mixtures into columns containing cation-exchanged ETS-4 and RPZ-1 materials. Retention times for ethylene and ethane generally decrease with temperature (Table 6-1), but the IGC profiles do not change qualitatively from 303 to 343 K.

Separation of ethylene and ethane can be clearly observed for columns containing zinc-exchanged ETS-4 and RPZ-1. Separation is also possible with Ca/H-ETS-4 and Ca/H-RPZ-1, although the ethylene and ethane signals are not baseline-resolved. Separation was not observed with strontium- or barium-exchanged materials.

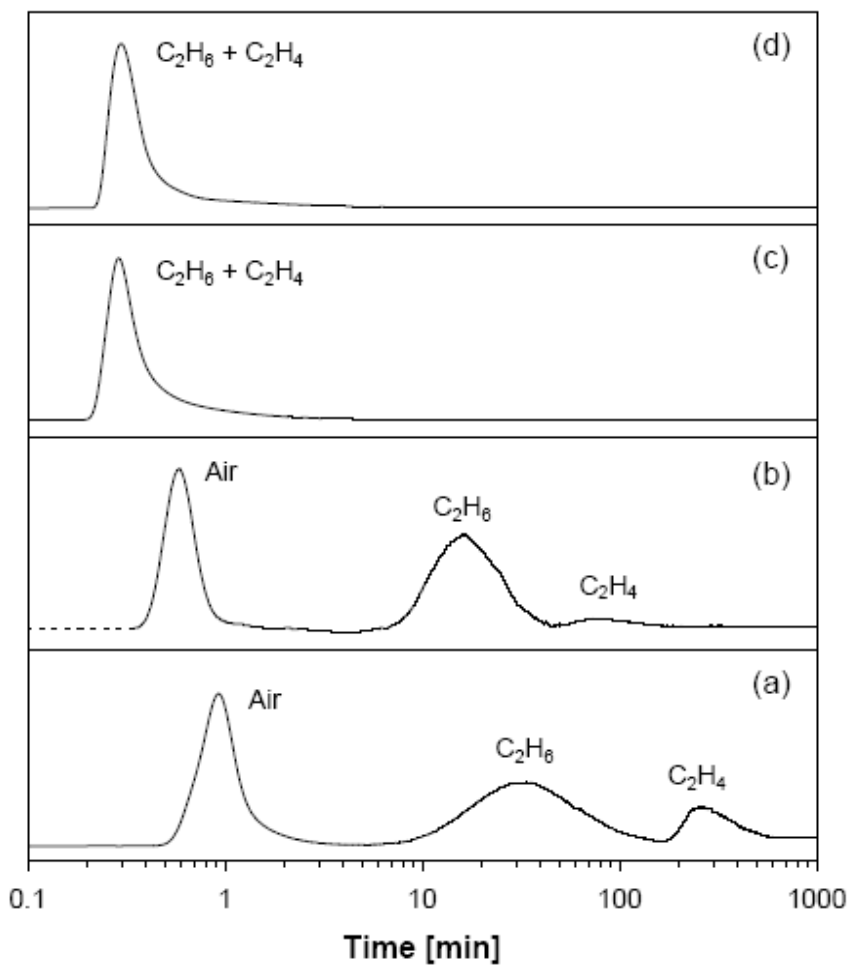


Figure 6-1. IGC profiles at 323 K for (a) Zn-, (b) Ca/H-, (c) Sr-, and (d) Ba-ETS-4.

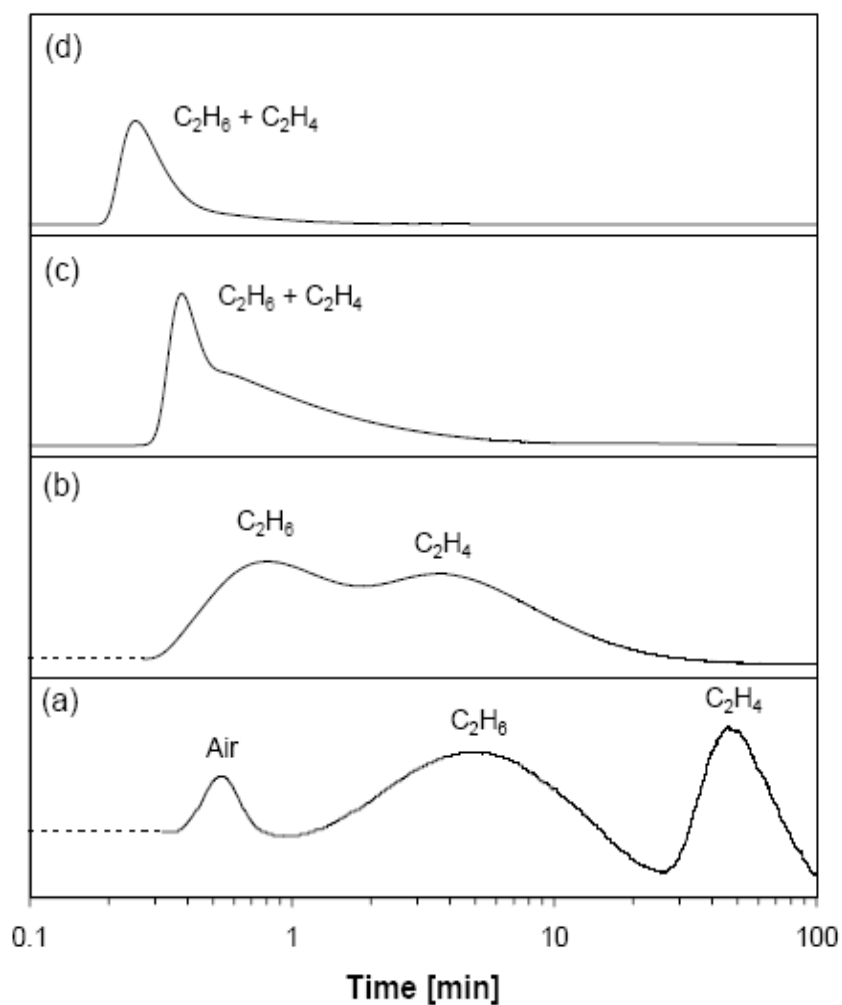


Figure 6-2. IGC profiles at 343 K for (a) Zn-, (b) Ca/H-, (c) Sr-, and (d) Ba-RPZ-1.

Table 6-1. IGC Retention Times for the Adsorption of Ethylene and Ethane on Cation-Exchanged ETS-4 and RPZ-1 at Selected Temperatures

| Adsorbent | Time [min] at 303 K | | | Time [min] at 323 K | | | Time [min] at 343 K | | |
|------------|---------------------|-------------------------------|-------------------------------|---------------------|-------------------------------|-------------------------------|---------------------|-------------------------------|-------------------------------|
| | Air | C ₂ H ₆ | C ₂ H ₄ | Air | C ₂ H ₆ | C ₂ H ₄ | Air | C ₂ H ₆ | C ₂ H ₄ |
| Zn-ETS-4 | 1.36 | 70.4 | 679 | 0.93 | 33.7 | 267 | 0.66 | 15.2 | 136 |
| Zn-RPZ-1 | 1.00 | 9.59 | 327 | 0.67 | 7.65 | 118 | 0.56 | 5.68 | 46.1 |
| Ca/H-ETS-4 | 0.85 | 38.1 | 244 | 0.59 | 16.1 | 73.7 | 0.50 | 8.75 | 34.1 |
| Ca/H-RPZ-1 | 0.70 | 2.06 | 20.6 | 0.48 | 1.30 | 8.62 | - | 0.83 | 3.62 |
| Sr-ETS-4 | - | 0.29 | - | - | 0.29 | - | - | 0.26 | - |
| Sr-RPZ-1 | - | 0.45 | 0.77 | - | 0.40 | - | - | 0.38 | - |
| Ba-ETS-4 | - | 0.33 | - | - | 0.30 | - | - | 0.28 | - |
| Ba-RPZ-1 | - | 0.38 | - | - | 0.31 | - | - | 0.25 | - |

Ethylene and ethane retention times for ETS-4 and RPZ-1 decrease with cation-exchange in the order of Zn > Ca/H > Sr \approx Ba (Table 6-1). Retention times for strontium- and barium-exchanged ETS-4 and RPZ-1 are very short, implying that ethylene and ethane molecules are not adsorbed. The pores of the strontium- and barium-exchanged materials are apparently too constricted to allow ethylene and ethane to reach the intrazeolitic adsorption sites in the short time that the gas mixture is in contact with the adsorbent in the chromatographic column.

Retention times for Zn- and Ca/H-RPZ-1 are shorter than for Zn- and Ca/H-ETS-4, respectively (Table 6-1). C₂H₄/C₂H₆ selectivity calculated from the IGC data for RPZ-1 is higher than for ETS-4, especially at the lowest temperature (Table 6-2). The highest selectivity of C₂H₄/C₂H₆, nearly 38, was obtained by Zn-RPZ-1.

Table 6-2. Limiting Selectivity (α) Calculated from Gravimetric Measurements at 298 K and IGC Measurements at 303 K, 323 K, and 343 K

| Adsorbent | α (298 K) | α (303 K) | α (323 K) | α (343 K) |
|------------|------------------|------------------|------------------|------------------|
| Zn-ETS-4 | 4.68 | 9.8 | 8.1 | 9.3 |
| Zn-RPZ-1 | 4.44 | 37.9 | 16.8 | 8.9 |
| Ca/H-ETS-4 | 10.3 | 6.5 | 4.7 | 4.1 |
| Ca/H-RPZ-1 | 5.31 | 14.6 | 9.9 | 4.4 |
| Sr-ETS-4 | 11.5 | - | - | - |
| Sr-RPZ-1 | 8.61 | 1.7 | - | - |
| Ba-ETS-4 | 7.92 | - | - | - |
| Ba-RPZ-1 | 8.87 | - | - | - |

Figures 6-3 and 6-4 depict gravimetric adsorption isotherms for ethylene and ethane on cation-exchanged ETS-4 and RPZ-1, respectively. A good correlation was obtained when the experimental data were fitted to the three-parameter UNILAN adsorption isotherm model. The three UNILAN parameters calculated for the isotherms (Figures 6-3 and 6-4) are listed in Tables 6-3 and 6-4, together with the Henry's law constants (K) calculated from the UNILAN parameters. As expected, the values of the Henry's law constants for zinc-exchanged ETS-4 and RPZ-1 are much higher than for the samples exchanged with Ca, Sr, and Ba.

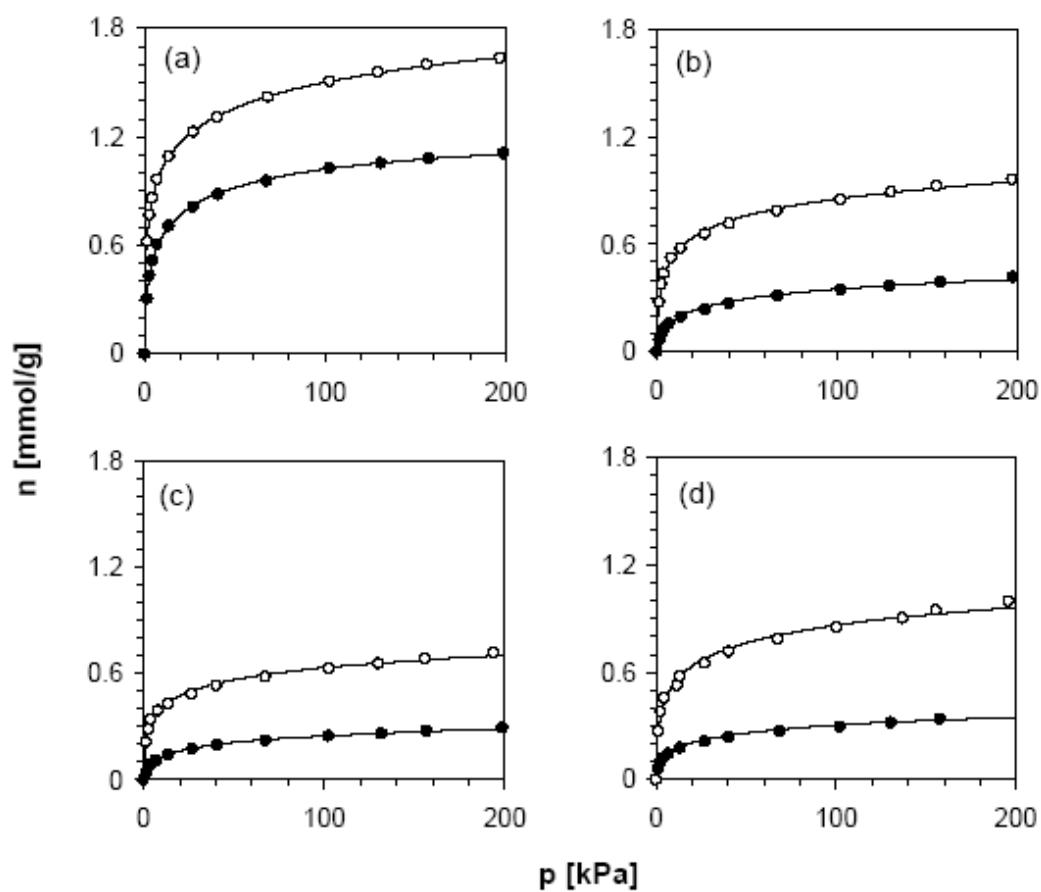


Figure 6-3. Ethylene (white circles) and ethane (black circles) adsorption isotherms at 298 K for (a) Zn-, (b) Ca/H-, (c) Sr-, and (d) Ba-ETS-4.

Table 6-3. UNILAN Parameters for Ethylene Adsorption

| Adsorbent | n_m [mmol/g] | s | c [kPa] | K [mmol/g kPa] |
|------------|----------------|------|-------------------|----------------|
| Zn-ETS-4 | 2.85 | 6.95 | 69.0 | 3.10 |
| Zn-RPZ-1 | 1.79 | 4.96 | 8.14 | 3.16 |
| Ca/H-ETS-4 | 3.72 | 13.6 | $1.57 \cdot 10^5$ | 0.70 |
| Ca/H-RPZ-1 | 3.48 | 10.6 | $2.33 \cdot 10^4$ | 0.28 |
| Sr-ETS-4 | 2.51 | 12.6 | $5.21 \cdot 10^4$ | 0.57 |
| Sr-RPZ-1 | 2.22 | 11.5 | $3.23 \cdot 10^4$ | 0.29 |
| Ba-ETS-4 | 3.51 | 12.3 | $5.18 \cdot 10^4$ | 0.61 |
| Ba-RPZ-1 | 0.57 | 3.50 | 19.9 | 0.14 |

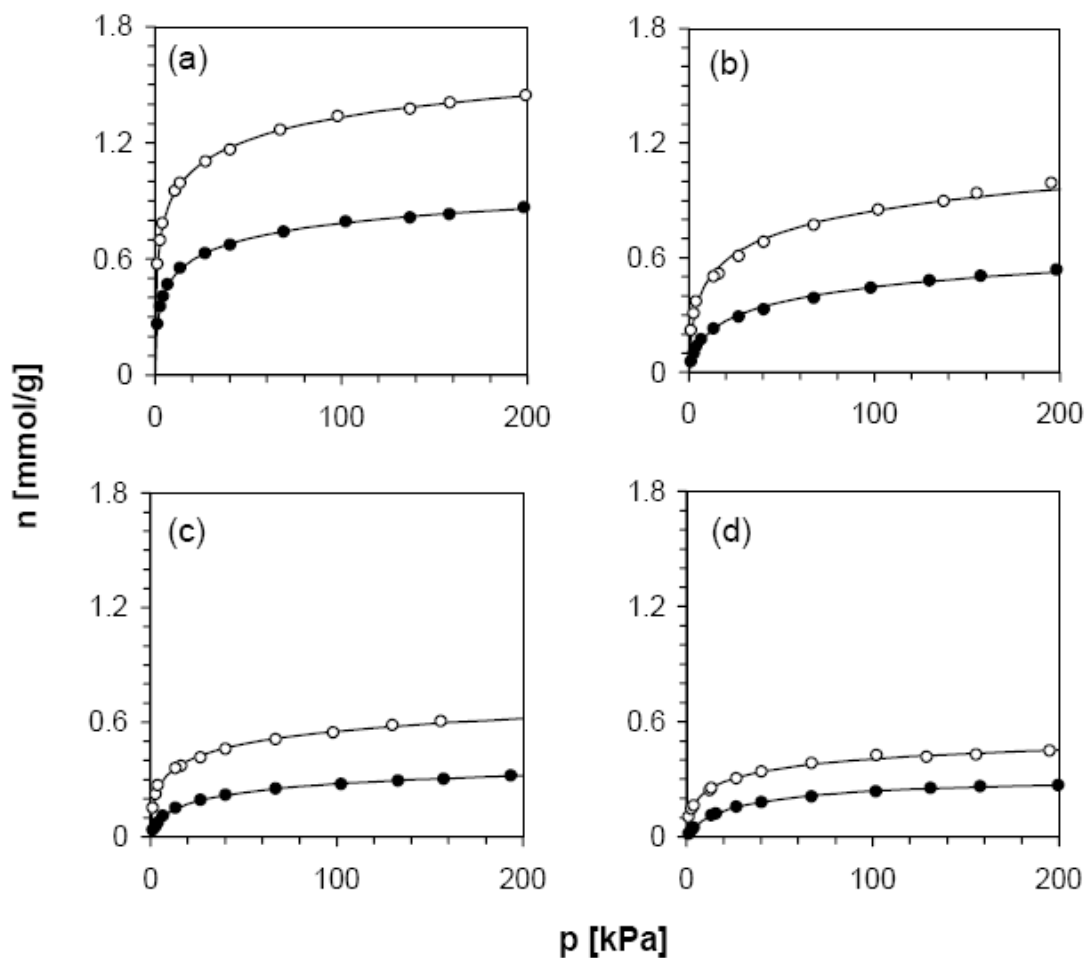


Figure 6-4. Ethylene (white circles) and ethane (black circles) adsorption isotherms at 298 K for (a) Zn-, (b) Ca/H-, (c) Sr-, and (d) Ba-RPZ-1.

Table 6-4. UNILAN Parameters for Ethane Adsorption

| Adsorbent | n_m [mmol/g] | s | c [kPa] | K [mmol/g kPa] |
|------------|----------------|------|-------------------|------------------|
| Zn-ETS-4 | 1.27 | 3.49 | 8.99 | 0.66 |
| Zn-RPZ-1 | 1.08 | 4.29 | 12.9 | 0.71 |
| Ca/H-ETS-4 | 2.75 | 17.7 | $5.55 \cdot 10^7$ | 0.07 |
| Ca/H-RPZ-1 | 2.60 | 11.2 | $1.60 \cdot 10^5$ | 0.05 |
| Sr-ETS-4 | 1.37 | 12.5 | $2.98 \cdot 10^5$ | 0.05 |
| Sr-RPZ-1 | 0.43 | 2.88 | 38.6 | 0.03 |
| Ba-ETS-4 | 2.08 | 16.4 | $1.10 \cdot 10^7$ | 0.08 |
| Ba-RPZ-1 | 0.32 | 1.47 | 29.3 | 0.02 |

Limiting selectivity (α) values for the separation of C_2H_4/C_2H_6 , as determined from gravimetric isotherm measurements, are listed in Table 6-2. Adsorption of ethylene is thermodynamically favored over ethane in all of the samples. Limiting selectivity varies

only slightly between the adsorbent samples, suggesting that the differences observed by the IGC analysis may be attributed to kinetic sieving effects, possibly related to the modifications of pore size induced by cation-exchange.

Figures 6-5 and 6-6 illustrate C_2H_4/C_2H_6 selectivity models for the cation-exchanged ETS-4 and RPZ-1 adsorbents at pressures up to 1000 kPa (10 bar), based on IAST calculations. Selectivity increases with pressure for all ETS-4 and RPZ-1 materials, particularly Sr- and Ba-ETS-4. In these cases, selectivity is predicted to increase to above 100 at 1000 kPa. Size effects could be playing an important role in the adsorption of ethylene and ethane at high pressures.

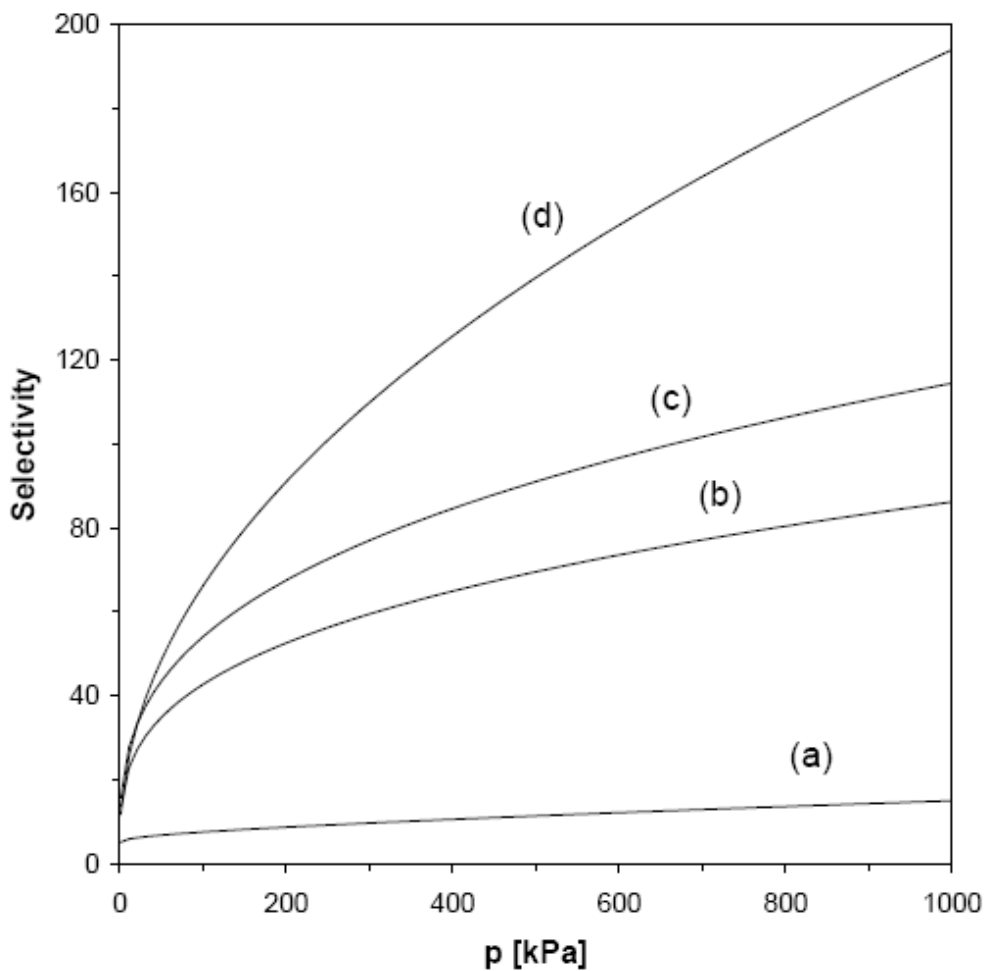


Figure 6-5. IAST model for C_2H_4/C_2H_6 selectivity at 298 K for (a) Zn-, (b) Ca/H-, (c) Sr-, and (d) Ba-ETS-4.

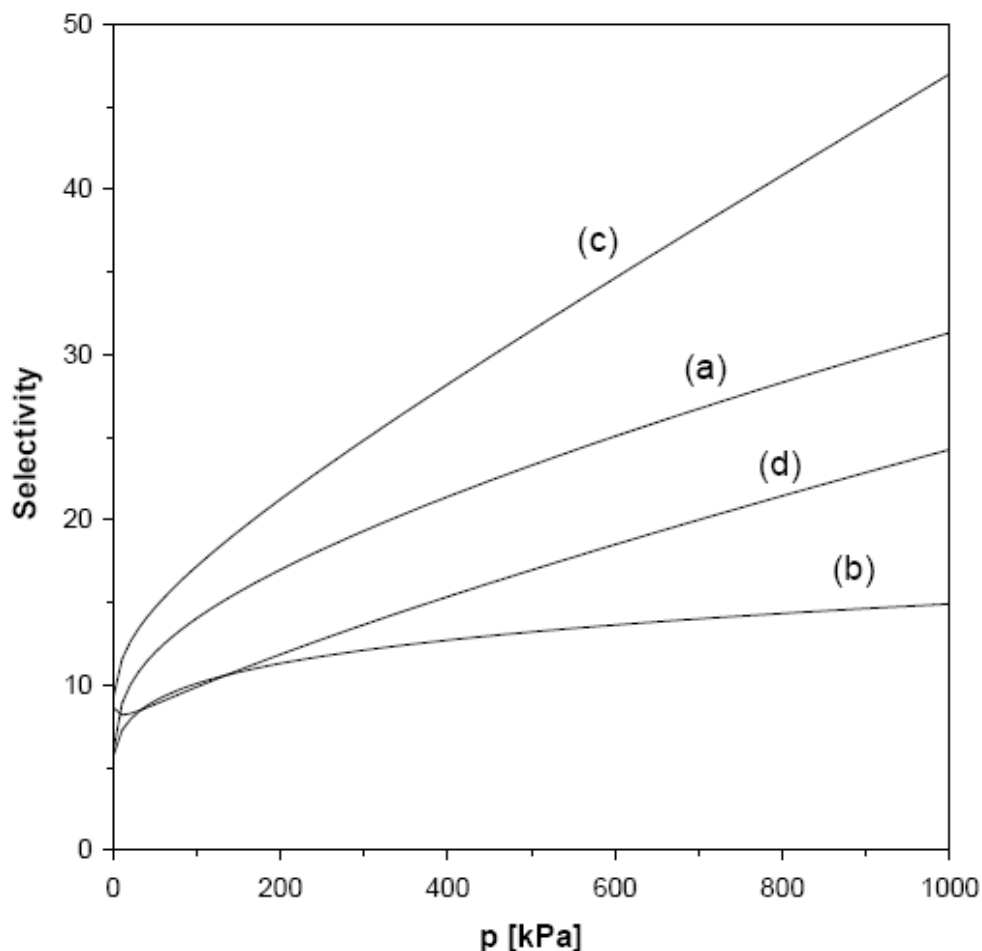


Figure 6-6. IAST model for C_2H_4/C_2H_6 selectivity at 298 K for (a) Zn-, (b) Ca/H-, (c) Sr-, and (d) Ba-RPZ-1.

The results for the adsorption of ethylene and ethane obtained from gravimetric and chromatographic measurements are quite different, especially for the strontium- and barium-exchanged samples. Based on the differences between these analysis techniques, it can be concluded that the contact time between the adsorbent and the C_2H_4/C_2H_6 mixture is a key factor affecting the separation of these gases. Contact time must be considered in the design of any pressure swing adsorption (PSA) process that utilizes adsorbents derived from ETS-4 or RPZ-1.

6.6 Conclusions

All of the cation-exchanged ETS-4 and RPZ-1 titanium silicate molecular sieves tested demonstrate selectivity for the adsorption of ethylene over ethane. Chromatographic separation of ethylene and ethane can be achieved by using ETS-4 or RPZ-1 exchanged with Zn or Ca/H. These materials could be appropriate adsorbents for the separation of ethylene from ethane by pressure swing adsorption. The highest chromatographic selectivity for C₂H₄/C₂H₆ (nearly 38) was observed on Zn-RPZ-1. In contrast, strontium- and barium-exchanged ETS-4 demonstrate very high gravimetric selectivity at high pressures. Combined results from both gravimetric and chromatographic separation techniques indicate that the adsorption of ethylene and ethane by cation-exchanged ETS-4 and RPZ-1 is dependent on the sieving nature of the frameworks, and that the contact time between the adsorbent and the C₂H₄/C₂H₆ mixture determines the outcome of the separation.

6.7 References

- (1) Choudary, N. V.; Kumar, P.; Bhat, T. S. G.; Cho, S. H.; Han, S. S.; Kim, J. N. *Ind. Eng. Chem. Res.* **2002**, *41*, 2728.
- (2) Van Miltenburg, A.; Zhu, W.; Kapteijn, F.; Moulijn, J. A. *Chem. Eng. Res. Des.* **2006**, *84*, 350.
- (3) Al-Baghli, N. A.; Loughlin, K. F. *J. Chem. Eng. Data* **2006**, *51*, 248.
- (4) Kuznicki, S. M. Large-Pored Crystalline Titanium Molecular Sieve Zeolites. U.S. Patent 5,011,591, April 30, 1991.
- (5) Kuznicki, S. M. Preparation of Small-Pored Crystalline Titanium Molecular Sieve Zeolites. U.S. Patent 4,938,939, July 3, 1990.
- (6) Kuznicki, S. M.; Sawada, J. A.; Rode, E. J.; Lin, C. C. H. Titanium Silicate Materials, Method for their Manufacture, and Method for Using Such Titanium Silicate Materials for Adsorptive Fluid Separations. International Patent WO/2008/002463, January, 3, 2008.
- (7) Sandomirskii, P. A.; Belov, N. V. *Sov. Phys. Crystallogr.* **1979**, *24*, 686.
- (8) Kuznicki, S. M.; Bell, V. A.; Petrovic, I.; Blosser, P. W. Separation of Nitrogen from Mixtures thereof with Methane Utilizing Barium Exchanged ETS-4. U.S. Patent 5,989,316, November 23, 1999.
- (9) Kuznicki, S. M.; Bell, V. A.; Petrovic, I.; Desai, B. T. Small-Pored Crystalline Titanium Molecular Sieve Zeolites and their Use in Gas Separation Processes. U.S. Patent 6,068,682, May 30, 2000.
- (10) Kuznicki, S. M.; Bell, V. A.; Nair, S.; Hillhouse, H. W.; Jacubinas, R. M.; Braunbarth, C. M.; Toby, B. H.; Tsapatsis, M. *Nature* **2001**, *412*, 720.
- (11) Kuznicki, S. M.; Bell, V. A. Olefin Separations Employing CTS Molecular Sieves. U.S. Patent 6,517,611, February 11, 2003.
- (12) Myers, A. L.; Prausnitz, J. M. *AIChE J.* **1965**, *11*, 121.
- (13) Danner, R. P.; Choi, E. C. F. *Ind. Eng. Chem. Fundam.* **1978**, *17*, 248.
- (14) Valenzuela, D. P.; Myers, A. L. *Adsorption Equilibrium Data Handbook*; Prentice Hall: Englewood Cliffs, 1989.

SEPARATION OF ETHYLENE AND ETHANE BY ADSORPTION ON LARGE-PORED TITANIUM SILICATE MOLECULAR SIEVES[†]

[†] A version of this chapter has been published. Reproduced with permission from Anson, A.; Wang, Y.; Lin, C. C. H.; Kuznicki, T. M.; Kuznicki, S. M. *Chem. Eng. Sci.* **2008**, *63*, 4171. Copyright 2008 Elsevier.

7.1 Summary

Ethylene and ethane adsorption isotherms were measured on several cation-exchanged forms of ETS-10. Isotherms for Na-, K-, and Ag-ETS-10 were found to be nearly rectangular, indicating strong interactions between the adsorbents and the adsorbates. In contrast, isotherms for Li-, Ba-, and Cu-ETS-10 show substantial curvature, suggesting a weakening of adsorption strengths for ethylene and ethane. Isotherms for the mixed cation forms (such as Ba/H and La/H) demonstrate the weakest ethylene and ethane adsorption, but possess substantial adsorption swing capacity between 1 and 200 kPa. Using the ideal adsorbed solution theory (IAST), it was determined that C_2H_4/C_2H_6 selectivity decreases in the order of $Na > K > Li > Cu \approx Ba > Ba/H > La/H$, while the adsorption swing capacity (from 1 to 200 kPa) shows a reversed trend. Therefore, it is possible to find a balance between selectivity and swing capacity in order to design an appropriate pressure swing adsorption (PSA) process for the separation of ethylene and ethane over a wide range of conditions using cation-exchanged ETS-10 adsorbents.

7.2 Introduction

The separation of ethylene and ethane is of key importance to the petrochemical sector. Annual global demand for ethylene, used to manufacture products such as plastic, rubber, and films, exceeds 100 million tonnes, making ethylene the largest product (by tonnage) of the petrochemical industry.¹ In Alberta, the petrochemical sector is one of the largest industries in the province, estimated at \$14 billion net sales per annum.² Clearly, the economic impact of ethylene production plays a significant role in Alberta's energy-driven economy, and this success is supported by the abundant, competitively-priced supply of hydrocarbon feedstocks unique to Alberta's petroleum-rich environment.

In Alberta, ethylene production is primarily based on ethane. Through steam cracking and thermal decomposition, ethane is converted into ethylene. However, this process results in a complex mixture of ethylene (principal component) and other hydrocarbons, including un-cracked ethane. Economically, it is desirable to recycle the un-cracked ethane via a C_2H_4/C_2H_6 separation process. Currently, this separation involves repeated compression and refrigeration, which is energy-intensive and contributes roughly 75% to the overall cost of olefin production. Therefore, if the separation of ethylene from ethane could be achieved through an adsorptive approach, the cost of ethylene production could be significantly reduced.

Al-Baghli and Loughlin recently reported experimental data and model predictions for the binary adsorption of ethylene and ethane on Na-ETS-10 – a large-pored, mixed octahedral/tetrahedral titanium silicate molecular sieve possessing a three-dimensional network of interconnecting channels.³⁻⁵ The channels of ETS-10 are uniquely configured to display a surface charge that is both shielded and homogenous. ETS-10, with an average pore size of $\sim 8 \text{ \AA}$,⁴ has been used extensively in ion-exchange, gas separation, and catalytic studies.⁶⁻⁸ The results of Al-Baghli and Loughlin suggest that the adsorptive separation of ethylene from ethane is highly favorable on Na-ETS-10.³ However, the rectangular-shaped isotherms of ethylene and ethane (at ambient temperature) would make pressure swing adsorption at ambient conditions nearly impossible. Although a

combined PSA and TSA (temperature swing adsorption) process may be utilized for the separation of ethylene from ethane on Na-ETS-10, the risk of ethylene polymerization at high temperatures, catalyzed by the ETS-10, would be a concern.

The adsorptive properties of most zeolite molecular sieves can be changed substantially by substituting different extra-framework cations. In ETS-10, different cationic species can occupy different lattice sites within the crystal framework⁹ and, consequently, alter the local electrostatic field that governs molecular adsorptive interactions. This phenomenon makes it possible to tailor ETS-10 adsorbents to have precise adsorptive characteristics over a wide range of conditions.

The objective of this study is to modify the shapes of the adsorption isotherms for ethylene and ethane on ETS-10 by cation-exchange, in order to improve performance in pure PSA separation processes. The C_2H_4/C_2H_6 selectivities are deduced from the pure-gas isotherms and by applying the ideal adsorbed solution theory.¹⁰

7.3 Experimental Methods

ETS-10 was synthesized hydrothermally as reported by Kuznicki.⁴ A typical sample involved thoroughly mixing 50.0 g of sodium silicate (28.80% SiO_2 , 9.14% Na_2O , Fisher), 3.2 g of sodium hydroxide (97+% NaOH, Fisher), 3.8 g of potassium fluoride (99% KF, Fisher), 4.0 g of HCl (1M), and 16.3 g of titanium trichloride (20% $TiCl_3$, 6% HCl, Fisher). The mixture was stirred in a blender for 1 h, and then reacted in a 125 mL sealed autoclave (PARR Instruments) at 488 K for 64 h. The resultant material was thoroughly washed with de-ionized water, and dried in a forced-air oven at 373 K.

Ion-exchanges were accomplished by exposing the Na-ETS-10 (as <150 μm powders) to an excess of aqueous ionic solutions (i.e. LiCl, KCl, $BaCl_2$, $AgNO_3$, or $CuSO_4$) at 373 K with stirring for 24 h. The exchanged materials were washed with de-ionized water, and dried at 373 K.

Mixed cation forms of ETS-10 (Ba/H and La/H) were prepared by exposing Na-ETS-10 powders to 1 meq/g of aqueous BaCl₂ or LaCl₃ solution at 373 K with stirring for 16 h. The partially-exchanged materials were then exposed to an HCl solution at pH 2 for 8 h at 293 K. The final products were washed with de-ionized water, and dried at 373 K.

Ethylene and ethane adsorption isotherms were measured with a Rubotherm magnetic suspension balance (accuracy $\pm 1 \mu\text{g}$) that is integrated with a gravimetric high pressure (GHP) adsorption system constructed by VTI Corporation (Hialeah, FL). Test samples were activated at 473 K for 6 h under a vacuum of greater than 10^{-4} Torr. Buoyancy effects were corrected with a helium displacement isotherm taken at the same conditions as the ethylene and ethane isotherms.

Nitrogen adsorption isotherms at 77 K were measured with an AUTOSORB-1-MP volumetric system from Quantachrome Instruments (Boynton Beach, FL). The nitrogen isotherms for the cation-exchanged ETS-10 samples are all Type I isotherms according to the IUPAC classification system.¹¹ Equivalent specific surface (S_{total}) was calculated by applying the BET equation. External surface (S_{ext}), internal surface (S_{int}), and micropore volume (V_{mic}) were calculated by the V-t method.^{11,12} Surface analysis results are summarized in Table 7-1.

Table 7-1. Surface Parameters for the Cation-Exchanged ETS-10 Samples

| Adsorbent | S_{total} [m ² /g] | S_{ext} [m ² /g] | S_{int} [m ² /g] | V_{mic} [cc/g] |
|-------------|--|--------------------------------------|--------------------------------------|-------------------------|
| Na-ETS-10 | 289 | 28 | 261 | 0.099 |
| Li-ETS-10 | 321 | 22 | 299 | 0.123 |
| K-ETS-10 | 178 | 28 | 150 | 0.067 |
| Ba-ETS-10 | 350 | 35 | 315 | 0.119 |
| Ba/H-ETS-10 | 417 | 30 | 387 | 0.146 |
| La/H-ETS-10 | 420 | 26 | 394 | 0.151 |
| Ag-ETS-10 | 209 | 19 | 190 | 0.071 |
| Cu-ETS-10 | 189 | 45 | 144 | 0.056 |

7.4 Theoretical Background

Model analysis of the ethylene and ethane adsorption isotherms followed the procedures of Al-Baghli and Loughlin.³ Experimental isotherms were fitted by applying the Tóth equation:

$$n = \frac{n_m \cdot p}{(b + p^t)^{1/t}} \quad (7-1)$$

Where n is the amount adsorbed at the pressure p , n_m is the monolayer adsorption capacity, t varies from 0 to 1, and b is related to the Henry's law constant (K) by the expression:

$$K = n_m \cdot b^{-1/t} \quad (7-2)$$

The selectivity at a specified temperature in the Henry's law region is defined as the ratio of the Henry's law constants between the pure-gas components. In this study, the selectivity of ethylene over ethane at 298 K is:

$$\alpha = \frac{K_{\text{ethylene}}}{K_{\text{ethane}}} \quad (7-3)$$

The Tóth equation is an empirical model used to characterize monolayer adsorption on heterogeneous surfaces. It is suitable for describing the adsorption of hydrocarbons, carbon oxides, hydrogen sulfide, and alcohols on activated carbons and molecular sieves. If the three parameters of the Tóth model (n_m , t , and b) are considered to be merely numerical fitting values, then the equation accurately fits all of the experimental ethylene and ethane isotherms reported in this work. Typically, the three parameters are allowed to vary until some optimum values are obtained, for example, by the least squares technique, with the only restrictions of n_m being higher than the highest value of n measured, and t varying from 0 to 1. However, the fitting parameters obtained by the

typical approach led to unrealistically high values for the monolayer capacity and selectivity, as noticed by Al-Baghli and Loughlin.¹³ In order to determine physically meaningful values for these parameters, they proposed a constrained method for the Tóth equation fitting. In the constrained approach, the monolayer adsorption capacity n_m is theoretically calculated, so only the parameters b and t can vary during the fitting. The theoretical monolayer capacity is calculated by:

$$n_m = 0.95 \cdot \frac{\varepsilon}{V^*} \quad (7-4)$$

Where ε is the monolayer volume of the adsorbent, V^* is the molar volume of the adsorbate at the temperature of the isotherm measurement, and the factor 0.95 accounts for steric effects.¹³ The monolayer volume ε can be calculated directly from the nitrogen isotherm at 77 K by applying the BET equation. Alternatively, it can also be determined from the surface parameters listed in Table 7-1 by:

$$\varepsilon = \frac{S_{\text{total}}}{S_{\text{int}}} \cdot V_{\text{mic}} \quad (7-5)$$

In the supercritical region, the molar volume of the adsorbate (V^*) can be approximated by the Van der Waals volume.¹³ The adsorbate molar volume (V^*) was taken to be 0.055 cm³/mmol for ethylene and 0.063 cm³/mmol for ethane.

The constrained Tóth equation fits reasonably well with the experimental ethylene and ethane isotherms for all of the cation-exchanged ETS-10 materials in the pressure range of 1-200 kPa (Figure 7-1). The largest deviation between the model and the experimental data is observed for ethylene adsorption on Li-ETS-10. However, even in this case, the deviations of the constrained Tóth model do not lead to qualitative changes in the conclusions presented, or to large quantitative differences with the predicted results.

Model predictions for the binary adsorption of C₂H₄/C₂H₆ were performed by applying the ideal adsorbed solution theory developed by Myers and Prausnitz.¹⁰ This theory has been successfully used to describe C₂H₄/C₂H₆ adsorption on titanium silicate ETS-10³ and on other related systems.^{10,14} The algorithm proposed by Valenzuela and Myers¹⁵ was applied for the IAST mathematical analysis. The constrained Tóth equation was used to model the pure compound isotherms for the IAST calculations. The constrained Tóth parameters for the IAST calculations are listed in Tables 7-2 and 7-3. The selectivity of the adsorbent (α) for the adsorption of ethylene from a C₂H₄/C₂H₆ mixture at a given total pressure is calculated by:

$$\alpha_{ij} = \frac{y_i \cdot x_j}{y_j \cdot x_i} \quad (7-6)$$

Where x_i and y_i are the molar fractions of ethane in the adsorbed and gas phase, respectively, and x_j , y_j are the corresponding molar fractions of ethylene. At the limit of $p = 0$, the selectivity α_{ij} is equivalent to the Henry's law selectivity.

Table 7-2. Constrained Tóth Parameters for the Adsorption of Ethylene at 298.5 K

| Adsorbent | n_m [mmol/g] | b [kPa ^t] | t | K [mmol/g kPa] |
|-------------|-------------------|----------------------------|------|---------------------|
| Na-ETS-10 | 1.89 | 0.24 | 0.37 | 89.45 |
| Li-ETS-10 | 2.28 | 0.51 | 0.50 | 8.77 |
| K-ETS-10 | 1.37 | 0.42 | 0.59 | 5.96 |
| Ba-ETS-10 | 2.28 | 0.86 | 0.48 | 3.12 |
| Ba/H-ETS-10 | 2.72 | 2.12 | 0.53 | 0.66 |
| La/H-ETS-10 | 2.78 | 3.36 | 0.56 | 0.32 |
| Ag-ETS-10 | 1.35 | 0.29 | 0.33 | 57.47 |
| Cu-ETS-10 | 1.27 | 1.89 | 0.53 | 0.38 |

Table 7-3. Constrained Tóth Parameters for the Adsorption of Ethane at 298.5 K

| Adsorbent | n_m [mmol/g] | b [kPa ^t] | t | K [mmol/g kPa] |
|-------------|-------------------|-----------------------------|------|---------------------|
| Na-ETS-10 | 1.65 | 0.54 | 0.40 | 7.70 |
| Li-ETS-10 | 1.99 | 1.37 | 0.63 | 1.21 |
| K-ETS-10 | 1.20 | 1.04 | 0.62 | 1.13 |
| Ba-ETS-10 | 1.99 | 1.71 | 0.58 | 0.79 |
| Ba/H-ETS-10 | 2.37 | 3.25 | 0.57 | 0.30 |
| La/H-ETS-10 | 2.43 | 3.36 | 0.55 | 0.27 |
| Ag-ETS-10 | 1.18 | 0.58 | 0.41 | 4.46 |
| Cu-ETS-10 | 1.11 | 2.01 | 0.47 | 0.25 |

7.5 Results and Discussion

Ethylene and ethane adsorption isotherms at 298 K for selected cation-exchanged ETS-10 samples are depicted in Figure 7-1. Isotherms for Na-ETS-10, especially ethylene, are nearly rectangular-shaped, indicating strong interactions between the Na-ETS-10 framework and the adsorbates. Similar results are obtained for K-ETS-10. However, the adsorption capacity of K-ETS-10, expressed on a gravimetric basis, is lower than Na-ETS-10 because potassium has a higher mass density than sodium. Isotherms for Li-ETS-10 are different from Na- and K-ETS-10, showing more progressive bending, leading to a larger swing capacity than both Na- and K-ETS-10 in the pressure range of 1-200 kPa. This is an interesting property of ETS-10, because lithium-exchanged classical zeolites typically demonstrate the opposite trend, showing stronger adsorption than their sodium and potassium counterparts.

Ethylene and ethane adsorption isotherms for Ba-ETS-10 (Figure 7-1) are less rectangular than for Na-ETS-10, suggesting a weakening of adsorptive interactions. Once again, ETS-10 behaves differently from classical zeolites which typically show stronger adsorption on divalent sites (such as Ca, Sr, or Ba) than on monovalent sites.¹⁶ The change in the isotherm shapes achieved with barium-exchange improves the swing capacity considerably between 1-200 kPa for both ethylene and ethane.

The swing capacity of Ba-ETS-10 can be further improved by making mixed Ba/H materials. Ba/H-ETS-10 is stable over a wide range of temperatures, and the bulk of its ethylene and ethane adsorption capacities manifest between 1 and 200 kPa (Figure 7-1). The insertion of trivalent cations into ETS-10 also leads to the modification of ethylene and ethane adsorption isotherms. On La/H-ETS-10 (Figure 7-1), the bending of the isotherms is even more pronounced than on Ba/H-ETS-10.

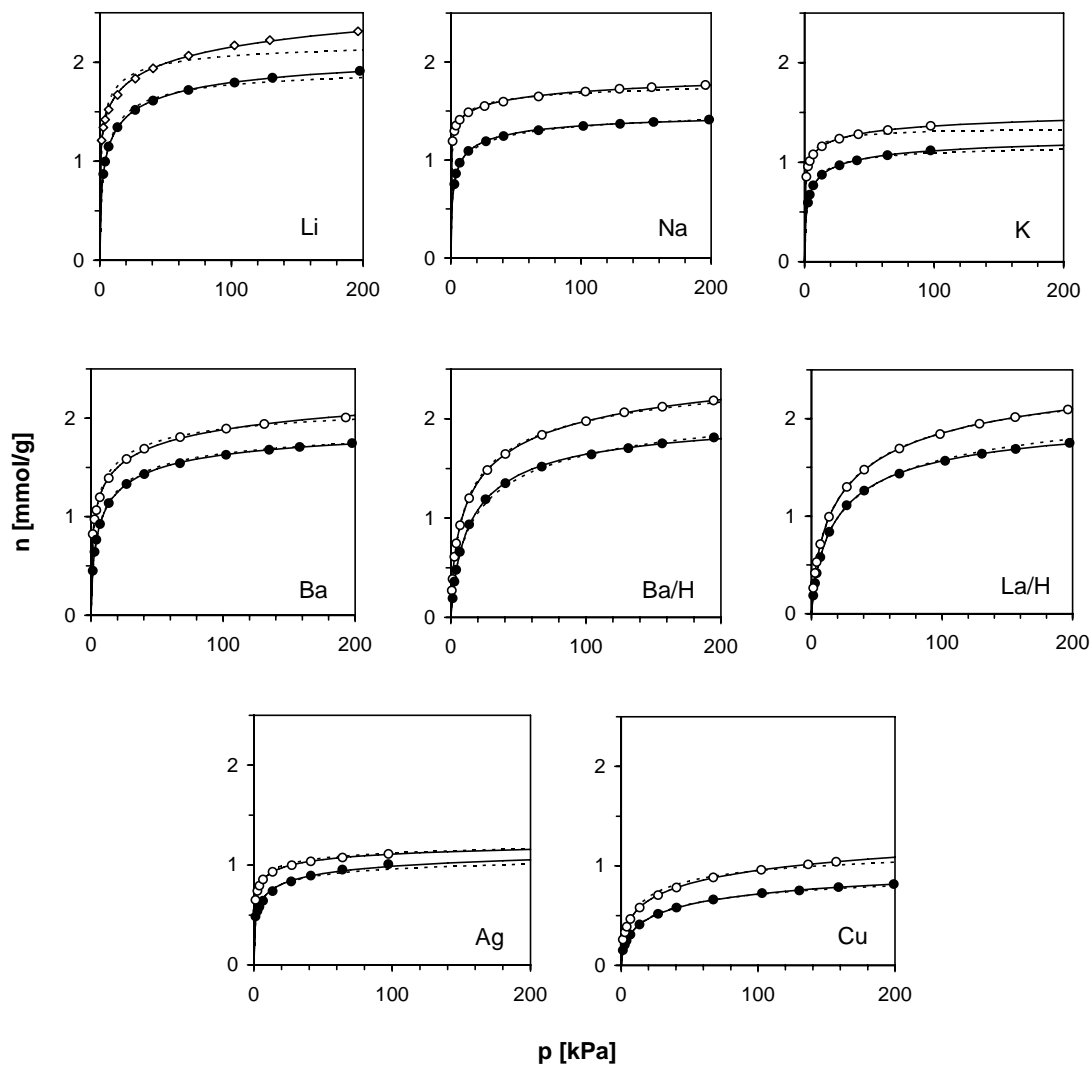


Figure 7-1. Ethylene (white circles) and ethane (black circles) adsorption isotherms at 298 K for selected cation-exchanged ETS-10 materials. Dotted lines represent the constrained Tóth model isotherms.

Silver and monovalent copper salts have been reported to show very good properties for the adsorptive separation of ethylene and ethane due to the interactions between the

compounds and the olefinic double bonds of ethylene.^{17,18} Isotherms of ethylene and ethane on Ag-ETS-10 (Figure 7-1) are very rectangular and the adsorption of both gases is essentially irreversible. This irreversibility may be due to the chemical state of the silver, which on ETS-10 reduces easily to metal by heat treatment (during the drying stage). In contrast, Cu-ETS-10 adsorbs ethylene and ethane reversibly. A change in the color from blue to green during the activation stage suggests that Cu^{2+} cations are reduced to Cu(I). Ethylene and ethane adsorption is believed to be predominantly on such sites. This is supported by infrared spectroscopy as reported by Bordiga et al.¹⁹ Cu-ETS-10 manifests most of its ethylene and ethane swing capacity in the pressure regime of 1-200 kPa.

Henry's law constants for the adsorption of ethylene and ethane on the cation-exchanged ETS-10 materials (Tables 7-2 and 7-3) show the following trend: $\text{Na} > \text{Ag} > \text{Li} > \text{K} > \text{Ba} > \text{Ba/H} > \text{Cu} \approx \text{La/H}$. The characteristics of ethylene and ethane adsorption on ETS-10 can be tuned quite precisely by cation-exchange, covering a range from weak adsorbents (such as silica)²⁰ to strong adsorbents (such as classical aluminosilicate zeolites).

The $\text{C}_2\text{H}_4/\text{C}_2\text{H}_6$ selectivities calculated from the IAST for selected cation-exchanged ETS-10 materials are presented in Figure 7-2 as a function of the total pressure. The IAST predicts that $\text{C}_2\text{H}_4/\text{C}_2\text{H}_6$ selectivity for Na-ETS-10 at 298 K increases with pressure. This tendency has been experimentally confirmed by Al-Baghli and Loughlin.³ The IAST predicts that the $\text{C}_2\text{H}_4/\text{C}_2\text{H}_6$ selectivity for Li- and K-ETS-10 also changes with pressure in a similar way, although the numerical values of the selectivity are less than Na-ETS-10. In general, the $\text{C}_2\text{H}_4/\text{C}_2\text{H}_6$ selectivity for alkali metal forms of ETS-10 decreases in the order of $\text{Na} > \text{K} > \text{Li}$. For divalent and mixed cation forms of ETS-10, the selectivity from 1-200 kPa decreases in the order of $\text{Ba} > \text{Cu} > \text{Ba/H} > \text{La/H}$.

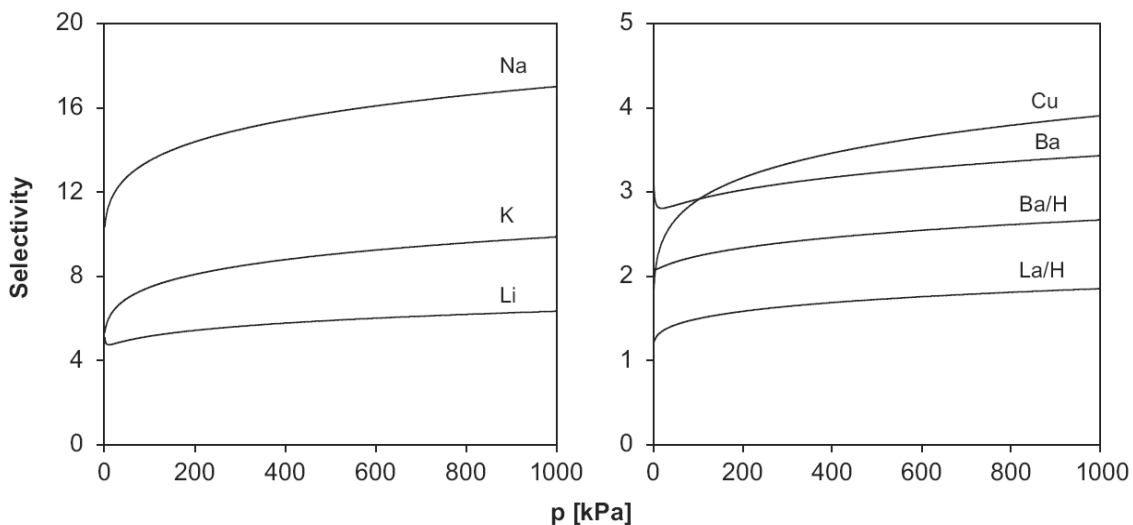


Figure 7-2. C_2H_4/C_2H_6 selectivity (from IAST) as a function of the total pressure for selected cation-exchanged ETS-10 materials at 298 K ($y = 0.5$).

Figure 7-3 depicts ethylene enrichment curves calculated for the entire set of cation-exchanged materials by the IAST. The enrichment of the adsorbed phase in ethylene decreases in the order of $Na > K > Li > Cu \approx Ba > Ba/H > La/H$ -ETS-10, similar to the adsorption strength.

In order to design a C_2H_4/C_2H_6 PSA separation process utilizing ETS-10, a compromise between selectivity and swing capacity appears to be necessary. Li-, Ba-, Ba/H-, and Cu-ETS-10 would appear to be more appropriate for a PSA process than Na-ETS-10 as proposed by Al-Baghli and Loughlin.³ In mixed cation forms, for example Ba/H-ETS-10, it should be possible to modify the compositional ratios of the cations continuously in order to obtain flexible adsorptive characteristics that can cover a wide range of PSA process conditions.

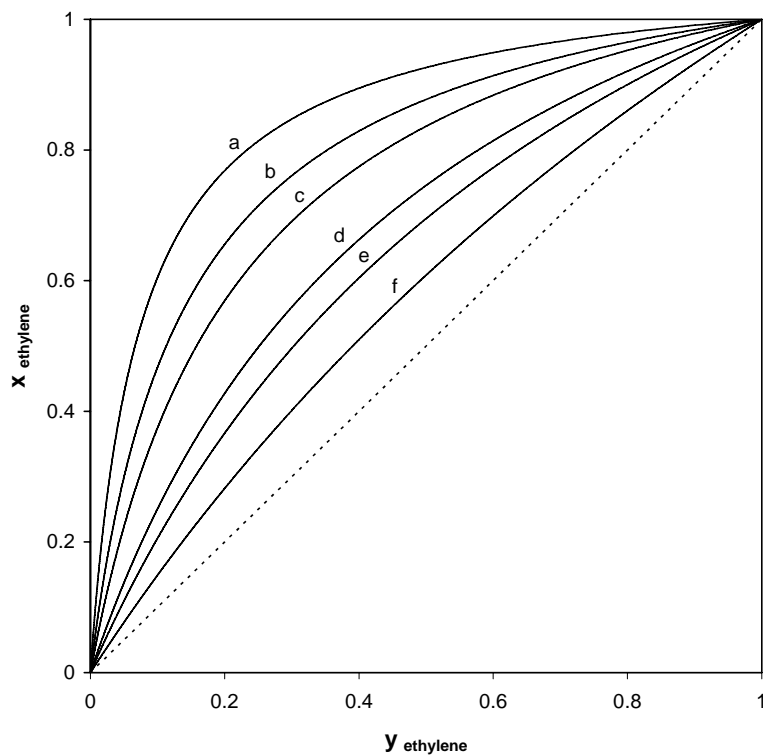


Figure 7-3. IAST plot of x_{ethylene} (molar fraction of ethylene in the adsorbed phase) vs. y_{ethylene} (molar fraction of ethylene in the gas phase) at 298 K and 150 kPa (total pressure) for (a) Na-, (b) K-, (c) Li-, (d) Cu- and Ba-, (e) Ba/H-, and (f) La/H-ETS-10.

7.6 Conclusions

Al-Baghli and Loughlin showed that Na-ETS-10 has a high selectivity for the separation of ethylene from $\text{C}_2\text{H}_4/\text{C}_2\text{H}_6$ mixtures. However, at ambient conditions, Na-ETS-10 possesses a low swing capacity for both ethylene and ethane, making its implementation in a PSA process impractical. The $\text{C}_2\text{H}_4/\text{C}_2\text{H}_6$ selectivities for several cation-exchanged forms of ETS-10 were investigated in this study, and were found to be uniformly lower than for Na-ETS-10, but the shapes of the adsorption isotherms can be tailored to substantially increase adsorption swing capacities in the regime of 1-200 kPa. A compromise between selectivity and swing capacity can be found on Li-, Ba-, Ba/H-, and Cu-ETS-10. The characteristics of ethylene and ethane adsorption on ETS-10 can be tuned quite precisely by cation-exchange, covering a range from weak adsorbents (such as silica) to strong adsorbents (such as classical aluminosilicate zeolites).

7.7 References

- (1) Storck, W. J. *Chem. Eng. News* **2006**, *84*, 59.
- (2) Alberta Industries. <http://www.albertacanada.com/industries/861.html> (accessed April 1, 2009).
- (3) Al-Baghli, N. A.; Loughlin, K. F. *J. Chem. Eng. Data* **2006**, *51*, 248.
- (4) Kuznicki, S. M. Large-Pored Crystalline Titanium Molecular Sieve Zeolites. U.S. Patent 5,011,591, April 30, 1991.
- (5) Anderson, M. W.; Terasaki, O.; Ohsuna, T.; Philippou, A.; Mackay, S. P.; Ferreira, A.; Rocha, J.; Lidin, S. *Nature* **1994**, *367*, 347.
- (6) Pavel, C. C.; Vuono, D.; Nastro, A.; Nagy, J. B.; Bilba, N. *Stud. Surf. Sci. Catal.* **2002**, *142 A*, 295.
- (7) Kuznicki, S. M.; Thrush, K. A.; Allen, F. M.; Levine, S. M.; Hamil, M. M.; Hayhurst, D. T.; Mansour, M. In *Synthesis of Microporous Materials: Molecular Sieves, Vol. 1*; Occelli, M. L.; Robson, H. E., Eds.; Synthesis and Adsorptive Properties of Titanium Silicate Molecular Sieves; Van Nostrand Reinhold: New York, 1992; pp 427-456.
- (8) Gervasini, A.; Picciau, C.; Auroux, A. *Microporous Mesoporous Mater.* **2000**, *35-36*, 457.
- (9) Anderson, M. W.; Agger, J. R.; Luigi, D.-P.; Baggaley, A. K.; Rocha, J. *PCCP* **1999**, *1*, 2287.
- (10) Myers, A. L.; Prausnitz, J. M. *AIChE J.* **1965**, *11*, 121.
- (11) Rouquerol, F.; Rouquerol, J.; Sing, K. S. W. *Adsorption by Powders and Porous Solids: Principles, Methodology and Applications*; Academic Press: London, 1999.
- (12) Gregg, S. J.; Sing, K. S. W. *Adsorption, Surface Area and Porosity*; Academic Press: London and New York, 1982.
- (13) Al-Baghli, N. A.; Loughlin, K. F. *J. Chem. Eng. Data* **2005**, *50*, 843.
- (14) Danner, R. P.; Choi, E. C. F. *Ind. Eng. Chem. Fundam.* **1978**, *17*, 248.
- (15) Valenzuela, D. P.; Myers, A. L. *Adsorption Equilibrium Data Handbook*; Prentice Hall: Englewood Cliffs, 1989.
- (16) Triebe, R. W.; Tezel, F. H.; Khulbe, K. C. *Gas Sep. Purif.* **1996**, *10*, 81.

- (17) Choudary, N. V.; Kumar, P.; Bhat, T. S. G.; Cho, S. H.; Han, S. S.; Kim, J. N. *Ind. Eng. Chem. Res.* **2002**, *41*, 2728.
- (18) Van Miltenburg, A.; Zhu, W.; Kapteijn, F.; Moulijn, J. A. *Chem. Eng. Res. Des.* **2006**, *84*, 350.
- (19) Bordiga, S.; Pazé, C.; Berlier, G.; Scarano, D.; Spoto, G.; Zecchina, A.; Lamberti, C. *Catal. Today* **2001**, *70*, 91.
- (20) Newalkar, B. L.; Choudary, N. V.; Turaga, U. T.; Vijayalakshmi, R. P.; Kumar, P.; Komarneni, S.; Bhat, T. S. G. *Microporous Mesoporous Mater.* **2003**, *65*, 267.

SEPARATION OF CARBON DIOXIDE, ETHANE, AND METHANE BY ADSORPTION ON MODIFIED TITANIUM SILICATE MOLECULAR SIEVES[†]

[†] A version of this chapter has been published. Reproduced with permission from Anson, A.; Lin, C. C. H.; Kuznicki, S. M.; Sawada, J. A. *Chem. Eng. Sci.* **2009**, *64*, 3683. Copyright 2009 Elsevier.

8.1 Summary

The separation of carbon dioxide from light hydrocarbons is a vital step in multiple industrial processes that could be performed by pressure swing adsorption (PSA), if appropriate adsorbents could be identified. To compare candidate PSA adsorbents, carbon dioxide, ethane, and methane adsorption isotherms were measured for cation-exchanged forms of titanium silicate molecular sieves ETS-10, ETS-4, and RPZ-1. Mixed cation forms, such as Ba/H-ETS-10, may offer appropriate stability, selectivity, and swing capacity to be utilized as adsorbents in CO₂/CH₄ PSA processes. Certain cation-exchanged forms of ETS-4 were found to partially or completely exclude ethane by size, and equivalent RPZ-1 materials were observed to exclude both ethane and methane, while allowing carbon dioxide to be substantially adsorbed. Adsorbents such as Ca/H-ETS-4 and Ca/H-RPZ-1 are strong candidates for use in PSA separation processes for both CO₂/C₂H₆ and CO₂/CH₄, potentially replacing current amine scrubber systems.

8.2 Introduction

The separation of carbon dioxide from light hydrocarbons is an important stage in the industrial production of ethane or methane from natural gas.¹ For some applications, such as the synthesis of ethylene by decomposition of ethane, the carbon dioxide content in the ethane stream must be reduced to trace levels. This can be accomplished by chemical absorption with amines, but the purification process is feasible only when the carbon dioxide content in the inlet stream is already moderately low (<3-5%).² The total or partial extraction of carbon dioxide from ethane or methane by pressure swing adsorption could reduce the chemical and energy costs of the purification process, while eliminating the need for environmental-unfriendly amine scrubbers.^{2,3}

The separation of carbon dioxide from ethane or methane could be performed by pressure swing adsorption using an appropriate adsorbent. Carbon dioxide, ethane, and methane adsorption isotherms for selected standard adsorbents are shown in Figure 8-1. The adsorption capacities on activated carbon molecular sieves at gas pressures below 1 bar (Figure 8-1a) typically decrease in the order of $C_2H_6 > CO_2 > CH_4$.^{4,5} Carbon molecular sieves are therefore selective toward ethane over carbon dioxide and cannot be effectively utilized to reduce carbon dioxide levels in ethane streams.

Most classical aluminosilicate zeolites selectively adsorb carbon dioxide over ethane and methane, as is illustrated for 13X zeolite in Figure 8-1b.⁶ Similar selectivity is observed for Na-Y, Na-mordenite, and 4A zeolite.^{6,7} The shape of the carbon dioxide isotherms for classical zeolites varies, but the curves are generally too steep for practical PSA processes and, therefore, classical zeolites are best suited for thermal swing adsorption (TSA) processes.

Not all molecular sieves preferentially adsorb carbon dioxide over ethane; some follow the capacity sequence of $C_2H_6 > CO_2 > CH_4$, as is illustrated for ALPO-5 in Figure 8-1c.⁸ Similar trends are observed for SAPO-5 and silicalite-1, with ethane selectivities in the order of silicalite-1 > ALPO-5 > SAPO-5.^{8,9}

Templated, high-silica zeolites usually follow the capacity sequence of $\text{CO}_2 > \text{C}_2\text{H}_6 > \text{CH}_4$, but present very small $\text{CO}_2/\text{C}_2\text{H}_6$ selectivity, as is observed for ZSM-5 in Figure 8-1d.¹⁰ These adsorbents cannot be used for the PSA separation of carbon dioxide from ethane but, with their nearly linear CO_2 isotherms, may be suitable for the PSA separation of carbon dioxide from methane. However, product recovery would suffer due to the adsorbent's significant methane capacity.

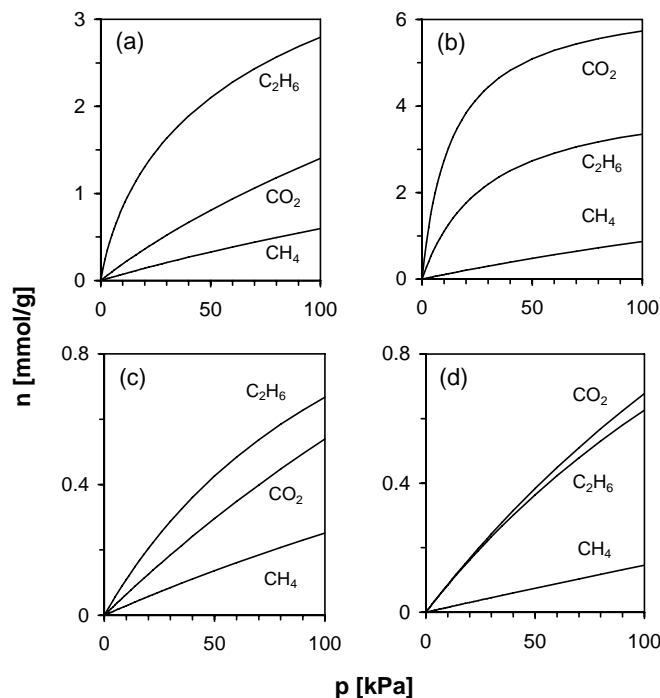


Figure 8-1. Carbon dioxide, ethane, and methane adsorption isotherms for (a) BPL activated carbon at 301 K, (b) 13X zeolite at 305 K, (c) ALPO-5 at 305 K, and (d) ZSM-5 at 298 K.

Engelhard Titanosilicate-10 (ETS-10) is a large-pored, titanium silicate molecular sieve with an average pore size of approximately 8 \AA .¹¹ Carbon dioxide and light hydrocarbons (such as ethane and methane) are all small enough to enter the pores of ETS-10 without constrictions, therefore no size-selectivity effects can be expected for the separation of carbon dioxide from ethane or methane. However, the shape of the adsorption isotherms and the strength of the adsorption for selected gases on ETS-10 can be widely modified by cation-exchange, and this characteristic could be exploited to design appropriate adsorbents for PSA-based carbon dioxide removal processes.

ETS-4 is a synthetic titanium silicate molecular sieve with a crystalline structure related to the mineral zorite,¹² possessing a pore size of 3-5 Å.¹³ Upon appropriate ion-exchange (usually with strontium or barium) followed by controlled temperature treatment, ETS-4 has been reported to be a size-selective adsorbent for small molecules with similar size, such as O₂/N₂, O₂/Ar, N₂/CH₄, CH₄/C₂H₆, and C₂H₄/C₂H₆.¹⁴⁻¹⁷ This phenomenon forms the basis of a pressure swing nitrogen rejection process used for the purification of natural gas.¹⁸ Since the kinetic diameter of CO₂ is smaller than those of O₂, N₂, Ar, CH₄, and C₂H₆, adsorptive separation of carbon dioxide from light hydrocarbons by size-selectivity may be possible using ETS-4.

Reduced Pore Zorite (RPZ), a synthetic titanium silicate, is a structural analog of ETS-4 and the mineral zorite.¹⁹ The size-selectivity and adsorptive characteristics of RPZ-1 can both be readily tailored. The pore size of RPZ-1 in the regime of 3-5 Å is controlled by the level of structural chloride anions. As the concentration of chlorides increases in the framework, the pores of RPZ-1 constrict progressively and systematically, which allows stable, size-selective materials to be prepared.²⁰ In addition to size-selectivity, ion-exchange of the extra-framework cations in RPZ-1 can also modify the isotherm profiles and adsorption strength for selected gases. Therefore, it may be possible to combine these features to synergistically prepare a highly selective adsorbent for PSA-based separations of carbon dioxide from ethane and/or methane.

In this investigation, we study the adsorption of carbon dioxide, ethane, and methane on selected cation-exchanged forms of ETS-10, ETS-4, and RPZ-1. The shape of the adsorption isotherms and adsorptive selectivity is modified by controlling the strength of the adsorption sites and/or controlling pore size to induce size-selectivity, in order to prepare enhanced adsorbents for the PSA separation of carbon dioxide from ethane and/or methane.

8.3 Experimental Methods

ETS-10, ETS-4, and RPZ-1 were synthesized hydrothermally as previously reported.^{11,13,19} Ion-exchanges were performed by exposing the as-synthesized molecular sieves (as <150 μm powders) to an excess of aqueous ionic solutions (i.e. BaCl_2 , ZnCl_2 , or CuSO_4) at 373 K with stirring for 24 h. The exchanged materials were washed with de-ionized water, and dried in a forced-air oven at 373 K.

The mixed cation forms of ETS-10 (Ba/H), ETS-4 (Ba/H, Ca/H), and RPZ-1 (Ca/H) were prepared by first exposing the as-synthesized molecular sieves in concentration-controlled aqueous solutions of BaCl_2 or CaCl_2 at 373 K with stirring for 24 h. These solutions were prepared by mixing 1, 4, or 6 meq of BaCl_2 or CaCl_2 with 10 g of de-ionized water per gram of molecular sieve. The partially-exchanged materials were then exposed to an HCl solution at pH 2 for 16 h at 293 K. The final products were washed with de-ionized water, and dried at 373 K.

Carbon dioxide, ethane, and methane adsorption isotherms at 298 K and up to 1 bar were measured with an AUTOSORB-1-MP volumetric system from Quantachrome Instruments (Boynton Beach, FL). This system is equipped with low pressure range transducers (0-1 Torr) that allow the direct measurements of very low pressure points of the adsorption isotherms, including those corresponding to the initial linear region (Henry's law region) of the carbon dioxide isotherms. Samples were activated at 473 K for 6 h under a vacuum of greater than 10^{-4} Torr, unless otherwise indicated.

Henry's law constants (K) were determined directly from the linear region of the isotherms, and were also calculated from the Langmuir equation applied to the low pressure adsorption data. Both methods for the determination of the Henry's law constants gave equivalent results. The selectivity of gas A over gas B in the Henry's law region, or the limiting selectivity (α), is defined as the ratio of the Henry's law constants of gas A and gas B:

$$\alpha(A/B) = \frac{K_A}{K_B} \quad (8-1)$$

In this study, the swing capacity (or working capacity) of an adsorbent is defined as the adsorption capacity between pressures of 1-100 kPa. A partial pressure of 1 kPa was selected to allow a common basis of comparison and because highly rectangular isotherms tend to hold a significant portion of their capacity below 1 kPa. Swing capacity percentage is normalized with respect to the total adsorption at 1 bar.

8.4 Results and Discussion

Figure 8-2 depicts carbon dioxide, ethane, and methane adsorption isotherms for three cation-exchanged forms of ETS-10: Na-, Ba-, and Ba/H- (1 meq Ba/g). Isotherms for Na-ETS-10 (Figure 8-2a) are similar in shape to those for 13X zeolite (Figure 8-1b), and follow the capacity sequence of $\text{CO}_2 > \text{C}_2\text{H}_6 > \text{CH}_4$. Carbon dioxide and ethane isotherms for Ba-ETS-10 (Figure 8-2b) are less rectangular than for Na-ETS-10. This phenomenon is opposite to what is generally observed in classical zeolites exchanged with divalent cations, such as Ca, Sr, or Ba.⁷ For Ba/H-ETS-10 (1 meq Ba/g), carbon dioxide and ethane isotherms are even less rectangular than for fully-exchanged Ba-ETS-10. This result is in agreement with observations from classical zeolites, where H^+ is the weakest of all possible cationic adsorption sites.

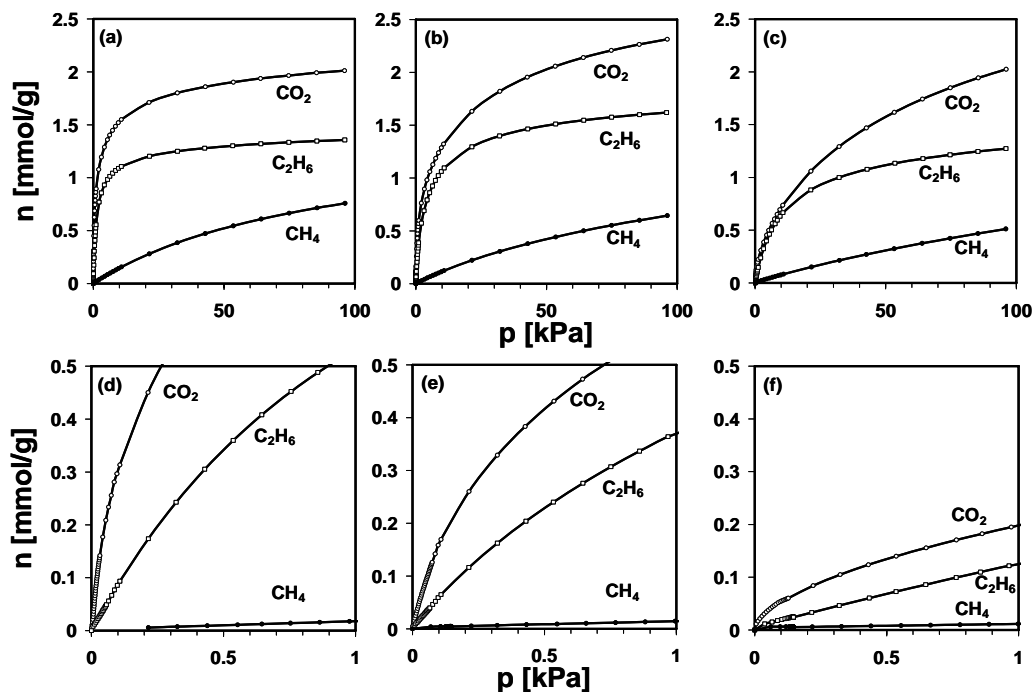


Figure 8-2. Carbon dioxide, ethane, and methane adsorption isotherms (up to 100 kPa) at 298 K for (a) Na-ETS-10, (b) Ba-ETS-10, and (c) Ba/H-ETS-10 (1 meq Ba/g). Equivalent data (up to 1 kPa) for (d) Na-ETS-10, (e) Ba-ETS-10, and (f) Ba/H-ETS-10 (1 meq Ba/g) are also presented.

The Henry's law constants for the adsorption of carbon dioxide, ethane, and methane on ETS-10 materials decrease with cation-exchange in the order of Na > Ba > Ba/H, but the limiting selectivity of carbon dioxide over ethane and methane does not undergo appreciable changes (Table 8-1). The swing capacity of carbon dioxide for ETS-10 materials increases in the order of Na < Ba < Ba/H (Table 8-2). More than 90% of the total carbon dioxide capacity for Ba/H-ETS-10 (1 meq Ba/g) is observed within 1-100 kPa, yet this material still demonstrates high carbon dioxide selectivity over ethane (nearly 9) and methane (around 150). From this result, Ba/H-ETS-10 (1 meq Ba/g) could be an effective adsorbent for the PSA separation of carbon dioxide from light hydrocarbons, especially methane. Fully-exchanged Ba-ETS-10 also demonstrates a large carbon dioxide swing capacity and, under certain conditions, could also be appropriate for the PSA separation of carbon dioxide from methane.

Table 8-1. Henry's Law Constants (K) and Limiting Selectivities (α) for the Adsorption of Carbon Dioxide, Ethane, and Methane on Selected Titanium Silicate Molecular Sieves

| | K [mmol·g ⁻¹ ·kPa ⁻¹] | | | | |
|--------------------------|--|-------------------------------|----------------------|--|-----------------------------------|
| | CO ₂ | C ₂ H ₆ | CH ₄ | $\alpha(\text{CO}_2/\text{C}_2\text{H}_6)$ | $\alpha(\text{CO}_2/\text{CH}_4)$ |
| Na-ETS-10 | 5.2 | 9.5·10 ⁻¹ | 1.6·10 ⁻² | 5.5 | 3.2·10 ² |
| Ba-ETS-10 | 2.1 | 6.2·10 ⁻¹ | 1.2·10 ⁻² | 3.4 | 1.7·10 ² |
| Ba/H-ETS-10 ^a | 1.2 | 1.4·10 ⁻¹ | 7.8·10 ⁻³ | 8.8 | 1.5·10 ² |
| Ba-ETS-4 | 34 | 1.1·10 ⁻¹ | 9.8·10 ⁻³ | 3.1·10 ² | 3.5·10 ³ |
| Ca/H-ETS-4 ^b | 1.3 | 7.8·10 ⁻² | 4.4·10 ⁻³ | 16 | 2.8·10 ² |
| Zn-ETS-4 | 1.6 | 3.6·10 ⁻¹ | 9.7·10 ⁻³ | 4.6 | 1.7·10 ² |
| Cu-ETS-4 | 1.3 | 3.2·10 ⁻¹ | 8.6·10 ⁻³ | 4.2 | 1.5·10 ² |
| Ba-RPZ-1 | 22 | 8.0·10 ⁻³ | 0.7·10 ⁻³ | 2.8·10 ³ | 3.2·10 ⁴ |
| Ca/H-RPZ-1 ^b | 7.7 | 7.2·10 ⁻² | 1.2·10 ⁻³ | 1.1·10 ² | 6.4·10 ³ |
| Zn-RPZ-1 | 2.0 | 2.1·10 ⁻¹ | 6.6·10 ⁻³ | 9.2 | 3.0·10 ² |
| Cu-RPZ-1 | 9.5·10 ⁻¹ | 2.0·10 ⁻¹ | 5.1·10 ⁻³ | 4.8 | 1.8·10 ² |

^a 1 meq Ba/g, ^b 4 meq Ca/g

Table 8-2. Swing Capacities (1-100 kPa) for the Adsorption of Carbon Dioxide, Ethane, and Methane on Selected Titanium Silicate Molecular Sieves

| | CO ₂ | | C ₂ H ₆ | | CH ₄ | |
|--------------------------|-----------------|----|-------------------------------|----|-----------------|----|
| | mmol/g | % | mmol/g | % | mmol/g | % |
| Na-ETS-10 | 1.14 | 57 | 0.82 | 61 | 0.76 | 98 |
| Ba-ETS-10 | 1.78 | 77 | 1.26 | 72 | 0.64 | 98 |
| Ba/H-ETS-10 ^a | 1.88 | 91 | 1.14 | 90 | 0.51 | 99 |
| Ba-ETS-4 | 0.78 | 37 | 0.04 | 66 | 0.53 | 98 |
| Ca/H-ETS-4 ^b | 1.94 | 82 | 0.24 | 85 | 0.27 | 98 |
| Zn-ETS-4 | 1.59 | 76 | 0.53 | 73 | 0.49 | 98 |
| Cu-ETS-4 | 1.36 | 76 | 0.54 | 75 | 0.44 | 98 |
| Ba-RPZ-1 | 0.44 | 34 | 0.01 | 80 | 0.04 | 98 |
| Ca/H-RPZ-1 ^b | 1.13 | 60 | 0.12 | 79 | 0.11 | 99 |
| Zn-RPZ-1 | 1.36 | 73 | 0.41 | 76 | 0.33 | 98 |
| Cu-RPZ-1 | 1.30 | 81 | 0.49 | 79 | 0.28 | 98 |

^a 1 meq Ba/g, ^b 4 meq Ca/g

The shape of the adsorption isotherms for ETS-4 and RPZ-1 can be modified, much like ETS-10, by cation-exchange. However, some exchanged forms of ETS-4 and RPZ-1 are not stable to thermal activation and, unlike ETS-10, cannot be utilized as effective adsorbents. Na-ETS-4 loses its crystallinity upon mild temperature treatments,¹⁶ as do other ETS-4 materials exchanged with monovalent cations. In order to induce thermal stability for activation (and adsorption), ETS-4 and RPZ-1 require exchanges with large size di or trivalent cations such as Ba or La.¹³ Figure 8-3 depicts the carbon dioxide isotherms for Ba/H-ETS-4 materials exchanged with different levels of Ba and H, under selected activation conditions. The carbon dioxide capacity for Ba/H-ETS-4 materials depends on the temperature of activation (Figure 8-3), because the interatomic distances and the pore size of ETS-4 progressively shrink with increased activation temperature.¹⁶ Ba/H-ETS-4 (4 meq Ba/g), Ba/H-ETS-4 (6 meq Ba/g), and fully-exchanged Ba-ETS-4 were found to be stable upon heating up to 423-473 K, at which point they are sufficiently activated for adsorption. Differences in the carbon dioxide adsorption capacities (mmol/g) observed for thermally-stable materials are influenced by the charge and mass density of the cationic sites.

As with Ba, exchange in the presence of at least 4 meq of Sr, Ca, Zn, or La per gram of Na-ETS-4 stabilizes the ETS-4 crystal structure and allows activation at 393-473 K. The levels of di or trivalent cations that are needed to stabilize the crystal structure of RPZ-1 are similar to those of ETS-4.

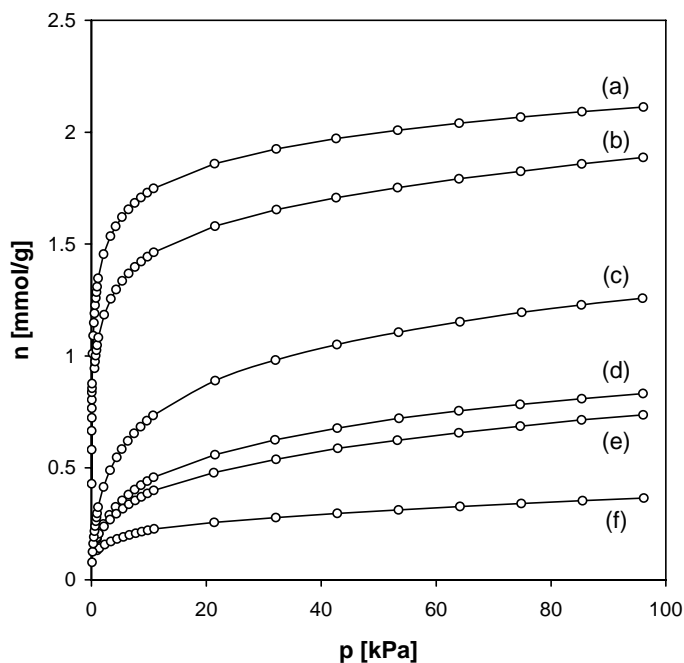


Figure 8-3. Carbon dioxide adsorption isotherms for (a) Ba/H-ETS-4 (6 meq Ba/g) activated at 473 K, (b) fully-exchanged Ba-ETS-4 activated at 473 K, (c) Ba/H-ETS-4 (4 meq Ba/g) activated at 423 K, (d) Ba/H-ETS-4 (1 meq Ba/g) activated at 373 K, (e) Ba/H-ETS-4 (1 meq Ba/g) activated at 393 K, and (f) Ba/H-ETS-4 (1 meq Ba/g) activated at 473 K.

Figure 8-4 depicts carbon dioxide, ethane, and methane adsorption isotherms for Ba-, Ca/H-, and Zn-ETS-4. Sieving properties of ETS-4 are clearly observed from the ethane isotherms. Ethane adsorption capacity is low in all cases and decreases with cation-exchange in the order of Zn > Ca/H > Ba, indicating a progressive reduction in the pore size of the adsorbent with exchange. The carbon dioxide isotherm for Ba-ETS-4 is nearly rectangular, with only a 37% swing capacity under the test conditions. Carbon dioxide isotherms for Ca/H- and Zn-ETS-4 are less rectangular than for Ba-ETS-4, showing swing capacities on the order of 80% (Table 8-2).

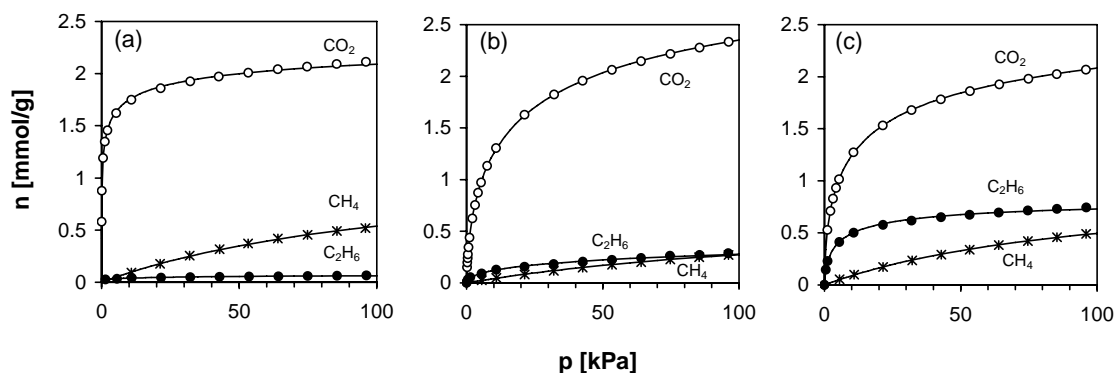


Figure 8-4. Carbon dioxide, ethane, and methane adsorption isotherms at 298 K for (a) Ba-ETS-4, (b) Ca/H-ETS-4 (4 meq Ca/g), and (c) Zn-ETS-4.

The Henry's law selectivity of $\text{CO}_2/\text{C}_2\text{H}_6$ for Ba-ETS-4 is approximately 310, which is nearly two orders of magnitude higher than for ETS-10 materials (Table 8-1), indicating significant enhancement from the size exclusion of ethane. The limiting selectivity of $\text{CO}_2/\text{C}_2\text{H}_6$ for ETS-4 materials decreases with the extra-framework cation type in the order of $\text{Ba} > \text{Ca/H} > \text{Zn} \approx \text{Cu}$ (Table 8-1). Ca/H-ETS-4 (4 meq Ca/g) appears to partially exclude ethane and demonstrates a limiting selectivity of 16 for $\text{CO}_2/\text{C}_2\text{H}_6$. The selectivities for Zn- and Cu-ETS-4 are similar to the values obtained for ETS-10, indicating little if any enhancement by size-selectivity. From this group, Ca/H-ETS-4 exchanged with at least 4 meq of Ca per gram of sample seems to be the most appropriate ETS-4 material for the PSA separation of carbon dioxide from ethane.

Values of CO_2/CH_4 selectivity for ETS-4 materials also reflect size effects, although these effects are much smaller than in the case of $\text{CO}_2/\text{C}_2\text{H}_6$. Methane molecules are smaller than ethane, and the pores of certain stabilized ETS-4 materials are too large to constrict the passage of methane, including fully-exchanged Ba-ETS-4. The limiting CO_2/CH_4 selectivity for ETS-4 materials decreases with cation-exchange in the order of $\text{Ba} > \text{Ca/H} > \text{Zn} \approx \text{Cu}$ (Table 8-1). Because of the nearly rectangular isotherm for carbon dioxide, the selectivity of CO_2/CH_4 for Ba-ETS-4 is quite high, reaching approximately 3500, but the selectivity values for other cation-exchanged ETS-4 are similar to those obtained for ETS-10 materials. Taking into account carbon dioxide swing capacities

(Table 8-2) and CO_2/CH_4 selectivity values (Table 8-1), Ca/H- and Zn-ETS-4 would appear to be the best adsorbents for the PSA separation of carbon dioxide from methane.

Size effects for the separation of $\text{CO}_2/\text{C}_2\text{H}_6$ and CO_2/CH_4 on RPZ-1 titanium silicates are greater than on ETS-4 containing equivalent extra-framework cations. Figure 8-5 illustrates carbon dioxide, ethane, and methane adsorption isotherms for Ba-, Ca/H-, and Zn-RPZ-1. The methane adsorption capacity for Ba-RPZ-1 is very low due to the size exclusion of methane molecules, while carbon dioxide is still adsorbed. $\text{CO}_2/\text{C}_2\text{H}_6$ and CO_2/CH_4 limiting selectivity values for RPZ-1 materials are uniformly higher than for ETS-4 exchanged with the same cations (Table 8-1). From this, it appears that RPZ-1 channels are more constricted than the channels of ETS-4. For Ba-RPZ-1 and Ca/H-RPZ-1 (4 meq Ca/g), the selectivity values for both CO_2/CH_4 and $\text{CO}_2/\text{C}_2\text{H}_6$ are approximately an order of magnitude higher than for Ba-ETS-4 and Ca/H-ETS-4 (4 meq Ca/g). The carbon dioxide adsorption isotherm for Ba-RPZ-1 is essentially rectangular, but Table 8-2 indicates that carbon dioxide swing capacity improves significantly for Ca/H-RPZ-1 (4 meq Ca/g). Therefore, Ca/H-RPZ-1 exchanged with at least 4 meq of Ca per gram of the Na-RPZ-1 precursor could be a promising adsorbent for the PSA separation of carbon dioxide from ethane and/or methane.

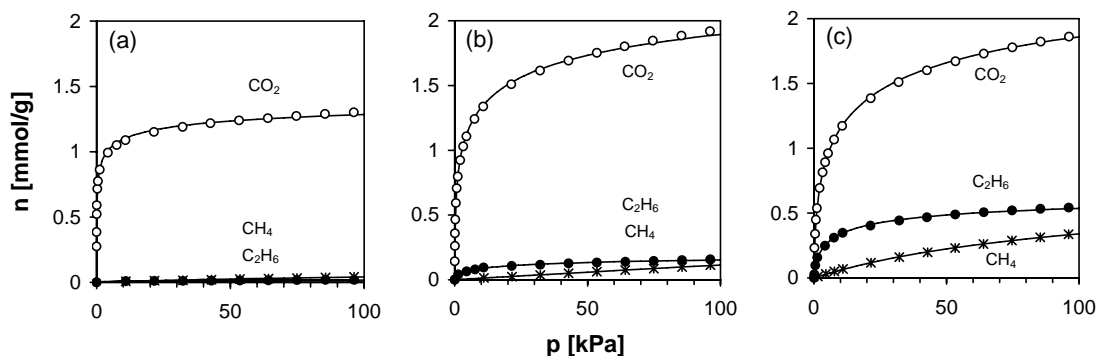


Figure 8-5. Carbon dioxide, ethane, and methane adsorption isotherms at 298 K for (a) Ba-RPZ-1, (b) Ca/H-RPZ-1 (4 meq Ca/g), and (c) Zn-RPZ-1.

8.5 Conclusions

Titanium silicate molecular sieves (ETS-10, ETS-4, and RPZ-1) can be modified by cation-exchange to prepare adsorbents with the appropriate characteristics of selectivity and swing capacity for the PSA separation of carbon dioxide from ethane and/or methane. Large-pored adsorbents such as Ba/H-ETS-10 with low Ba content could be utilized for the separation of carbon dioxide from methane by cationic site modification. This effect can be further enhanced by size-selectivity in small-pored titanium silicates such as ETS-4 and RPZ-1. While adsorbing substantial amounts of carbon dioxide, stabilized ETS-4 can exclude ethane by size and similarly modified RPZ-1 materials can exclude both ethane and methane. Ca/H-ETS-4 and Ca/H-RPZ-1 containing high levels of Ca appear to be excellent candidates for the PSA separation of carbon dioxide from ethane and/or methane.

8.6 References

- (1) Cavenati, S.; Grande, C. A.; Rodrigues, A. E. *Energy Fuels* **2006**, *20*, 2648.
- (2) Rao, A. B.; Rubin, E. S.; *Environ. Sci. Technol.* **2002**, *36*, 4467.
- (3) Collie, J.; Hlavinka, M.; Ashworth, A. In Proceedings of the 48th Annual Laurence Reid Gas Conditioning Conference, Norman, OK, March 1-4, 1998; pp 175-193.
- (4) Laukhuf, W. L. S.; Plank, C. A. *J. Chem. Eng. Data* **1969**, *14*, 48.
- (5) Reich, R.; Ziegler, W. T.; Rogers, K. A. *Ind. Eng. Chem. Process Des. Dev.* **1980**, *19*, 336.
- (6) Choudhary, V. R.; Mayadevi, S.; Singh, A. P. *J. Chem. Soc. Faraday Trans.* **1995**, *91*, 2935.
- (7) Breck, D. W. *Zeolite Molecular Sieves: Structure, Chemistry and Use*; Wiley: New York, 1974.
- (8) Choudhary, V. R.; Mayadevi, S. *Langmuir* **1996**, *12*, 980.
- (9) Choudhary, V. R.; Mayadevi, S. *Zeolites* **1996**, *17*, 501.
- (10) He, Y.; Seaton, N. A. *Langmuir* **2006**, *22*, 1150.
- (11) Kuznicki, S. M. Large-Pored Crystalline Titanium Molecular Sieve Zeolites. U.S. Patent 5,011,591, April 30, 1991.
- (12) Sandomirskii, P. A.; Belov, N. V. *Sov. Phys. Crystallogr.* **1979**, *24*, 686.
- (13) Kuznicki, S. M. Preparation of Small-Pored Crystalline Titanium Molecular Sieve Zeolites. U.S. Patent 4,938,939, July 3, 1990.
- (14) Kuznicki, S. M.; Bell, V. A.; Petrovic, I.; Blosser, P. W. Separation of Nitrogen from Mixtures thereof with Methane Utilizing Barium Exchanged ETS-4. U.S. Patent 5,989,316, November 23, 1999.
- (15) Kuznicki, S. M.; Bell, V. A.; Petrovic, I.; Desai, B. T. Small-Pored Crystalline Titanium Molecular Sieve Zeolites and their Use in Gas Separation Processes. U.S. Patent 6,068,682, May 30, 2000.
- (16) Kuznicki, S. M.; Bell, V. A.; Nair, S.; Hillhouse, H. W.; Jacobinas, R. M.; Braunbarth, C. M.; Toby, B. H.; Tsapatsis, M. *Nature* **2001**, *412*, 720.
- (17) Kuznicki, S. M.; Bell, V. A. Olefin Separations Employing CTS Molecular Sieves. U.S. Patent 6,517,611, February 11, 2003.

- (18) Butwell, K. F.; Dolan, W. B.; Kuznicki, S. M. Selective Removal of Nitrogen from Natural Gas by Pressure Swing Adsorption. U.S. Patent 6,315,817, November 13, 2001.
- (19) Kuznicki, S. M.; Sawada, J. A.; Rode, E. J.; Lin, C. C. H. Titanium Silicate Materials, Method for their Manufacture, and Method for Using Such Titanium Silicate Materials for Adsorptive Fluid Separations. International Patent WO/2008/002463, January, 3, 2008.
- (20) Lin, C. C. H.; Sawada, J. A.; Wu, L.; Haastrup, T.; Kuznicki, S. M. *J. Am. Chem. Soc.* **2009**, *131*, 609.

SEPARATION OF NITROGEN, ARGON, AND OXYGEN BY ADSORPTION ON SILVER-EXCHANGED MOLECULAR SIEVES[†]

[†] A version of this chapter has been published. Reproduced with permission from Anson, A.; Kuznicki, S. M.; Kuznicki, T.; Hastrup, T.; Wang, Y.; Lin, C. C. H.; Sawada, J. A.; Eyring, E. M.; Hunter, D. *Microporous Mesoporous Mater.* **2008**, *109*, 577. Copyright 2008 Elsevier.

9.1 Summary

The adsorption of nitrogen, argon, and oxygen were studied on silver-exchanged titanium silicate molecular sieve ETS-10 and silver-exchanged aluminosilicate mordenite by inverse-phase gas chromatography and volumetric adsorption isotherm measurements. Silver-exchanged zeolites, especially Ag-mordenite, have been noted to demonstrate some degree of selectivity for argon over oxygen. Ag-ETS-10 was found to have a selectivity of 1.49 for argon over oxygen at 303 K in the Henry's law region. This is substantially higher than 1.25 obtained for Ag-mordenite under the same conditions. Ag-mordenite has been proposed as a useful adsorbent for the removal of argon from a 95-5% O₂/Ar stream generated by many adsorptive air separation processes. With its higher limiting argon selectivity, Ag-ETS-10 would appear to be a promising potential adsorbent for the production of high purity oxygen from such streams.

9.2 Introduction

Silver-exchanged zeolites exhibit unusual adsorptive properties, especially toward the “inert gases” such as argon, krypton, and xenon. The nature of this phenomenon may be related to the directional properties given by the d orbitals of the silver ions.¹ Ag⁺ in silver zeolites react, upon heating, to generate clusters with a wide range of compositions including metal nanoensembles and groupings which may be composed of a combination of silver ions and silver atom clusters. The clusters can occupy different sites in the zeolitic structure.² This variability in the composition and location of the clusters results in materials that can express many different colors (from white or light yellow to dark gray), depending on the state of the silver and its thermal history.²⁻⁴

Enhanced interaction between xenon and silver-exchanged zeolites X and Y has been reported, including xenon adsorption isotherms and xenon NMR.⁵⁻⁷ The initial isosteric heat of xenon adsorption for silver zeolites is uniformly higher than for their sodium analogs, and a substantial displacement of the chemical shift has been observed in the ¹²⁹Xe NMR spectrum with silver present. The adsorption capacity of xenon and krypton on Ag-mordenite has also been reported to be substantially higher than for other cation forms of mordenite as well as 5A zeolite and activated carbon, especially at very low pressures.⁸

Although the strength of the interaction between silver zeolites and noble gases decreases remarkably in the order of Xe > Kr > Ar, the sorption affinity for argon is still significant, and some silver zeolites possess the unique property of being measurably selective in adsorbing argon (vs. oxygen). The separation of argon and oxygen by adsorption-based methods is difficult due to the similar diameter and polarizability of the argon atoms and oxygen molecules. However, molecular sieves and microporous polymers with some degree of selectivity for oxygen (vs. argon) are known and have been applied since the 1960s for the chromatographic resolution of nitrogen, argon, and oxygen.⁹⁻¹⁴ Moreover, oxygen over argon kinetic selectivity in certain carbon adsorbents has been employed for the production of purified argon and oxygen by pressure swing adsorption (PSA).^{15,16}

The preceding methods for the separation of argon and oxygen are based on adsorbents that show selectivity for oxygen over argon. In contrast, Ag-mordenite has been reported to manifest some argon selectivity (vs. oxygen).¹⁷ Pressure swing adsorption simulations and experiments were successfully performed for the purification of oxygen (to at least 99.7% purity) from a feed gas comprising of 95% O₂ and 5% Ar at 333-363 K.¹⁷ While Ag-mordenite appears to be the most widely reported zeolite-based argon-selective adsorbent, silver-exchanged zeolites X,¹⁸ Li-Na-LSX,^{19,20} A,^{21,22} Y, L, BEA, and ZSM-15⁴ have all been reported to show some degree of argon selectivity (vs. oxygen).

Nitrogen also interacts strongly with silver-exchanged zeolites. The nitrogen adsorption capacity and isosteric heat of adsorption of fully-exchanged zeolite Ag-X was found to be significantly higher than that of Na-X and Li-X.²³ This effect was explained by means of the π -complexation mechanism, which would involve donation of the π -bond electrons of the nitrogen molecule to the empty s orbital of Ag, and back-donation of electrons from the d orbital of silver to the empty π -antibonding orbital of nitrogen.²³ The basic concept for π -complexation was first described by Dewar.²⁴ The N₂/O₂ selectivity for Ag-X zeolite is also reported to be higher than for other cation forms of zeolite X. This effect has also been explained by the π -complexation theory. The π -antibonding electrons of the oxygen molecule do not allow the back-donation of electrons from the silver d orbital and, therefore, oxygen shows a weaker binding affinity than nitrogen on Ag-X zeolites.

It is known that by combining the potentials of lithium and silver, a hybrid Li-Ag-X zeolite can be superior to Li-X for air separation under certain circumstances. For example, it has been reported that a small amount of Ag substitution in Li-X can improve N₂/O₂ separation properties.²⁵ Other silver-exchanged zeolites, such as Ag-mordenite²⁶ and Ag-A,²² have also been reported to possess enhanced nitrogen capacities and N₂/O₂ selectivities compared to materials without silver.

Engelhard Titanosilicate-10 (ETS-10) is a mixed-coordination titanium silicate molecular sieve with a Si/Ti ratio of approximately five and two exchangeable (monovalent) cations for each structural titanium. ETS-10 is usually synthesized in the sodium form.²⁷ Silver-

exchanged ETS-10 was recently discovered to be an unusually strong adsorbent for xenon.²⁸ For this study, silver-exchanged ETS-10 was examined for its interactions with the constituents of air (nitrogen, argon, and oxygen). Since Ag-mordenite has a widely recognized preference for argon over oxygen, it was chosen as a comparison.

9.3 Experimental Methods

ETS-10 was synthesized under hydrothermal conditions as reported by Kuznicki.²⁷ The ETS-10 adsorbent was ion-exchanged by adding 5 g of ETS-10 powder to 10 g of silver nitrate (99+% AgNO₃, Fisher) in 50 g of de-ionized water. The mixture was heated to 353 K for a period of 1 h. The silver-treated material was filtered, washed with de-ionized water, and the exchange procedure was repeated twice more (for a total of three exchanges). The silver-exchanged ETS-10 was then dried in a forced-air oven at 353 K. Elemental analysis indicated that the Ag-ETS-10 was in essence quantitatively silver-exchanged with Ag constituting slightly more than 30 wt % of the finished material.

In order to obtain Ag-mordenite, H-mordenite (from Zeolyst Corporation) was silver-exchanged in a manner similar to that of Ag-ETS-10. With its inherently lower exchange capacity, the silver loading on mordenite was found to be only approximately 8 wt % by elemental analysis.

Inverse-phase gas chromatography (IGC) was performed on a Varian 3800 gas chromatograph (GC) utilizing a thermal conductivity detector (TCD). Test adsorbents were packed into 10" long, 0.25" OD copper columns using a plastic funnel. Typical columns contained approximately 3 g of the test adsorbents. The test columns were treated at 623 K and 0.5 psig for 16 h under 30 cm³/min of helium carrier flow. Characterization gases were composed of 1 mL injections of pure argon, pure oxygen, and a 50-50% mixture of O₂/Ar, which were performed at 303 K and 0.5 psig with 30 cm³/min of helium carrier flow.

Low pressure (up to 120 kPa) adsorption isotherms for nitrogen, argon, and oxygen were measured at 303 K in a Micromeritics (ASAP 2010) volumetric adsorption system. Test samples were dried (423 K for Ag-ETS-10 and 623 K for Ag-mordenite) for 6 h under a vacuum of greater than 10^{-4} Torr. Adsorption isotherms were fitted to the classical Langmuir equation:

$$n = \frac{n_m \cdot K_L \cdot p}{1 + K_L \cdot p} \quad (9-1)$$

Where n is the amount adsorbed ($\text{mmol}\cdot\text{g}^{-1}$) at the pressure p (kPa), and n_m and K_L are the fitting parameters. According to the Langmuir model, n_m is interpreted as the monolayer coverage ($\text{mmol}\cdot\text{g}^{-1}$), and the product $n_m \cdot K_L$ ($\text{mmol}\cdot\text{g}^{-1}\cdot\text{kPa}^{-1}$) equals the Henry's law constant at low loadings, i.e. when $p \rightarrow 0$. The selectivity (α) was calculated from the pure-gas Langmuir isotherms:

$$\alpha(A/B) = \frac{K_A}{K_B} \quad (9-2)$$

Where $\alpha(A/B)$ is the limiting selectivity of gas A over gas B at low loadings and expressed as the ratio of their respective Henry's law constants K_A and K_B ($K = n_m \cdot K_L$).

9.4 Results and Discussion

Color changes were noted for both Ag-ETS-10 and Ag-mordenite during activation. Ag-ETS-10 was initially light brown and became dark gray after heating to 423 K in a vacuum. Ag-mordenite changed from a light greenish yellow to a light gray with activation at 623 K. The color change infers a change in the state of silver during activation, presumed to be partial or total reduction to metal. Mordenite required the higher temperature for complete activation.

Figure 9-1 shows the IGC profiles for Ag-ETS-10 and Ag-mordenite with injections of pure argon, pure oxygen, and a 50-50% mixture of O₂/Ar. The retention times for pure argon were larger than for pure oxygen in both Ag-ETS-10 and Ag-mordenite, indicating an affinity for argon over oxygen, although chromatographic splitting was much more obvious for Ag-ETS-10 than Ag-mordenite when the 50-50% mixture of O₂/Ar was injected.

Figure 9-2 shows nitrogen, argon, and oxygen adsorption isotherms for Ag-ETS-10 and Ag-mordenite together with their Langmuir fitting curves up to a pressure of 120 kPa. An enhancement of the isotherm data at lower pressures (up to 8 kPa) is included as an insert. Up to 120 kPa, all experimental isotherms fit the Langmuir model. The parameters of these Langmuir isotherms are listed in Table 9-1, together with their standard deviations (σ):

$$\sigma = \frac{\Sigma(n_{\text{exp}} - n_{\text{calc}})}{N - m} \quad (9-3)$$

Where n_{exp} is the experimentally measured adsorption (mmol·g⁻¹) at pressure p (kPa) and n_{calc} is the adsorption calculated from the Langmuir equation at the same pressure. N is the number of experimental points taken and m is the number of fitting parameters (2 for the Langmuir equation).

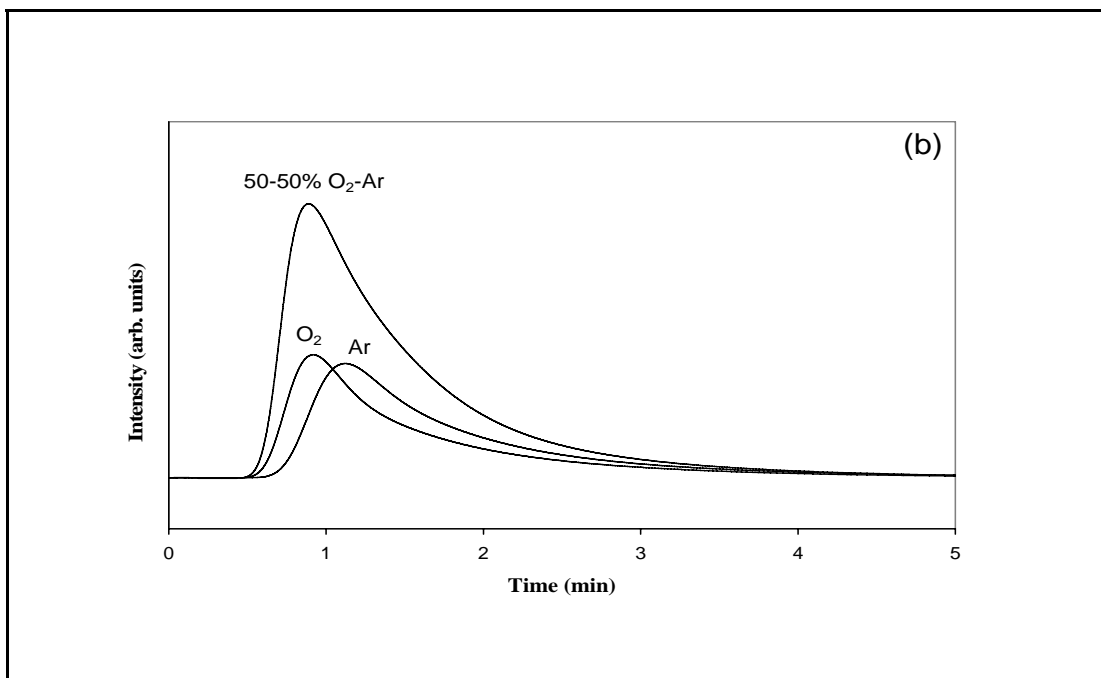
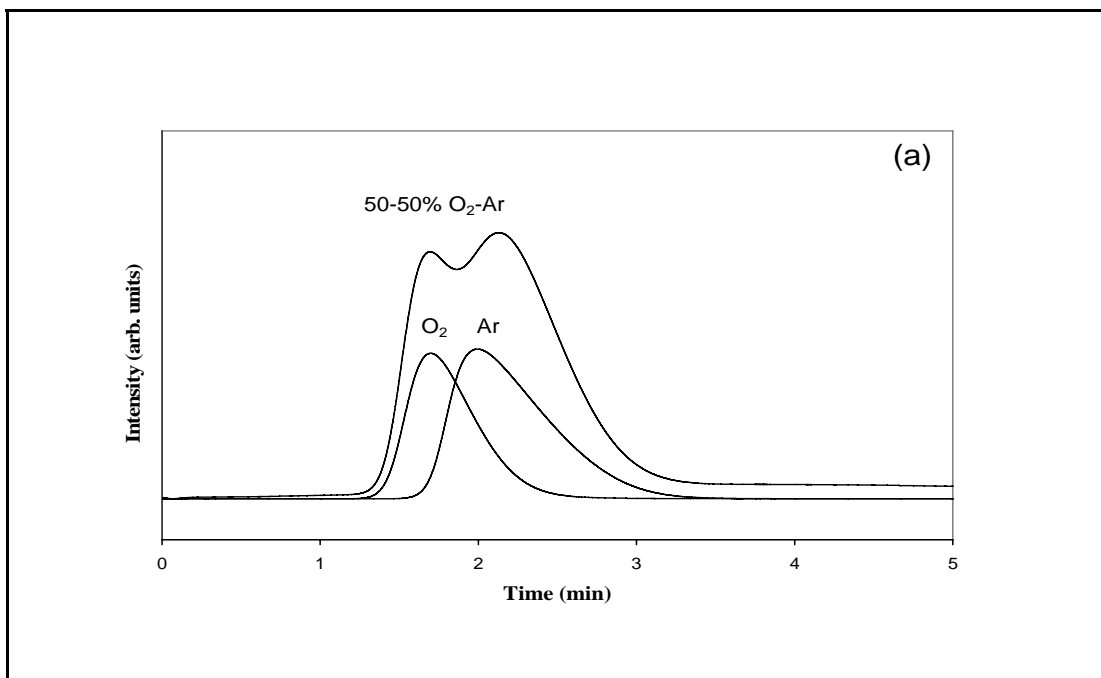


Figure 9-1. IGC profiles obtained at 303 K with 30 cm³/min of helium carrier flow for argon, oxygen, and a 50-50% mixture of O₂/Ar on (a) Ag-ETS-10 and (b) Ag-mordenite.

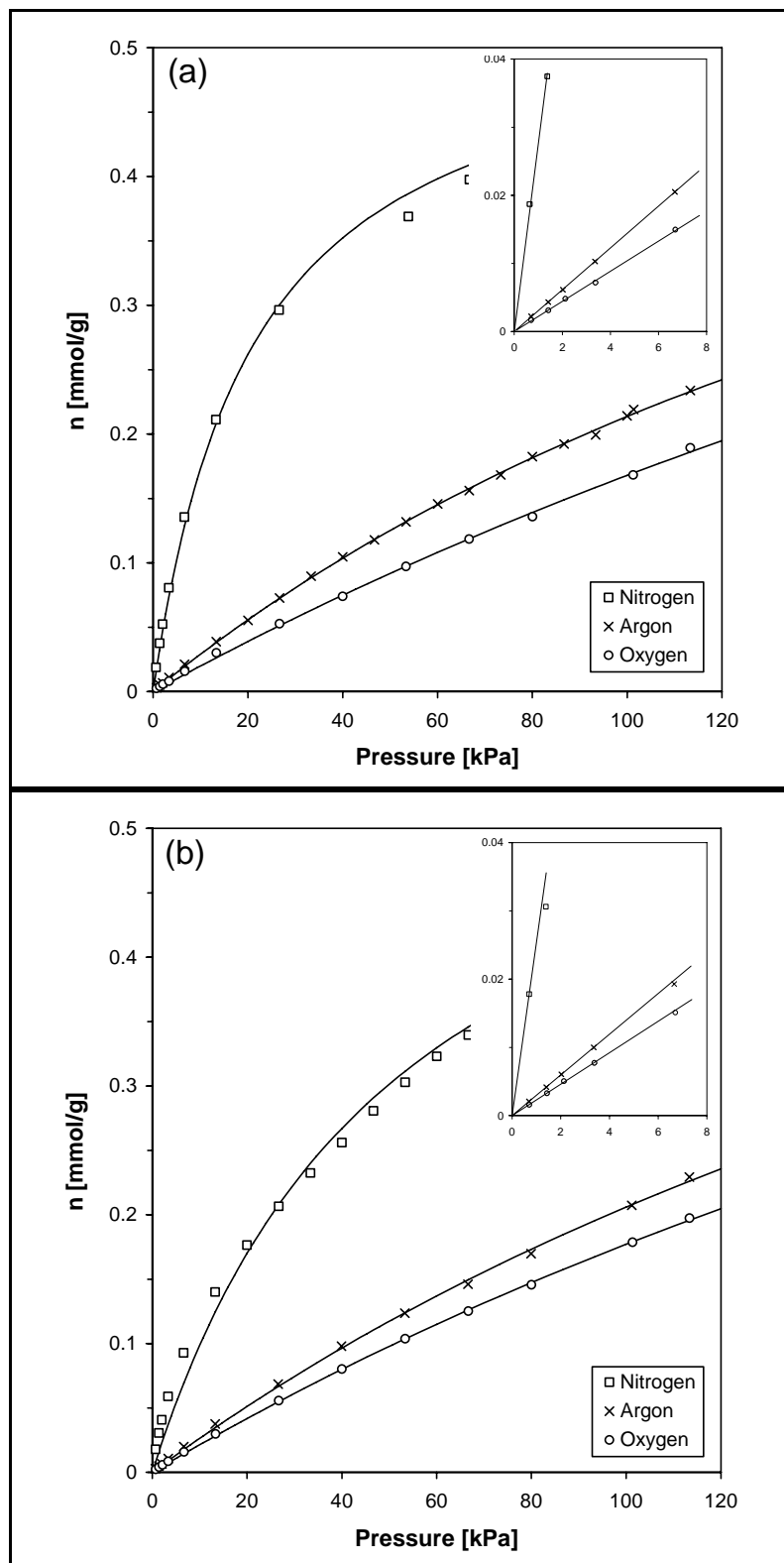


Figure 9-2. Nitrogen, argon, and oxygen adsorption isotherms at 303 K on (a) Ag-ETS-10 and (b) Ag-mordenite, with Langmuir fitting curves up to a pressure of 120 kPa. The inserts expand the lower pressure regimes.

The calculated Langmuir adsorption isotherms were used to predict the selectivity of Ag-ETS-10 and Ag-mordenite for nitrogen, argon, and oxygen. The resulting selectivities for the Henry's law limiting region are included in Table 9-1. Both Ag-ETS-10 and Ag-mordenite demonstrate some selectivity for argon over oxygen at atmospheric pressure, and this is magnified at low pressure, especially in the case of Ag-ETS-10, which reaches a selectivity of 1.49 at its limit. Both materials show strong selectivity for nitrogen over argon and oxygen at low pressures, especially Ag-ETS-10 where the limiting N₂/O₂ selectivity exceeds 10. Considering that Ag-ETS-10 is approximately twice as dense as Ag-mordenite, differences in actual bed selectivities would probably be greater than indicated by the isotherms.

Table 9-1. Langmuir Parameters for the Adsorption Data from 0-120 kPa

| Langmuir (0-120 kPa) | | Ag-ETS-10 | Ag-mordenite |
|----------------------|--|-----------|--------------|
| Nitrogen | n_m (mmol·g ⁻¹) | 0.53865 | 0.62092 |
| | $K_L \cdot n_m$ (mmol·kPa ⁻¹ ·g ⁻¹) | 0.02546 | 0.01171 |
| | $\sigma \cdot 10^3$ | 0.108 | 0.148 |
| Argon | n_m (mmol·g ⁻¹) | 0.73262 | 0.84651 |
| | $K_L \cdot n_m$ (mmol·kPa ⁻¹ ·g ⁻¹) | 0.00302 | 0.00272 |
| | $\sigma \cdot 10^3$ | 0.002 | 0.005 |
| Oxygen | n_m (mmol·g ⁻¹) | 0.98753 | 0.93305 |
| | $K_L \cdot n_m$ (mmol·kPa ⁻¹ ·g ⁻¹) | 0.00202 | 0.00218 |
| | $\sigma \cdot 10^3$ | 0.004 | 0.001 |
| | α (N ₂ /Ar) | 8.44 | 4.30 |
| | α (N ₂ /O ₂) | 12.58 | 5.36 |
| | α (Ar/O ₂) | 1.49 | 1.25 |

9.5 Conclusions

From chromatographic analyses and volumetric isotherm measurements, both Ag-ETS-10 and Ag-mordenite demonstrate adsorptive selectivity for argon over oxygen at 303 K over a wide range of pressures. This selectivity increases with decreasing pressure, especially in the case of Ag-ETS-10, where it reaches 1.49 in the Henry's law region. Ag-mordenite has been proposed as a useful adsorbent for the production of high purity oxygen (>99%) from a previously enriched oxygen stream (from PSA air separation)

containing approximately 95% O₂ and 5% Ar. Ag-ETS-10, with its higher Ar/O₂ selectivity (vs. Ag-mordenite) at low argon partial pressures, would appear to be a strong candidate to improve oxygen generation under these conditions.

9.6 References

- (1) Habgood, H. W. *Can. J. Chem.* **1964**, *42*, 2340.
- (2) Sun, T.; Seff, K. *Chem. Rev.* **1994**, *94*, 857.
- (3) Hutson, N. D.; Reisner, B. A.; Yang, R. T.; Toby, B. H. *Chem. Mater.* **2000**, *12*, 3020.
- (4) Sebastian, J.; Jasra, R. V. *Ind. Eng. Chem. Res.* **2005**, *44*, 8014.
- (5) Grosse, R.; Burmeister, R.; Boddenberg, B.; Gedeon, A.; Fraissard, J. *J. Phys. Chem.* **1991**, *95*, 2443.
- (6) Grosse, R.; Gedeon, A.; Watermann, J.; Fraissard, J.; Boddenberg, B. *Zeolites* **1992**, *12*, 909.
- (7) Watermann, J.; Boddenberg, B. *Zeolites* **1993**, *13*, 427.
- (8) Munakata, K.; Kanjo, S.; Yamatsuki, S.; Koga, A.; Ianovski, D. *J. Nucl. Sci. Technol.* **2003**, *40*, 695.
- (9) Lard, E. W.; Horn, R. C. *Anal. Chem.* **1960**, *32*, 878.
- (10) Jones, K.; Halford, P. *Nature* **1964**, *202*, 1003.
- (11) Walker, J. A. *J. Nature* **1966**, *209*, 197.
- (12) Pollock, G. E.; O'Hara, D.; Hollis, O. L. *J. Chromatogr. Sci.* **1984**, *22*, 343.
- (13) Pollock, G. E. *J. Chromatogr. Sci.* **1986**, *24*, 173.
- (14) Maroulis, P. J.; Coe, C. G. *Anal. Chem.* **1989**, *61*, 1112.
- (15) Rege, S. U.; Yang, R. T. *Adsorption* **2000**, *6*, 15.
- (16) Jin, X.; Malek, A.; Farooq, S. *Ind. Eng. Chem. Res.* **2006**, *45*, 5775.
- (17) Knaebel, K. S.; Kandybin, A. Pressure swing Adsorption System to Purify Oxygen. U.S. Patent 5,226,933, July 13, 1993.
- (18) Kandybin, A. I.; Anderson, R. A.; Reichley, D. L. System for Separation of Oxygen from Argon/Oxygen Mixture. U.S. Patent 5,470,378, November 28, 1995.
- (19) Chiang, R. L.; Whitley, R. D.; Ostroski, J. E.; Dee, D. P. Argon/Oxygen Selective X-Zeolite. U.S. Patent 6,432,170, August 13, 2002.
- (20) Dee, D. P.; Chiang, R. L.; Miller, E. J.; Whitley, R. D. High Purity Oxygen Production by Pressure Swing Adsorption. U.S. Patent 6,544,318, April 8, 2003.

- (21) Sebastian, J.; Jasra, R. V. Process for the Preparation of Molecular Sieve Adsorbent for Selective Adsorption of Nitrogen and Argon. U.S. Patent 6,572,838, June 3, 2003.
- (22) Sebastian, J.; Jasra, R. V. *Chem. Commun.* **2003**, 2, 268.
- (23) Yang, R. T.; Chen, Y. D.; Peck, J. D.; Chen, N. *Ind. Eng. Chem. Res.* **1996**, 35, 3093.
- (24) Dewar, M. J. S. *Bull. Soc. Chim. Fr.* **1951**, 18, C71.
- (25) Hutson, N. D.; Rege, S. U.; Yang, R. T. *AIChE J.* **1999**, 45, 724.
- (26) Salla, I.; Salagre, P.; Cesteros, Y.; Medina, F.; Sueiras, J. E. *J. Phys. Chem. B* **2004**, 108, 5359.
- (27) Kuznicki, S. M. Large-Pored Crystalline Titanium Molecular Sieve Zeolites. U.S. Patent 5,011,591, April 30, 1991.
- (28) Kuznicki, S. M.; Anson, A.; Kuznicki, T. M.; Hastrup, T.; Eyring, E. M.; Hunter, D. *J. Phys. Chem. C* **2007**, 111, 1560.

CONCLUSIONS

10.1 Conclusions

The discovery of zeolite molecular sieves has reshaped the chemical processing industry for applications ranging from adsorption to catalysis and ion-exchange. The objective of this research was to develop new molecular sieve materials and to examine their applications in adsorptive gas separation processes. Several techniques to modify zeolite molecular sieve materials have been developed, including a new pore size control mechanism and novel surface modification procedures. The new materials derived from these modification techniques have been successfully applied to commercially-relevant adsorptive gas separation processes.

Chapter three detailed the development of a novel mechanism to systematically control the pore size of titanium silicate molecular sieves through halogen substitution of terminal hydroxyl groups. These halogen containing zorites represent a new class of size-selective adsorbents with readily tailored and highly specific pore sizes. The promise of anion-controlled titanium silicate molecular sieves in multiple areas of size-based separation, particularly light hydrocarbon purification and permanent gas separation, was explored.

To demonstrate the effectiveness of the anion-controlled zorite analogs, a small-pored, halogen containing titanium silicate molecular sieve adsorbent, Ba-RPZ-1, was synthesized and its utility in light hydrocarbon purification and permanent gas separation was evaluated. In chapter four, we showed that Ba-RPZ-1 had much better nitrogen selectivity and (volumetric) nitrogen capacity than the commercial Molecular Gate[®] adsorbent ETS-4 in the separation of N₂/CH₄. In chapter five, mixtures of oxygen and argon were cleanly resolved at room temperature using Ba-RPZ-1 as the adsorbent. Inorganic crystalline adsorbents with the ability to resolve oxygen and argon more rapidly and reproducibly than carbon molecular sieves could find widespread applications in oxygen purification and argon generation, particularly in rapid cycle pressure swing adsorption processes. Both of these innovations arose from the use of anionic halides as structural barriers to adsorption in zorite-like titanium silicates.

The separation mechanism of the anion-controlled zorite analogs discussed in chapters three to five was primarily steric. In chapter six, the separation of ethylene and ethane was performed through the kinetic phenomenon using surface modified, small-pored titanium silicate molecular sieve adsorbents. While this method was promising, chapter seven described an alternative approach for separating ethylene and ethane through an equilibrium process, based on electrostatic interactions and thermodynamic affinities. The adsorptive properties of modified Engelhard Titanosilicate-10 (ETS-10) were controlled by the type and quantity of its extra-framework cations, altering both the thermodynamic selectivities and swing capacities of the modified ETS-10 adsorbents in order to improve the separation of ethylene and ethane.

In chapter eight, all of the modification techniques were synergistically integrated to illustrate that multi-functional adsorbents can be designed and prepared for many target separations. This approach was demonstrated using the separations of $\text{CO}_2/\text{C}_2\text{H}_6$ and CO_2/CH_4 as model systems. Anion-controlled adsorbents that can selectively exclude ethane and methane by the steric effect were designed and synthesized. The equilibrium and kinetic properties of the same adsorbents were concomitantly adjusted by surface modification.

Lastly, chapter nine introduced the concept of gas adsorption and separation through nanometals interaction. Nanometals, such as nanosilver, formed on molecular sieve surfaces were used as unique adsorbents to separate gas mixtures, such as Ar/O_2 and N_2/O_2 . Nanosilver, when formed on titanium silicate ETS-10, yielded one of the most selective materials reported to date for the separation of Ar/O_2 . Adsorptive gas separation utilizing nanometals interaction has unbounded potential and will clearly be an area of great interest in the research and development of new molecular sieve nanomaterials.

Whether it is pore size control by anion substitution, or surface modification by cation-exchange, or interaction with specialized metal nanoparticles, we have developed many techniques to generate new molecular sieve materials for adsorptive gas separation

processes. Continual research and development in new microporous materials will be crucial to the chemical processing industry, and should be viewed as an avenue for the discovery of next-generation adsorptive gas separation technologies.

10.2 Recommendations

Several innovative techniques to modify zeolite molecular sieve materials, including a new pore size control mechanism and novel surface modification procedures, have been identified in this research. The next logical step will be to investigate how to apply these modified materials to real-world separation systems. Efforts to scale-up modified adsorbents are already underway. The optimization of an adsorbent depends not only on the physical properties of the material, but also on the process conditions unique to each separation system. The transition from materials development to process implementation will require considerable effort, and will be a result of the intense ongoing collaborations between this academic research group and its industrial partners.

The future of zeolite molecular sieves and adsorptive gas separation processes depends on continual research and development with the objective of designing and modifying new microporous materials targeted toward specific applications.